

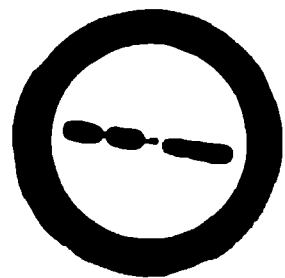
G1 8591

**STUDIES ON PREPARATION AND
CHARACTERIZATION OF HTS CURRENT
LEADS USING MULTIFILAMENTARY Ag AND
Ag-ALLOY SHEATHED (Bi,Pb)-2223
SUPERCONDUCTING TAPES**

*Thesis submitted to the
Cochin University of Science and Technology
For the degree of
DOCTOR OF PHILOSOPHY
in
PHYSICS*

By

ALOYSIUS. R. P.

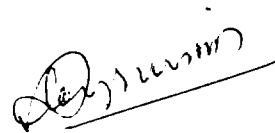


**REGIONAL RESEARCH LABORATORY
COUNCIL OF SCIENTIFIC AND INDUSTRIAL RESEARCH
THIRUVANANTHAPURAM -695 019
INDIA**

December 2002

DECLARATION

I, Aloysius. R. P., hereby declare that, this thesis entitled "STUDIES ON PREPARATION AND CHARACTERIZATION OF HTS CURRENT LEADS USING MULTIFILAMENTARY Ag AND Ag – ALLOY SHEATHED (Bi,Pb)-2223 SUPERCONDUCTING TAPES" is a bonafide record of the research work done by me and that no part of this thesis has been presented earlier for any degree, diploma of any other University.



Aloysius. R. P.

Trivandrum
30 December 2002





**COUNCIL OF SCIENTIFIC AND INDUSTRIAL RESEARCH [CSIR]
REGIONAL RESEARCH LABORATORY
TRIVANDRUM - 695 019, INDIA**

Dr. U. Syamaprasad

Scientist E II

Phone : 0091-0471-515233 (O), 741830 (R)

Fax : 0091- 0471- 491712, 490186; Grams : CONSEARCH

Email:syam@csrrltd.ren.nic.in; usyamaprasad@hotmail.com

30 December 2002

CERTIFICATE

*This is to certify that the thesis entitled " **STUDIES ON PREPARATION AND CHARACTERIZATION OF HTS CURRENT LEADS USING MULTIFILAMENTARY Ag AND Ag - ALLOY SHEATHED (Bi,Pb)-2223 SUPERCONDUCTING TAPES** " is an authentic record on the research work carried out by Mr. Aloysius. R. P., under my supervision in partial fulfilment of the requirement for the degree of **Doctor Of Philosophy** of the Cochin University of Science and Technology and further that no part of this thesis has been presented before for any other degree.*

U. Syamaprasad

Dedicated to my parents.

ACKNOWLEDGEMENTS

With great pleasure, I express my deep sense of gratitude and indebtedness to Dr. U. Syamaprasad, my supervising guide, Regional Research Laboratory, Trivandrum for his valuable guidance, constant encouragement and continuous support throughout the period of my Ph.D. work.

I am grateful to Dr. B.C. Pai, Acting Director, Regional Research Laboratory, Trivandrum and Dr. G. Vijay Nair and Prof. Javed Iqbal, former Directors of RRL, Trivandrum, for providing all the facilities to carry out this work and for their encouragement and valuable suggestions during this work.

I owe my sincere gratitude to my colleague Mrs. A. Sobha for her sincere help, constant encouragement, invaluable suggestions and the warmth of friendship during the entire course of this work.

I am greatly indebted to Mr. P. Guruswamy, Technical Officer, Regional Research Laboratory, and Trivandrum for his encouragement, invaluable suggestions and help during the entire course of this work.

My sincere thanks are due to Dr. K.G.K. Warriar, Dr. C. Pavithran, Dr. Peter Koshy and Mr. P. Prabhakar Rao, and Mr. V. Muraleedharan, Scientists, Regional Research Laboratory, Trivandrum for their help during this work.

I owe my sincere gratitude to my senior colleagues Dr. M. Sankara Sarma, Lecturer, Govt. Women's College, Trivandrum, Dr. Jose Kurian, Post Doctoral Fellow, NTT, Japan, for their sincere help, constant encouragement and invaluable suggestions.

It is with great pleasure that I thank my colleagues, Mr. Jolly Bose R., Mr. Rajeev Kumar R., Ms. Prabitha, Mr. N.A. Madhu, Mr. O.B. Satheesh Kumar, Dr. M.A. Suresh and Dr. T.P.D. Rajan, for their help at various stages of this work.

My heartfelt thanks are due to Mr. S.G.K. Pillai, Mr.K.V. Oonnikrishnan, Mr. Krishna Pillai, Mr. K.K. Ravikumar, Mr. K. P. Sadasivan, Mr. P. Mukundan and Mr. M.R. Nair, for extending different instrumental facilities.

I express my sincere gratitude to Dr. K. P. Vijayakumar, Head, Department of Physics, Cochin University of Science and Technology, Trivandrum for his kind cooperation and support at various stages of this work.

Finally I express my deep sense of gratitude to the Council of Scientific and Industrial Research, New Delhi for the award of Senior Research Fellowship.

Aloysius. R. P.

CONTENTS

	Page
Preface.....	i
List of Publications.....	vi
1 INTRODUCTION.....	1
1.1 History of Superconductivity.....	1
1.2 Distinguishing Characteristics of Copper oxide Superconductors.....	5
1.3 Type II nature and Irreversibility line of High-Tc superconductors (HTS).....	13
1.4 Theoretical Efforts and Developments.....	13
1.5 Application Environment of Superconductors.....	16
1.6 The BSCCO System of Superconductors.....	20
1.6.1 Structural features.....;	20
(a) Bi-2201 phase.....	20
(b) Bi-2212 phase.....	21
(c) Bi-2223 phase.....	21
1.6.2 Thermodynamic and kinetic aspects.....	22
1.6.3 Importance of Pb substitution.....	23
1.7 Powder-in-tube Technique for BPSCCO Tape Fabrication.....	24
1.8 Important Considerations in the PIT Technique for BPSCCO Tape Fabrication.....	25

1.8.1	Choice of sheath metal.....	25
1.8.2	Choice of Precursor powder.....	26
1.8.3	Choice of mechanical deformation procedures.....	27
1.8.4	Formation and stability of 2223 phase.....	28
	(a) Formation mechanism.....	29
	(b) Stability of 2223 phase.....	30
1.8.5.	Critical current density of (Bi,Pb)-2223/Ag tapes.....	30
	(a) Flux pinning and its significance.....	31
	(b) Weak links and intergranular connectivity.....	32
	(c) Other limitations.....	33
1.8.6	Importance of multifilamentary geometry.....	34
1.9	Achievements and State of the Art Developments of HTS.....	35
1.9.1	International Scenario.....	35
1.9.2	National Scenario.....	38
1.10	HTS Current Leads.....	38
1.10.1	Conditions cooled and vapour cooled current leads.....	40
1.10.2	Material choices for HTS current leads.....	41
1.10.3	HTS current leads in bulk rods or tubes.....	42
1.10.4	HTS current leads tape form.....	42
1.10.5	Operation and stability of HTS current leads	43
	(a) Heat leak.....	44
	(b) Thermal and mechanical stability.....	44
	(c) Field tolerance.....	45
1.10.6	Design aspects of the current leads.....	45
1.11.	Scope of the Present Work.....	46
	References.....	49

2	PREPARATION AND CHARACTERIZATION TECHNIQUES.....	60
2.1	Introduction.....	60
2.2	Preparation of Mono and Multifilamentary Tapes.....	60
2.2.1	Monofilament tapes.....	60
2.2.2	Multifilamentary tapes.....	61
2.2.3	Preparation of current leads.....	61
2.3	Analytical Methods.....	62
2.3.1	X-ray Diffraction Technique.....	62
2.3.2	Microstructural analysis.....	63
2.3.3	Scanning Electron Microscopy (SEM).....	64
2.3.4	Optical Microscopy.....	64
2.3.5	Thermal Analysis.....	65
2.4	Superconductivity Measurements.....	65
2.4.1	J_c measurement.....	65
2.4.2	V-I or E-J characteristics.....	68
2.4.3	J_c -B measurement.....	69
2.4.4	Measurement of $I_c - \sigma$ and $I_c - \epsilon$ (mechanical properties).....	69
2.5	Conclusions.....	73
	References.....	74
3	STUDIES ON ALTERNATE SHEATH ALLOYS FOR THE PREPARATION OF (BI,PB)-2223/AG TAPES.....	75
3.1	Introduction.....	75
3.2	Superconducting Properties.....	76
3.2.1	Experimental.....	76
	(a) Alloy preparation.....	76
	(b) Tape preparation.....	76

(c) Heat treatment and temperature optimization.....	77
3.2.2 Results and discussion.....	79
I Ag-Cu alloy system.....	79
(a) Optimization of sintering temperature for the precursors	
CD and CR.....	79
(b) Phase evolution study.....	81
(c) Critical current density of the tapes.....	88
II Ag-Au alloy system.....	91
3.3 Mechanical Properties.....	96
3.3.1 Mechanical behaviour of BPSCCO composite tapes.....	96
3.3.2 Experimental.....	98
3.3.3 Results and Discussion.....	99
3.4 Electrical and Thermal Properties.....	110
3.5 Conclusions.....	113
References.....	117
4 EFFECT OF NANO SIZE MGO ADDITION: ENHANCED	
FLU PINNING IN (BI,PB)-2223/AG TAPES.....	119
4.1 Introduction.....	119
4.2 Experimental.....	120
4.3 Results and Discussion.....	121
4.4 Conclusions.....	127
References.....	129

5	STUDIES ON THE OPTIMIZATION OF PROCESS PARAMETERS FOR THE PREPARATION OF MULTIFILAMENTARY (BI,PH)-2223/AG TAPES.....	131
5.1.	Introduction.....	131
5.2.	Optimization of Powder Packing Density in Monofilamentary Tapes.....	133
5.2.1	Experimental.....	133
5.2.2	Results and Discussion.....	135
5.2.3	Conclusions.....	142
5.3	Preparation of Multifilamentary Tapes: Optimization of Geometrical Parameters.....	143
5.3.1	Experimental.....	143
5.3.2	Results and Discussion.....	144
5.3.3	Conclusions.....	150
5.4	Optimization of Thermo-mechanical Processing/Heat Treatment Schedules of (Bi,Pb)-2223/Ag Multifilamentary Tapes.....	151
5.4.1	Experimental.....	151
5.4.2	Results and Discussion.....	152
5.4.3	Conclusions.....	159
	References.....	160
6	PREPARATION AND CHARACTERIZATION OF HTS CURRENT LEADS USING MULTIFILAMENTARY (BI,PB)-2223/AG AND AG-ALLOY SHEATHED TAPES.....	162
6.1	Introduction.....	162

6.2	Optimization of Uniaxial Pressure for the Preparation of Multifilamentary Tapes.....	163
6.2.1	Experimental.....	163
6.2.2	Results and Discussion.....	164
6.2.3	Conclusions.....	170
6.3	Preparation and characterization of Prototype HTS Current Leads.....	170
6.3.1	Experimental.....	171
6.3.2	Results and Discussion.....	173
6.3.3	Testing of Current leads.....	175
	(i) Thermal Recycling Tolerance.....	175
	(ii) Transient Quench Stability.....	176
	(ii) Heat Leak Estimation.....	177
6.4	Conclusions.....	178
	References.....	179
7	SUMMARY AND CONCLUSIONS.....	181

PREFACE

The application vistas of superconductors have widened very much since the discovery of high T_C superconductors (HTS) as many of the applications can be realised at 77 K rather than going down to 4.2 K, the liquid He temperature. One such application is the HTS current lead which is used to connect a superconducting system with a room temperature power source. Minimising heat leak to the cryogenic environment is the main advantage of introducing current leads into superconducting systems. The properties of HTSs like zero resistance (avoiding joule heating) and very low thermal conductivity (minimized conductive heat transfer) make them ideal candidates to be used as current leads. There are two forms of HTS current leads. (i) bulk form (tube or rod) prepared either from YBCO or BSCCO and (ii) tape form prepared from Bi-2223 multifilamentary tapes. The tape form of current leads has many advantages with respect to the mechanical and thermal stability related criteria. Crucial information on various aspects of HTS current lead development are not available in the literature as those are kept proprietary by various companies around the world. The present work has been undertaken to tailor the properties of multifilamentary tapes for the current lead application and to optimise the processing parameters of the same for enhanced critical current density and field tolerance. Also it is the aim of the present investigation is to prepare prototype current leads engineered for operation in conduction cooled mode and test them for operational stability.

First chapter is the overview of the properties and processing aspects of HTS materials, their application vistas and state of the art developments

in the processing of (Bi,Pb)-2223/Ag multifilamentary tapes. It also gives a brief account of the material choices and requirements such as reducing the thermal conductivity of the sheath, increasing the fill factor of superconductor, enhancing the field tolerance of HTS for use as current leads. Also the design aspects of the current leads and the different cooling schemes employed for operation of the HTS current leads are discussed. The second chapter deals with the preparation and characterisation techniques used in the present study.

Chapter-3 describes the studies conducted on alternate sheath alloys to replace pure Ag for better mechanical strength and reduced thermal conductivity. The alloy systems selected were Ag-Cu (Cu: 0-12 at%) and Ag-Au (Au: 0-6 at%). It was found that the percentage of Cu in the sheath affects both the phase evolution as well as the ultimate phase fraction of Bi-2223 in the tapes. Moreover the Cu percent in the sheath has to be optimised with respect to the Cu stoichiometry in the precursor and a Cu deficient precursor is favoured for preparing (Bi,Pb)-2223/Ag-Cu tapes. 6 at% Cu doping in the sheath was found to be optimum for a precursor having a stoichiometry of $\text{Bi}_{1.8}\text{Pb}_{0.4}\text{Sr}_{2.0}\text{Ca}_{2.2}\text{Cu}_{3.0}$ with respect to the phase evolution, ultimate phase fraction of Bi-2223 and the J_C . Phase formation, microstructure and J_C of the Ag-Au alloy sheathed tapes are comparable to that of pure Ag sheathed tapes which shows that Au alloying in the sheath is less sensitive to the superconducting properties. But the J_C -B characteristics of Ag-Au alloy sheathed tapes show a slight improvement over the pure Ag sheathed samples. The mechanical strength of Ag-Cu alloys improved considerably upon Cu doping. Both the irreversible strain limit and stress tolerance of Ag-Cu alloy sheathed tapes are higher than the pure Ag

sheathed tapes. Both electrical and thermal conductivities of Ag-Au alloys are considerably lower than the Ag-Cu alloys and decreases with increase in Au concentration and temperature. It was concluded that a multifilamentary geometry with inner Ag-Au alloy sheath and outer Ag-Cu alloy sheath (with optimum Cu %) is an ideal combination for preparing (Bi,Pb)-2223 multifilamentary tapes for use as current leads.

Chapter-4 describes the studies conducted to improve the flux pinning strength (field tolerance) of the (Bi,Pb)-2223/Ag tapes. Nano size MgO particles (0-0.6 wt%) were added to the precursor for this purpose. It was found that addition of MgO retards the phase formation of Bi-2223 to a slight extend. The amount of Bi-2212 left after the final stage sintering was found to increase with the percentage of MgO. 3 wt% MgO added sample showed considerable enhancement for both self filed J_C and the J_C -B characteristics. SEM microstructure examination of the longitudinal sections of pure and MgO added samples shows the same structure with nearly the same orientation and texture. Considering XRD results, SEM observations, J_C and J_C -B characteristics it was concluded that 0.3 wt% MgO added to the system improves the J_C and J_C -B characteristics of the tapes due to enhanced flux pinning strength.

Chapter-5 describes the optimisation studies conducted in mono and multifilamentary tapes. Fill factor, ff (ratio of superconductor to metal Ag) in monofilament tapes was optimised with respect to tape dimensions. Starting packing density of the precursor was varied from 27 to 40 wt%. Highly packed samples (Higher fill factors) led to oozing out of the liquid phase through the sheath and caused reduced sintered density and J_C . SEM

observations on the etched surface of the highly packed sample revealed a glassy phase showing the melting of the core and oozing out of the liquid phase. A packing density of 27-33.5 wt% is found to be optimum for preparing (Bi,Pb)-2223/Ag monofilamentary tapes with higher sintered density and J_C . The number of filaments, starting wire diameter prior to flat rolling and thickness of multifilamentary tapes have been optimised. The filament count was varied from 20 to 100. It was found that the thickness of multifilamentary tapes is the crucial parameter and it has to be optimised with respect to the number of filaments and tape dimensions. The thermomechanical processing and heat treatment schedules of multifilamentary tapes have been optimised for obtaining higher J_C s in the finished tapes. It was found that the phase fraction of Bi-2223 prior to the last stage deformation and heat treatment is a crucial parameter affecting the J_C , J_C -B, and microstructure of the finished tapes.

Chapter-6 describes the preparation and characterisation of HTS current leads using (Bi,Pb)-2223 multifilamentary tapes. The raw material, i.e., (Bi,Pb)-2223 multifilamentary tapes prepared in length of ~10 cm with rolling as the deformation technique showed inconsistency and inhomogeneity of J_C along the length of the tape. So it was decided to apply uniaxial pressing prior to the last stage sintering and a detailed investigation was carried out to optimise the uniaxial pressure. It was found that a pressure of 50 MPa enhances the J_C as well as the J_C homogeneity along the length of the tapes compared to the rolled samples. The J_C -B characteristics of pressed tapes were also found to be better compared to the rolled tapes. Finally HTS prototype current leads were designed and fabricated. A combination of inner Ag-Au (Au- 6at%) alloy and an outer Ag-Cu (Cu-6

at%) sheath were selected for preparing multifilamentary tapes for current leads. This combination yielded reduced thermal conductivity as well as better mechanical strength to the raw material. A Glass fibre reinforced epoxy rod with compatible thermal expansion coefficient compared to pure silver was selected for the housing current leads for better mechanical rigidity. Finally the prepared leads were tested for its mechanical, thermal and transient quench stability. The estimated heat leak of Ag-alloy sheathed current leads when anchored between 77 K and 4.2 K was found to be about two orders of magnitude lesser than the corresponding pure Ag sheathed one.

Chapter- 7 gives the overall summary and conclusions drawn from the present investigation.

LIST OF PUBLICATIONS OF ALOYSIUS. R. P.

I. Research Papers Published in International Journals

1. Superconducting and Mechanical Properties of (Bi,Pb)-2223/Ag Tapes in the Wire-In-Tube Geometry, *Physica C*, accepted for publication 2002
2. Development of HTS conductors for electrical power applications *Metals Materials And Processes*, 2001, Vol. 13, No. 2&3
3. Phase evolution, microstructure and transport property of (Bi, Pb)-2223/Ag tapes prepared using powders of varying particle size distribution *Superconductor Science and Technology* (UK) 14 (2001) 417-424
4. Bend Strain and tensile Stress Characteristics of (Bi, Pb)-2223/Ag-Cu alloy sheathed tapes *Superconductor Science and Technology* (UK) 14 (2001) 85-89
5. Strain tolerance and tensile strength of Ag added mono and multifilamentary (Bi, Pb)-2223/Ag tapes *Superconductor Science and Technology* (UK) 13 (2000) 1487-1491
6. Processing of Long Multifilamentary HTS Tapes and Coils *Metals Materials And Processes*, 2000, Vol. 12, No. 4, pp 301-310
7. Fabrication of (Bi, Pb)-2223/Ag-Cu alloy sheathed tapes: Optimization of Cu composition in the sheath with respect to the Cu stoichiometry in the system. *Physica C* 328 (1999) 221-229 (NH).
8. Effects of Ag, Ag₂O and AgNO₃ additions in (Bi, Pb)-2223/Ag powder-in-tube tapes. *Physica C* 316(1999) 63-68 (NH)
9. Optimisation of tape width and powder packing density in the

- powder-in-tube processing of (Bi, Pb)-2223/Ag tapes.
Physica C (NH) 309(1998) 203-207
10. Phase evolution in Ag, Ag₂O and AgNO₃ added (Bi, Pb)-2223 superconductor *Physica C* (NH) 307 (1998) 277-283
 11. Enhanced critical current density in multilayered Ag/(Bi,Pb)2223 tapes prepared using pretextured monolayered tapes *Superconductor Science and Technology* (UK) 10 (1997) 987-990
 12. Nano size MgO addition: Enhanced flux pinning in (Bi,Pb)-2223/Ag superconducting tapes. Communicated to *Superconductor Science and Technology(UK)*
 13. Optimization of geometrical and processing parameters of (Bi,Pb)-2223 multifilamentary tapes for current lead application. Communicated to *Physica C(NH)*

II. PAPERS PUBLISHED IN SEMINARS/SYMPOSIA **PROCEEDINGS**

1. Ag addition in (Bi, Pb)-2223 superconductor: Effects of Ag, Ag₂O and AgNO₃ on the phase evolution. Presented at DAE *Solid State Physics Symposium SSPS'97*, Kochi, Dec. 27-31.p- 286 (1997)
2. Effects tape width and powder packing density in the PIT processing (Bi, Pb)-2223/Ag superconducting tapes.
Presented at DAE *Solid State Physics Symposium SSPS'97*, Kochi, Dec. 27-31.p-287 (1997)
3. Structural and superconducting properties of mono and multilayered Ag/(Bi,Pb)-2223 tapes.
Presented at the *XXI National Conference on Electron Microscopy Society of India*, Trivandrum, Dec. 17-19 (1997)
4. Development of long length multilayered Ag/(Bi,Pb)-2223 superconducting tapes and pancake coils.
DAE-BRNS Workshop on Thin Film Multilayers. BARC, Mumbai, Oct. 6-8 (1999)

III. Patents Filed

1. Conduction cooling high temperature superconducting current lead
Indian Patent NF-390/99 dated 11.01.2000
2. Liquid nitrogen level sensor-monitor device using high TC
superconductors and method of manufacture thereof
US Patent Application No. 4062-25 filed on 20.03.2002.

CHAPTER 1

INTRODUCTION

1.1. History of Superconductivity

After the discovery of superconductivity in Hg by Kammerlingh-Onnes [1], a revolution in physics, especially in condensed matter has started prompting scientists/researchers all over the world to search for this phenomenon in newer materials and for exploiting the peculiar property of zero resistance for practical applications. Also some of the renowned theoreticians actively engaged in formulating new theories to explain the phenomenon of superconductivity. Superconductivity is a remarkable phenomenon with its many manifestations, the resistivity to the passage of electrical current for certain materials drops to zero below a particular temperature called the transition temperature or the critical temperature, T_C . However existence of superconductivity in a material depends not only on its T_C , but also on the strength of the ambient magnetic field, arising from either a current flow or an applied magnetic field. In addition to having electrical resistance, an ordinary type – I superconductor has the ability to shield itself completely from magnetic fields. But above a critical field, H_C , the superconductivity is destroyed. However in 1930's, it was noticed that an applied magnetic field could partially penetrate some materials eventually called 'Type – II' superconductors, and the sample would remain superconducting. Magnetic flux flows through magnetic vortices, whose cores behave as simple metallic conductors, surrounded by superconducting regions. When the field is high enough the number of vortices occupies the total volume of the sample, and all superconductivity is lost. All practical superconductors are type – II.

These magnetic vortices are the source of another operating limit on superconductors – the maximum superconducting current they can transport. When a current flows in a type – II superconductor it produces a force on the magnetic vortices, causing them to move and creating electrical resistance through friction with the atomic lattices. But defects in a material can fix or pin enough vortices such that they remain stationary, at least until the current and field become sufficiently strong that the vortices are unpinned and so generate resistance. The behaviour of the vortices therefore defines the maximum current, J_c and magnetic field H^* , for a given temperature and material. Thus the three boundary

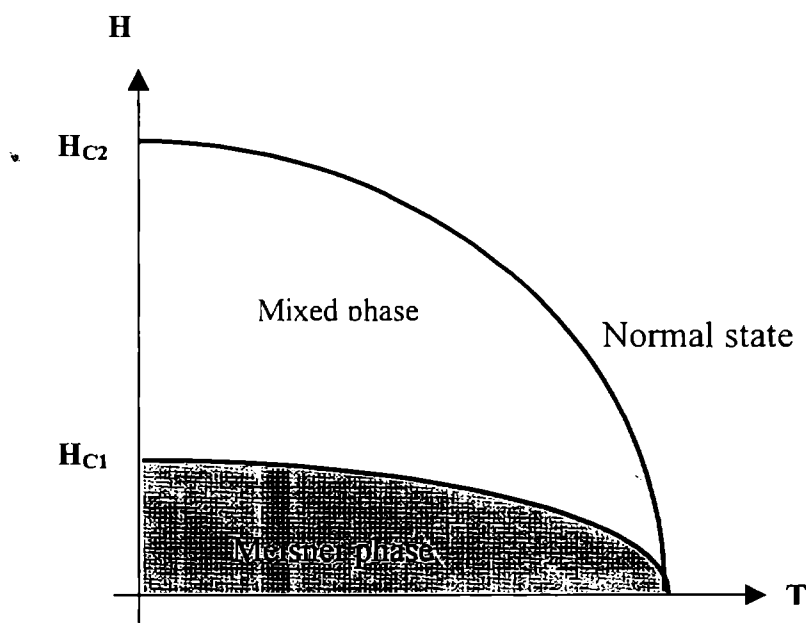


Fig. 1.1 Phase diagram of a type II superconductor. Below the lower critical field H_{C1} magnetic fields are expelled from the superconductor but it becomes energetically favourable to include some of the magnetic fields as flux lines above H_{C1} . Superconductivity is suppressed when the cores of the flux lines overlap at the upper critical field H_{C2} .

conditions viz. transition temperature T_C , critical field H_C , and current density J_C are the boundary conditions for the existence of superconductivity in a material. Figure 1.1 shows a typical phase diagram of a type II superconductor.

Over the last ninety years, several superconducting materials have been discovered with T_C ranging from a few Kelvin to 164 K [2] (in Hg-based cuprate under pressure). This wide variety of compounds can be classified according to a list given in Table 1.1.

Other important event of this period was the development of a theoretical model that finally successfully explained how superconductivity could occur. The theory was proposed by John Bardeen (the inventor of transistor) Leon Cooper and J. Robert Schrieffer (The BCS theory) [12] in the late 1950's. BCS theory explains that, below the critical temperature in superconducting materials, pairs of electrons are formed, for which the possible energy states are quantified. The energies of the possible states are sufficiently high that the electron pairs cannot absorb the low energy from the lattice vibrations and other low energy events in the solid. They cannot absorb the energy of normal scattering mechanisms experienced by ordinary conducting electrons and therefore move completely freely through the solid. Experiments soon showed that electrons in the pairs, expect to repel each other because of their like electrical charge, were held together by an attractive interaction mediated through coupling electrons to vibrations of underlying crystal lattice ("electron – phonon – coupling"). This coupling is at the basis of what is now called "conventional"

Table 1.1 Various families of superconductors and their Transition temperatures [3-11]

Sl.No.	Type	Example	T _c (K)
1	Amorphous superconductors	Amorphous Ga	8.4
2	Cheveral phases M _x Mo ₆ X ₈ (M = Pb, Sn, Cu, Ag, La; X = S, Se, Te)	PbMo ₆ S ₈	12.5-14.7
3	Elements	Nb	9.3
4	Carbides	NbC	11
5	Nitrides	NbN	15
6	Transition metal alloys	MoTc	16
7	C15 type Laves Phases	V ₂ Zr	9
8	Nitrocarbides	NbN _{0.7} C _{0.3}	18
9	A15 type Laves Phases	Nb ₃ Ge	23
10	Intercalation compounds	TaS ₂ (C ₃ H ₅ N) _{1/2}	3.5
11	Organic superconductors	(TMTSF) ₂ PF ₆	1 (at 12 kbar)
12	Semi-metal superconductors	La ₃ Se ₄	10
13	HeavyFermion superconductors	UPt ₃	
14	Magnetic superconductors	ErRh ₄ B ₄	8.6
15	Oxides	BaPb _{0.75} Bi _{0.25} O ₃	13
16	Cuprates	YBa ₂ Cu ₃ O _{7-δ}	92
17	Bismuthates	(Ba _{0.6} K _{0.4})BiO ₃	30
18	Oxycarbonates	Bi ₂ Sr ₄ Cu ₂ CO ₃ O ₈	
19	Borocarbides	YNi ₂ B ₂ C	15
20	Fullerides	Rb ₂ C ₆₀	45
21	Borides	MgB ₂	39

superconductivity. It is operating in most known superconducting materials but is not responsible for superconductivity in the cuprate superconductors.

The discovery of superconductivity in a copper oxide system containing La, Ba and Cu in 1986 by J.G. Bednorz and K.A.Muller [13]

was an important breakthrough in the field materials science/physics as this system was unknown for any sign of superconductivity and was the start of many other discoveries soon followed, which raised the T_C to well above the boiling point of liquid nitrogen, by various groups in the world. Table 1.2 lists some of the copper oxide superconductors with their T_{CS} [14,15].

The importance of T_C having above 77 K lies in the fact that the applications of superconductivity could be raised to the boiling point of liquid nitrogen, which is relatively cheap as compared to the earlier applications which were realized only at 4.2 K, the boiling point of liquid He, which is expensive and rare.

1.2. Distinguishing Characteristics of Copper oxide Superconductors

There are several chemical, structural and electronic aspects of copper oxide superconductors that distinguish them from other electronic oxides even those that are electrically conducting. In conducting oxides, the individual transition metal orbitals overlap and interact forming a band of allowed energy states that is partially filled by the electrons available. These partially filled electron bands are the basis of electrical conduction of oxides. The energy states of the oxygen play only a minor or insignificant role. In the copper oxides, however, the difference in energy between the oxygen and metal orbitals is very small resulting in electronic energy bands in which the oxygen orbitals play a major role in the vicinity of the highest occupied electronic states. Thus oxygen is as highly involved in the conductivity, as is copper, a rare situation in conducting oxides.

Table 1.2. Compounds of HTSC cuprate family of superconductors [14-15]

Compound	Tc (K)
$\text{La}_{1.85}(\text{Ba}/\text{Sr})_{0.15}\text{CuO}_4$	35
$\text{La}_2\text{CuO}_{4+\delta}$	45
$\text{La}_{1.6}\text{Sr}_{0.4}\text{CaCu}_2\text{O}_{6+\delta}$	60
$\text{YBa}_2\text{Cu}_3\text{O}_7$	92
$\text{YBa}_2\text{Cu}_3\text{O}_8$	82
$\text{TlBa}_2\text{Ca}_{n-1}\text{Cu}_n\text{O}_{2n+3}$	120 (n = 3)
$\text{TlBa}_2\text{Ca}_{n-1}\text{Cu}_n\text{O}_{2n+4}$	127 (n = 3)
$\text{Bi}_2\text{Sr}_2\text{Ca}_{n-1}\text{Cu}_n\text{O}_{2n+4}$	110 (n = 3)
$\text{HgBa}_2\text{Ca}_{n-1}\text{Cu}_n\text{O}_{2n+2+\delta}$	134 (n = 3)
$\text{CuBa}_2\text{Ca}_{n-1}\text{Cu}_n\text{O}_7$	120
$\text{Sr}_2\text{Ca}_{n-1}\text{Cu}_n\text{O}_4$	90
$\text{Pb}_2\text{Sr}_2(\text{Ca}, \text{Y}, \text{Nd})\text{Cu}_3\text{O}_8$	70
$\text{Pb}_2(\text{Sr}, \text{La})_2\text{Cu}_2\text{O}_6$	32
$\text{PbBaSrYCu}_3\text{O}_8$	50
$(\text{Pb}, \text{Cu})(\text{Ba}, \text{Sr})_2(\text{Y}, \text{Ca})\text{Cu}_2\text{O}_7$	53
$\text{Pb}_{0.5}\text{Sr}_{2.5}(\text{Y}, \text{Ca})\text{Cu}_2\text{O}_7$	104
$(\text{Pb}, \text{Cu})(\text{Sr}, \text{La})_2\text{CuO}_5$	32
$(\text{Nd}, \text{Ce})_2\text{CuO}_{4-\delta}$	24
$(\text{Nd}, \text{Ce}, \text{Sr})\text{CuO}_{4-\delta}$	28
$(\text{Pb}, \text{Cu})(\text{Eu}, \text{Ce})_2(\text{Sr}, \text{Eu})_2\text{Cu}_2\text{O}_9$	25
$(\text{Eu}, \text{Ce})_2(\text{Ba}, \text{Eu})_2\text{Cu}_3\text{O}_{10}$	43
$\text{Bi}_2\text{Sr}_2(\text{Gd}, \text{Ce})_2\text{Cu}_2\text{O}_{10}$	34
$\text{Tl}_{0.5}\text{Pb}_{0.5}\text{Sr}_4\text{Cu}_2(\text{CO}_3)\text{O}_7$	70
$(\text{BaSr})_2\text{CuO}_2(\text{CO}_3)$	40
$\text{Sr}_{4-x}\text{Ba}_x\text{TlCu}_2(\text{CO}_3)\text{O}_7$	62
$\text{Tl}_{0.5}\text{Pb}_{0.5}\text{Sr}_2\text{Gd}_{2-x}\text{Ce}_x\text{Cu}_2\text{O}_{9-\delta}$	45
$\text{NbSr}_2(\text{GdCe})_2\text{Cu}_2\text{O}_y$	27
$\text{Bi}_2\text{Sr}_{6-x}\text{Cu}_3\text{O}_{10}(\text{CO}_3)_2$	40
$(\text{Cu}_{0.5}\text{Co}_{0.5})\text{Ba}_2\text{Ca}_{n-1}\text{Cu}_n\text{O}_{2n+3}$	117 (n = 4)
$\text{YCaBa}_4\text{Cu}_5(\text{NO}_3)_{0.3}(\text{CO}_3)_{0.7}\text{O}_{11}$	82
$\text{CuSr}_{2-x}\text{La}_x\text{YCu}_2\text{O}_7$	60
$\text{GaSr}_2\text{Ln}_{1-x}\text{Ca}_x\text{Cu}_2\text{O}_7$	73
$(\text{C}_{0.35}\text{Cu}_{0.65})\text{Sr}_2(\text{Y}_{0.73}(\text{Ce}_{0.27})_2\text{Cu}_2\text{O}_x$	18
$\text{Bi}_4\text{Sr}_4\text{CaCu}_3\text{O}_{14+x}$	84

The second factor is that the electronic configuration of the Cu^{2+} ions that form the basis of superconductivity in oxide superconductors is $3d^9$: nine of the ten available d-orbital energy states are filled. In the Cu-O coordination polyhedra (octahedra, pyramids and squares) that form in the cuprate superconductors, these energy levels are non-degenerate. The t_{2g} orbitals, which are directed between the oxygen atoms are at low energy and therefore are completely filled with electrons (six). The shapes of the Cu-O coordination polyhedra are such that there are four near in-plane oxygen neighbours and one (pyramidal) or two (octahedral fig.1.2a) oxygen atoms more distant when present. This makes the energies of the orbitals with z components (i.e. toward the apices) lower because of lower repulsion from the oxygen orbitals. The result is that the nine-electron configuration has a single unpaired electron in the $dx^2 - y^2$ orbital (Fig.1.2b), which points towards the in-plane oxygen. The single unpaired electron carries a spin of $1/2$. This low spin value allows for the possibility of non-classical (e.g. quantum mechanical) interactions between spins in the solid, which is different from the more familiar case of the spins in ferrites.

In isolated atoms, these orbitals are discrete energy states, but in solids where the atoms are close together, the orbitals interact, and the sharp atomic energy states become bands of energies. The similar energy of the O 2p states and the Cu 3d states leads to the situation shown in Fig.1.2c. The electrons fill half of the Cu $dx^2 - y^2$ derived band, and the high energy part of the oxygen derived band has almost the same energy as the highest occupied copper states. This shows that Cu^{2+} oxides with the superconducting structure types should be metallic conductors (i.e. the electrons are in partially filled bands with available

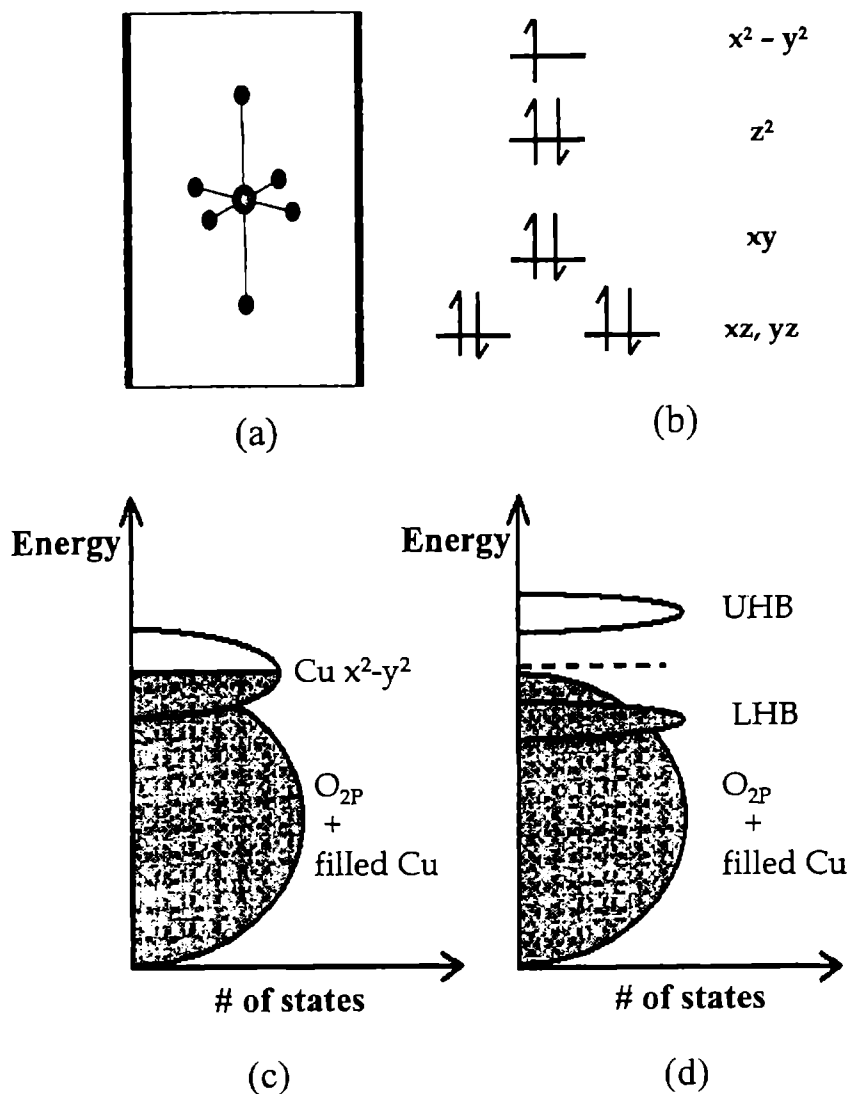


Fig. 1.2 (a) Cu-O coordination polyhedra found in copper oxide superconductors. (b) d electron configuration of Cu^{2+} , (c) schematic picture of the energy states in copper oxide superconductors, and (d) split dx^2-y^2 band for interacting electrons in cuprates (UHB is upper Hubbard band and LHB is lower Hubbard band)

states close by). They are instead electrical insulators. The standard picture for the electronic properties of the solids assumes that the electrons are not interacting with each other, only with the underlying

atomic lattice. In the cuprate superconductors this is not the case, they do interact. This interaction is the key factor of why it is taking so long to understand the mechanisms of high T_C superconductivity. The interaction between electrons is greatest in half filled bands which is exactly the case for cuprates. The addition of several electrons to the $dx^2 - y^2$ orbital takes a significant amount of extra energy, because it is repelled by the electron already present (called the “on-site repulsion energy”). The result is that the energy states of the second electron are higher than those for the first electron, and there is a gap of non-allowed energies between the two. The band gap between the highest occupied oxygen states and the empty part of the now split-in-two Cu $dx^2 - y^2$ band (Fig.1.2d) is what leads to the insulating behaviour.

A generalised view of the structure of cuprate superconductors is shown in Fig.1.3. At their electronic heart are infinite CuO_2 plane (Fig.1.3a) made from checkerboard like pattern of the in-plane basal squares of the Cu-O coordination polyhedra (such as the octahedra shown in Fig.1.2a) sharing corners with each other. Each of the four oxygens in the CuO_4 squares is shared with another copper, resulting in 180° (or $\sim 180^\circ$) Cu – O – Cu bonds and an overall stoichiometry of CuO_2 . Between these CuO_2 layers are other layers, known as “charge reservoir layers” (Fig.1.3b). These layers serve to control through chemistry. The number of electrons in the available electronic states in the CuO_2 planes and to electronically connect or isolate the CuO_2 planes in the third dimension. The key to determination of the superconducting transition temperatures within the family of cuprate superconductors depends on large part on the chemistry of these charge reservoir layers.

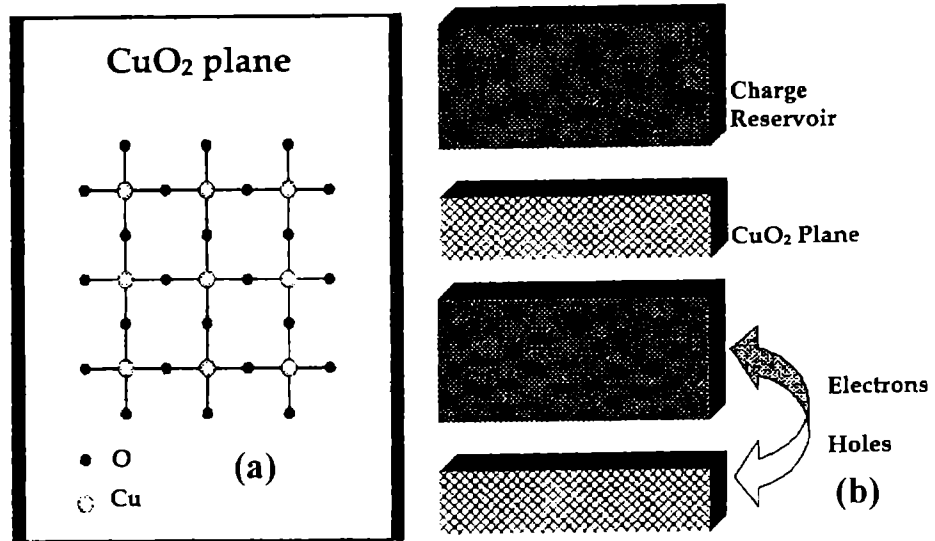


Fig. 1.3 (a) CuO_2 planes made from CuO_4 squares sharing corner oxygens and (b) schematic view of the electronic layers in copper oxide superconductors

In the copper oxide superconductor parent materials, the Cu^{2+} spin $1/2$ ions (one unpaired electron per copper in the $dx^2 - y^2$ orbital) in this CuO_2 plane are ordered antiferromagnetically at high temperatures and the material is insulating as previously discussed. The high antiferromagnetic ordering temperature indicates that the copper spins are coupled very strongly. Superconductivity is induced when the electron count on the CuO_2 plane is changed from one electron per Cu site: i.e. the compounds are doped to make the formal copper valence different from Cu^{2+} , typically higher. This is accomplished through manipulation of the charge reservoir layer, either by adding oxygen by partial substitution of one atom of higher or lower valence for another, or by the naturally occurring electron count present because of the valences of the atoms in the compound. Examples of these three cases

are the inducement of superconductivity on oxygen intercalation from $\text{YBa}_2\text{Cu}_3\text{O}_6$ to $\text{YBa}_2\text{Cu}_3\text{O}_7$ in the 123 compounds, the partial substitution of Sr for La in a solid solution in $\text{La}_{2-x}\text{Sr}_x\text{CuO}_4$, and the naturally occurring copper valence in the stoichiometric compound $\text{Tl}_2\text{Ba}_2\text{CaCu}_3\text{O}_8$. In the semiconductor language, parent compound is doped by either electrons or holes and the antiferromagnetic ordering changes to superconductivity. This happens at an excess electron doping of ~ 0.2 electrons per copper (the formal reduction of Cu to $\text{Cu}^{1.8+}$) or on the introduction of electron deficiency (here doping, the formal oxidation of Cu to $\text{Cu}^{2.2+}$). At higher doping concentrations, the materials become “normal” metallic conductors and are non-superconducting. A generic electronic phase diagram is given in Fig. 1.4, and it represents the behaviour of cuprates under different electron concentrations.

When hole doping is done on the cuprate superconductors, it appears that it should be going into oxygen p states. If this is the case, then the Cu^{2+} ions keeps its $1/2$ spin (the copper orbitals are not at the Fermi Level and would not change electron count on hole doping) and the hole introduced is centered on oxygen p states. The spin (the unpaired electron on the copper) and the charge (the doped hole on the oxygen) are separated. The common belief is that the doped hole is in the electronic states in the square of four oxygen atoms surrounding the copper. The system becomes less magnetic on doping, because the hole in the oxygen states also have a spin, in the opposite direction as the copper spin, and effectively cancels it out [16,17]. This entity with zero net spin and one deficient electron (called a Zhang-Rice singlet) has to move through a lattice of strongly antiferromagnetically coupled copper spins, in order to carry a current. Proper understanding of this exotic

conduction process will give insight to the problem of high- T_C superconductivity. Somehow, at just right concentration of these entities

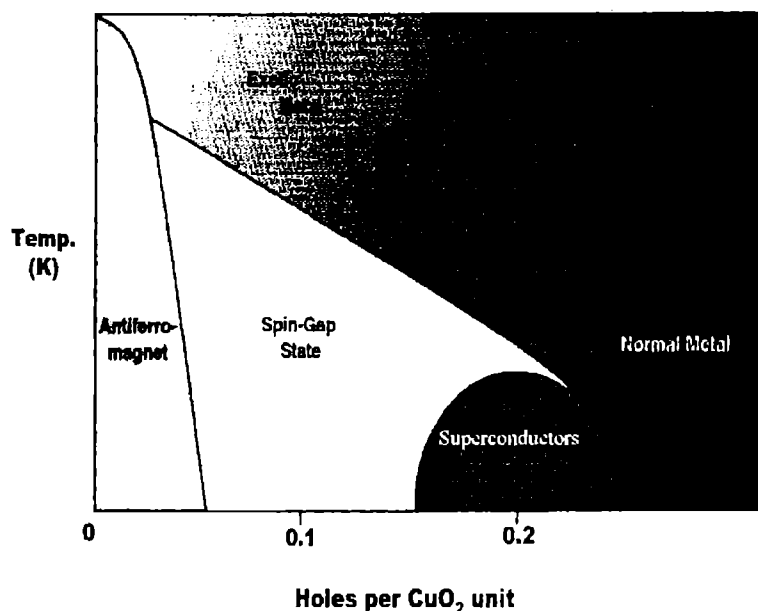


Fig. 1.4 Generic electronic phase diagram of copper oxide superconductors

wandering around in the CuO_2 plane, their complex interactions result in superconductivity. Sophisticated neutron-scattering experiments have confirmed that the interactions between spins remain present in the superconducting materials, even though they no longer show conventional magnetic ordering. But spectroscopic results suggest that the overall electronic picture moves toward the case shown in Fig.1.2(c), on doping, i.e. a conventional electronic band structure. Some believe strongly that it is one peculiar characteristic of this recovered otherwise normal looking band structure (known as van Hove singularity) that results in superconductivity. There is evidence for other factors to consider as well, such as the possible influence of electronic excitations and the coupling of the charge carriers to the lattice.

1.3. Type II nature and Irreversibility line of High- T_C Superconductors (HTS)

Cuprate HTS can be classified as Type II superconductors with their upper critical field H_{c2} of the order of 100 T, which is much larger than that of conventional superconductors. However unlike conventional superconductors the supercurrent in HTS vanishes above an irreversible field, H^* , which is considerably less than H_{c2} at the same temperature (see Fig.1.5). This existence of an irreversibility line [18-20] (IL, the line in $H - T$ plane above which J_C vanishes) is thought to arise from thermally activated flux flow, as coherence is lost among the supercurrents above irreversibility temperature. Many models such as collective flux creep [19], the vortex lattice melting [20] and Boss glass melting, etc. [21] have been forwarded for explaining the origin of IL.

1.4. Theoretical Efforts and Developments

Even though the much celebrated BCS theory [22] could explain the properties of conventional or low- T_C (LTS) superconductors rather satisfactorily, with the advent of high- T_C or cuprate superconductors, theorists thought of modifying the BCS theory or to formulate new theories to account for the higher transition temperatures, and the experimentally observed energy gap which is twice as high as predicted by BCS theory. Electron pairing is the key to BCS theory. Pairing is promoted by crystal lattice vibrations or phonons. Thus the basic mechanism which is responsible for the occurrence of superconductivity in traditional (low- T_C) superconductors is the interaction between

electrons and phonons. The paired electrons are called cooper pairs and displays s-wave symmetry as the pairs can be modeled by a single wave function whose solution gives a spherical area of probability, indicating

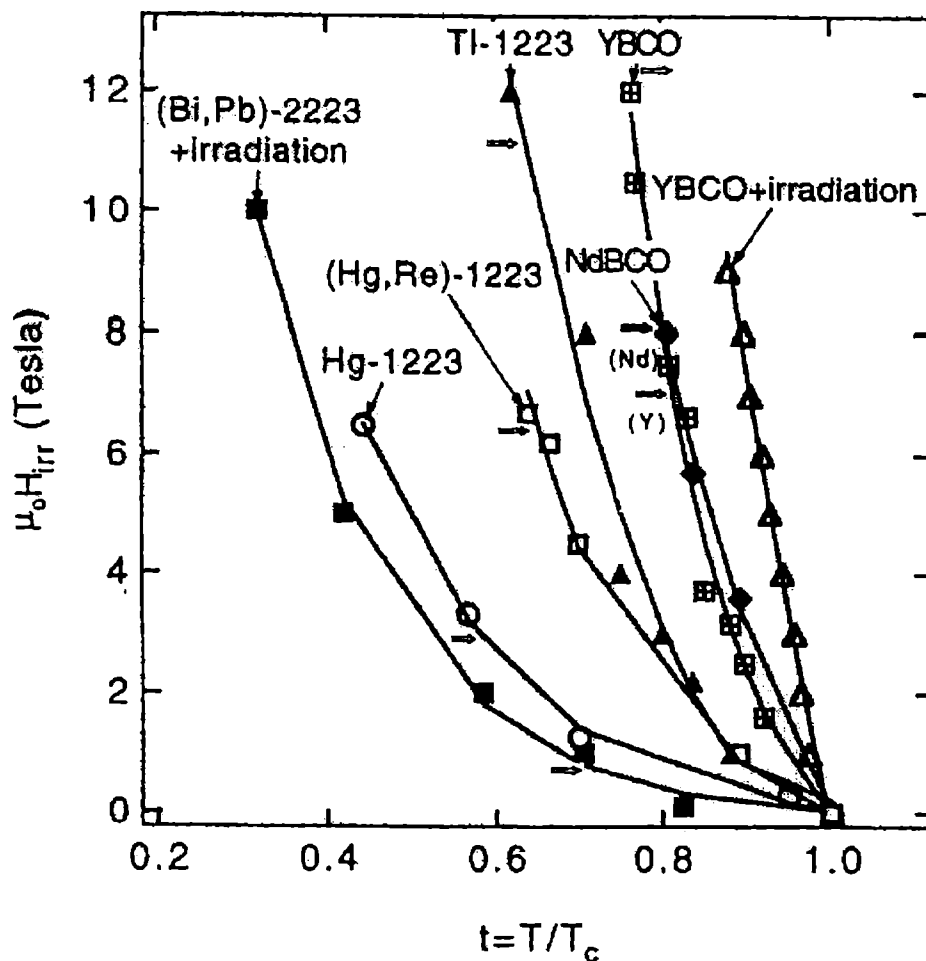


Fig. 1.5 Irreversibility field ($\mu_0 H$) as a function of reduced temperature (T/T_c) for most of the widely studied superconducting compounds. 77 K is indicated on each curve by an arrow.

that a plot of the location of the second electron of the pair with the first kept at the centre is equally likely in any position within a spherical area surrounding the first electron. As a result, the total angular momentum of the pair is zero. But in the case of HTS, experimental evidence

But in the case of HTS, experimental evidence suggest that the pairing symmetry is not the S-wave, but favours for a higher angular momentum state with either $dx^2 - y^2$ (d-wave symmetry or at least orthorhombically distorted d-wave (d+s-wave) symmetry. In the d-wave symmetry electrons can only move along 45° diagonals to the plane (see Fig.1.6b). This would allow the two electrons of the pair to be further away from each other, weakening the repulsion between the two electrons, for their linear distance from each other has increased, but allowing them to remain paired. This indicates that the pairing mechanism is different from the electron phonon interaction. Considering the possibilities of new and different pairing mechanisms, new theories have been proposed

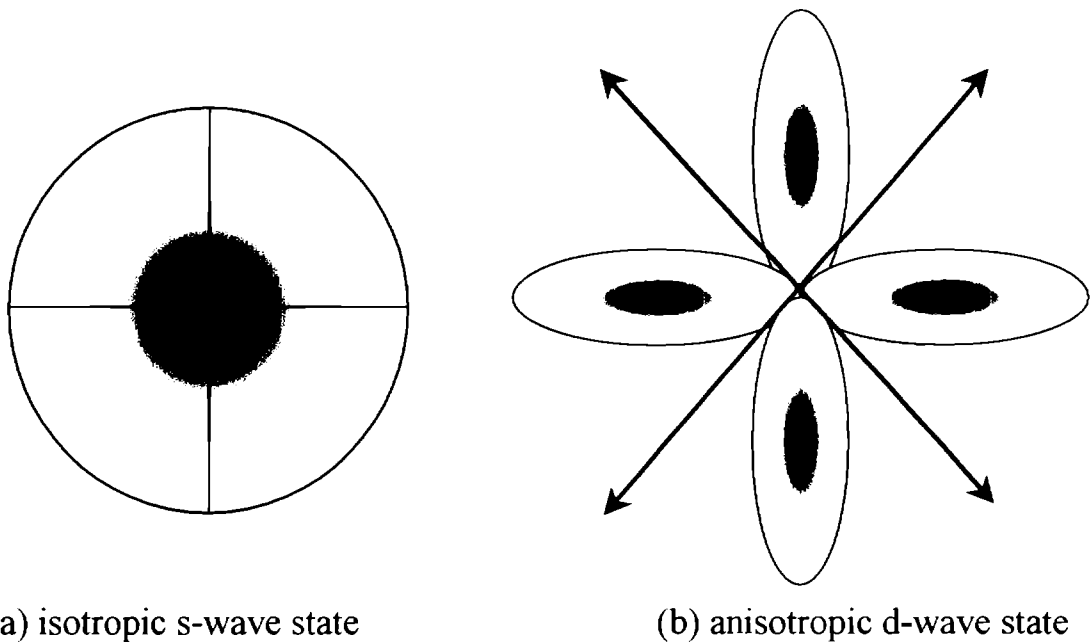


Fig 1.6 The shapes of electron pair wave functions of (a) isotropic s-wave and (b) anisotropic d – wave state which may describe electron pairs in high- T_C materials

such as interaction with antiferromagnetic spin fluctuations [23,24], phonon mechanism with interlayer coupling [25], anyon theory

[26], resonating valence bond theory (RVB) [27] etc. More recently a theory based on $SO(5)$ symmetry [28] has been proposed to unify the entire phase diagram, encompassing both superconductivity and antiferromagnetism as a function of carrier concentration.

Low temperature STM studies on BSCCO (2212 phase) single crystals by substituting a Zn atom in the Cu site of the Cu-O layer, S.H. Pan et al. [29] made the first real space observation of d-wave symmetry in a HTSC superconductor. This throws light on the pairing mechanism, which involves magnetic spin fluctuations of the Cu atoms residing in the Cu-O layers. Much enthusiasm is generated among the theorists and we can hope that the ultimate mechanism of superconductivity will be revealed soon.

1.5. Application Environment of Superconductors

Application environment of superconductors is progressing steadily after the discovery of high T_c superconductors. It took more than fifty years to produce practical LTS wires of NbTi and Nb₃Sn after the 1911 discovery of superconductivity in Hg. But after the fifteen years of the era of HTS several companies and industries all over the world have actively engaged in the commercialization of HTS products. As a result, several prototype devices have been tested and some products are already on the market [30-39].

Widely there are two main streams of applications for the superconductors: (i) high power electric applications and (ii) low power electronic applications. While high power applications require conductors with high current densities available in long lengths, electronic applications require high quality thin films of

superconductors. Most of the high current applications still use LTS NbTi and Nb₃Sn multifilamentary wires, as these wires have been further advanced in recent years especially concerning J_c -B and ac losses. Very complicated conductor arrangements, well tailored for the specific purpose, became industrial standards: as can be seen in huge particle detectors, new accelerator magnets and fusion magnets. For example, the magnet coils for the international thermonuclear experimental reactor (ITER), which is being developed in Europe, uses coil conductors of Nb₃Sn [38]. Another large system under construction is superconducting Stellarator W-7-X which will be operational in 2005 [40] uses NbTi coils for the poloidal field system. Also the Large Hadron Collider (LHC) which is under construction in CERN also uses NbTi wires as the superconducting coils for producing fields of the order of 10 T [41].

HTS are entering slowly in the application areas, best so far via current leads, which improve and facilitate LTS equipment substantially. Crucial for the growth of HTS superconducting application at all, will be further improvement of the HTS wire properties especially of the wire cost compared to LTS. The key parameters that must be optimized for HTS systems to be commercially viable are: (i) critical current density, (ii) operating temperature and (iii) the cost performance.

Figure 1.7 illustrates the HTS wire requirements for various power applications in terms of the wire length in amp. meters to the engineering current density (J_e). A wire J_c of at least 10,000 A/cm² is required for nearly all important electric power applications. Also the HTS wire must be able to conduct high currents at the highest fields and

temperatures possible. The advantage of the operation of HTS equipments at higher temperatures is evident from Fig.1.8, where the power required for cooling an HTS equipment (in % of the requirement at 4.2 K) is plotted against the temperature. It is plausible from the figure that operation at liquid nitrogen temperature (77 K) saves 90% of the energy, and operation at 20 K saves 75% of the energy. Benefits will vary depending on the cooling schemes used. Operating at 35 K or

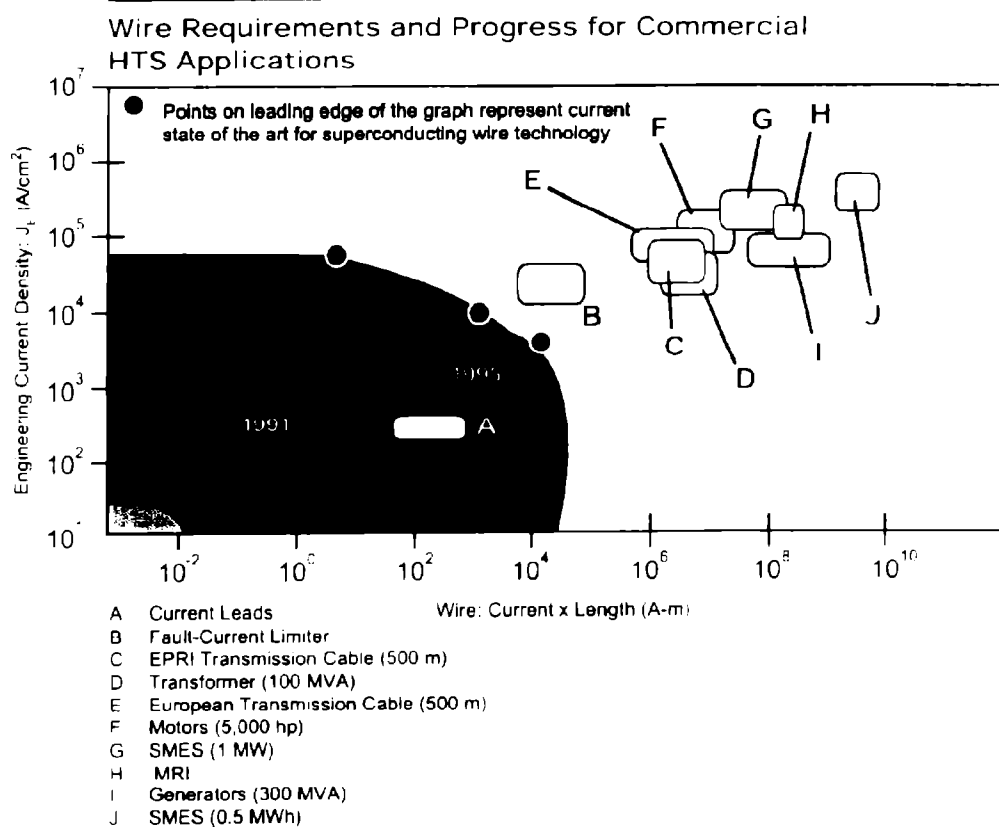


Fig. 1.7 Wire requirements of HTS for commercial applications in terms of engineering current density versus wire length in A-m

higher is much less demanding on cryogenic equipment, leading to greater system reliability, and service life, and lowering capital and operating costs dramatically.

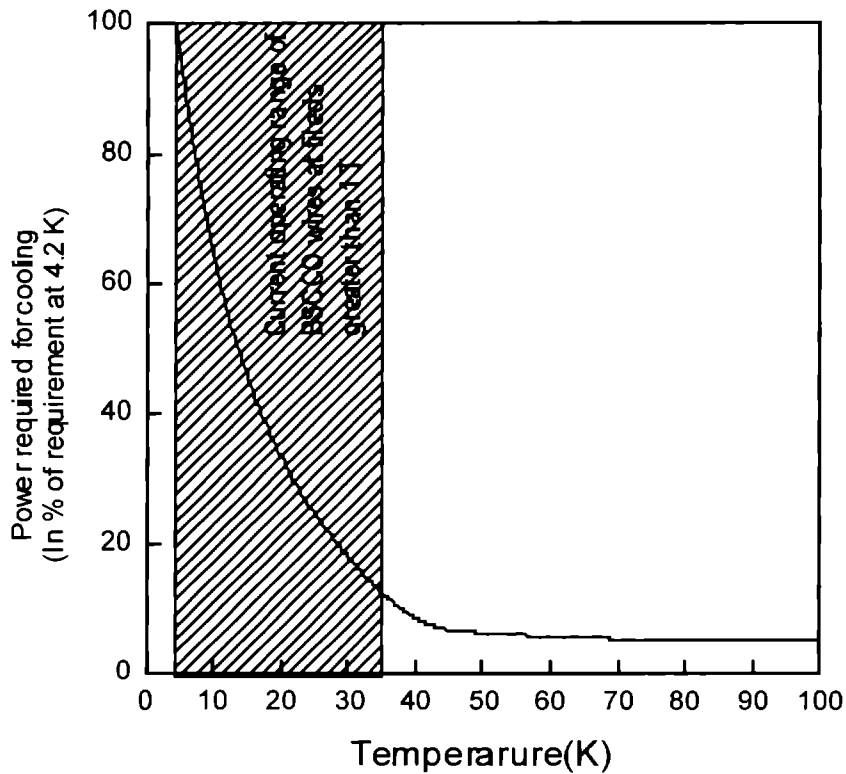


Fig. 1.8 The ideal power required for refrigeration for TS applications at 35 K is less than 10% of that for low temperature superconductivity applications 4.2 K. Actual power requirements will vary depending on cooling scheme chosen and system efficiency.

Presently the BSCCO system is the only conductor available in long lengths with moderate current carrying capacities. But inherent to this system are the drawbacks such as low flux pinning, which causes external magnetic field to adversely affect the operating temperature and critical current, and weak links which reduces the critical currents.

Strategic programs are now on pace in many laboratories around the world to develop alternate conductor technologies for other systems such as YBCO, TBCO and HBCCO etc., where the problem of flux pinning is less important with respect to BSCCO as the irreversibility lines of these systems are higher.

1.6. The BSCCO System of Superconductors

The BSCCO system of HTS materials can be represented by the homologue series $\text{Bi}_2\text{Sr}_2\text{Ca}_{n-1}\text{Cu}_n\text{O}_{2n+4+y}$. The first member of this series that was shown to superconduct was $\text{Bi}_2\text{Sr}_2\text{CuO}_6$ for which $T_C \sim 7$ to 20 K [42]. However, the $n = 2$ compound $\text{Bi}_2\text{Sr}_2\text{CaCu}_2\text{O}_{8+y}$ has a T_C of 85 K and $n = 3$ compound $\text{Bi}_2\text{Sr}_2\text{Ca}_2\text{Cu}_3\text{O}_{10+y}$ has a T_C of 110 K [43]. The $n = 4$ and $n = 5$ compounds are also described in the literature with $T_C = 90$ K [44] and 50 K [45] respectively, but have been shown to exist in thin film form or multiphase mixture in bulk. Therefore the most prominent members of the series are those with $n = 1, 2$ and 3 which will be denoted henceforth as Bi – 2202, Bi – 2212 and Bi – 2223 phases respectively.

1.6.1. Structural features

a) Bi-2201 phase

This system contains two distinct phases with closely related compositions. First correspond to a solid solution $\text{Bi}_{2-x}\text{Sr}_{2-y}\text{Cu}_1\text{O}_{6-\delta}$ shows a modulated structure and is superconducting phase. The average structure may be described in the orthorhombic Amm group with the cell parameters being $a = 5.36 \text{ \AA}$, $b = 5.37 \text{ \AA}$ and $c = 24.37 \text{ \AA}$ (see Fig.1.9). Also the number of formula units per unit cell, $z = 4$. This

superconducting phase is also known as Raveau phase. On the other hand, the near stoichiometric phase having a monoclinic symmetry is an insulator. The Cu – O coordination is octahedral.

b) Bi-2212 phase

In the 2212 phase, the double oxygen deficient perovskite layers are formed by two layers of corner sharing CuO_5 pyramid interleaved with a plane of Ca ions. The space group representing this phase has been A_{222} with $a = 5.414 \text{ \AA}$, $b = 5.428 \text{ \AA}$ and $c = 30.99 \text{ \AA}$, again with $z = 4$ (see Fig.1.9).

c) Bi-2223 phase

In 2223 phase, the triple perovskite layer is formed by one layer of corner sharing CuO_4 square planar groups sandwiched by two layers of corner sharing CuO_5 pyramids. Two planes of Ca ions are interleaved between these layers. The space group assigned to this phase is A_{222} with $a = 5.39 \text{ \AA}$, $b = 5.43 \text{ \AA}$ and $c = 37.1 \text{ \AA}$. For this compound, $z = 4$. All the three members of Bi series seem to show modulated structures [46,47]. As the modulated structures are difficult to study by conventional X-ray and Neutron diffraction techniques, electron microscopy has been used and many possibilities like excess oxygen in the Bi_2O_2 layers, Sr atom deficiency, atomic substitution (e.g. Bi for Cu) etc have been forwarded as the source of structural modulation. Another convenient arrangement has been the incommensurability between Bi – O layer and the perovskite layer. This mismatch introduces cooperative atom displacements or extra-oxygen in Bi – O layers [48].

An important aspect of the structure has been the double layer Bi – O characteristic to all three phases. The separation of 3.25 Å between Bi-O layers is supposed to occur due to $6s^2$ lone pair of Bi^{3+} ions [49]. This weak bonding leads to unit cell splitting into charge neutral sections and easy cleavage between Bi-O layers [50].

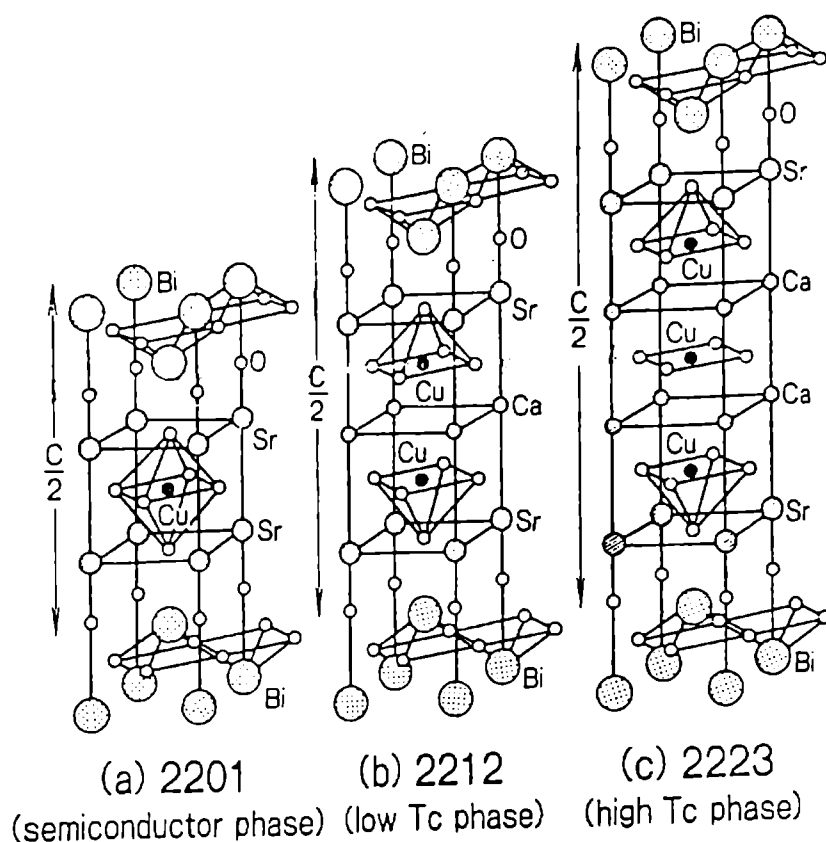


Fig 1.9 Crystal structures of BSCCO system of superconductors

1.6.2. Thermodynamic and kinetic aspects

Phase equilibria in the $\text{Bi}_2\text{O}_3 - \text{SrO} - \text{CaO} - \text{CuO}$ quaternary system, as well as different ternaries has been studied soon after the discovery of the system and it became clear that obtaining phase pure 2223 was a difficult task [51]. First of all, it can be seen that a large number of compounds can exist in this system and most of them with

compositional spread. On the basis of such studies, the following important aspects have been made clear.

- a) Of the three superconducting phases, the 2201 is thermodynamically stable over the widest temperature and in the presence of most of the compounds present in the system. In contrast 2223 phase is stable only over a narrow temperature range and exhibits phase equilibrium with fewer compounds.
- b) Extensive solid solution regions are observed for all the compounds in which they are perceptibly of single phase. However the single phase region is the least for 2223 phase. Apart from Sr and Ca mutual substitutions, Bi also seems to substitute at Sr and Ca sites.
- c) Another crucial aspect to be mentioned is the long duration of heat treatments required for the formation of 2223 phase compared to other two phases.

The solid state reaction

Bi-2212 phase + $\frac{1}{2}\text{CuO}$ \rightarrow Bi-2223 phase studied by Schulze et al. [52] failed to produce any significant formation of 2223 unless the reactant compositions are so chosen to include a liquid phase co-existent with the 2223 phase as well. The latter could be managed by adding excess quantity of CaO, CuO or Bi₂O₃.

1.6.3. Importance of Pb substitution

Partial substitution of Pb for Bi was found to be useful in stabilizing the high T_C phase [53,55]. Consequent to the addition of Pb, a shift in the stability domain of the phase to lower temperatures was

also observed [56]. Apart from accelerating the high T_C phase formation, Pb has been found to play other important roles in the BSCCO system. For example, the presence of a transient liquid phase has been evidenced by thermal studies on the formation of high T_C phase [57]. Pb containing intermediate phases, especially Ca_2PbO_4 has been found to closely associate with the formation of the liquid phase, which will be discussed later, is very important with respect to PIT fabrication of 2223 tapes.

1.7. Powder-in-tube Technique for BPSCCO Tape Fabrication

Essentially the powder-in-tube (PIT) technique refers to the production of flexible wires/tapes by mechanical diameter reduction of metallic tubes filled with oxide powder material. The advantage is that the ductility of the sheath metal makes mechanical working possible thereby enabling grain alignment, while heat treatments in the final stage sinters ceramic grains into a wholesome core. Such a metal clad geometry is desirable for HTS wires/tapes because the sheath not only protects the core from environmental corrosion and mechanical abrasion but also enhances the cryostability during operation. On the other hand, the PIT process brings with it a host of issues to be addressed properly for achieving the objective of high J_C . Right from the choice of sheath metal to the optimal conductor configuration, the parameter space is quite large and explains rather long gestation period before achieving reasonable J_C in HTS tapes. Moreover, the process is very much dependent on the characteristics of the superconducting system studied.

1.8. Important Consideration in the PIT Technique for BPSCCO Tape Fabrication

1.8.1. Choice of sheath metal

Silver has been found to be the most appropriate sheath metal for fabricating BPSCCO superconducting tapes. Apart from mechanical workability and high electrical and thermal conductivity, the properties which isolate silver as the option include its non-poisoning nature and compatibility at the processing temperature. Also silver is permeable to oxygen, which is important for the processing of ceramic inside the sheath. Nevertheless the mechanical weakness of Ag/Bi-Sr-Ca-Cu-O (BSCCO/Ag) tapes especially after long heat treatments [58] requires extra reinforcement to bear the winding and level strains, support the electromagnetic forces in operation and manage the cooling thermal stresses without dramatic decrease of critical currents [59,60]. This requires the use of Ag-alloys with better tensile strength and hardness. In fact the selection of Ag-alloy systems must fulfil the following requirements.

- (i) Tapes with alloyed cladding sheaths should have a considerable workability to follow successfully the PIT process.
- (ii) The metallic sheath must maintain enough oxygen permeability to allow the *in-situ* reaction of cladding precursor powders, providing appropriate oxygen balance for the growth of superconducting phases.
- (iii) Multifilamentary tapes having large areas of direct contact between the metallic sheaths and the BPSCCO cores would

enhance the chemical reactivity, which should not be detrimental to the formation and texturing of superconducting phases.

The above reasons greatly reduce the material choice for composite tapes to a few silver rich alloys. Additionally the improvement of alloy mechanical properties may require the introduction of high content of alloying elements, worsening the chemical compatibility. Moreover, as the preparation of BPSCCO tapes involves long sintering times in oxidizing atmospheres at high temperatures, the sheaths, except for some noble metal alloying elements, become composites of oxide precipitates dispersed in a metallic host matrix.

Another aspect of the selection of an Ag-alloy system is the type of application requirement. Strain tolerance and high conductivity is a primary requirement for applications of tapes in coil winding for magnets, high resistivity is a primary requirement for applications involving ac fields and low thermal conductivity is required for applications where the tape is being used as current lead.

Binary alloy systems such as Ag-Mg, Ag- Cu, Ag- Mn and ternary systems such as Ag – Mg – Ni, Ag – Au – Pd, Ag – Cu – Zr and Ag – Cu – Ti are the choices [61] for the preparation of (Bi,Pb)-2223/Ag tapes, wherein the useful properties of the alloys can be made use of.

1.8.2. Choice of precursor powder

The selection of a suitable precursor powder is the most important step in the powder-in-tube process. Researchers made it clear that filling a powder containing mostly Bi-2223 phase yields only tapes with

inferior properties with respect to transport current and phase purity. The reasons suggested for this were that the phase stability region of Bi-2223 is very narrow and is very much dependent on the temperature and atmosphere and that it cannot be melted to form a coherent structure for it decompose into Bi-2212 and other mixed oxides [62]. Supported by subsequent investigations, it became clear that the route of reaction sintering assisted by a transient liquid phase is the most suited approach if high currents are to be carried by tapes, while the presence of a liquid phase helps healing the microcracks produced by mechanical deformation procedures, its complete consumption in the finished tapes is a must for better transport properties. Consequently if a pre-reacted powder is to be filled in the tube it is important to optimize the cation stoichiometry, the starting phase assemblage and the powder characteristics such as particle size distribution which together will dictate the conversion to the desired 2223 phase under specific heat treatment conditions. Extensive studies carried out by our group [63-65] and various other groups in the world [66-69] have arrived at a conclusion that the precursor derived from a solution route, and having a phase assemblage consisting of 2212 as major phase, Ca_2PbO_4 and oxides as secondary phases yields better I_c transport properties for the PIT processed tapes.

1.8.3. Choice of mechanical deformation procedures

Mechanical working has multiple roles in PIT fabrication of BPSCCO/Ag tapes. Initially diameter reduction is one soul objective, while towards the final stages of tape processing, thickness reduction as well as improvisation of c-axis alignment of grains become important. Methods like wire drawing, swaging and groove rolling have been

utilized for fabrication, while subsequent flat rolling and often uniaxial pressing have been employed for making tapes. The importance of pressing as well as repeated thermo mechanical cycling has been emphasized by a large number of research groups.

1.8.4. Formation and stability of 2223 phase

After a PIT tape was fabricated, the precursor powder needs to be converted to 2223 phase. However converting a multiphase, overall $(\text{Bi,Pb})_2\text{Sr}_2\text{Ca}_2\text{Cu}_3\text{O}_x$ composition powder into phase-pure BPSCCO-2223 in Ag-clad tape can be a difficult task. Relatively small variations in starting chemistry, reaction temperature, and oxygen partial pressure can move the system into regions in phase space where 2223 formation is not reversible. For example, even in the optimum atmosphere for 2223 formation (oxygen partial pressure ~ 0.075 atm: often referred as simply 7.5% O_2), the activation energy for 2223 formation, E_a^{2223} has been shown to change from ~ 2700 kJ/mol to ~ 700 kJ/mol [70-71] over just a few degrees. This sharp change in E_a^{2223} is believed to be resulted from a change from a solid state to a liquid assisted formation process. As the activation energy for the formation of the impurity, or “second” phases in the system is only ~ 500 kJ/mol [72], it is very difficult to form single phase 2223. Since the BPSCCO system involves so many components and possible reaction pathways the initial phase assemblage, in addition to the overall chemical composition has a large effect on the post processing results. Furthermore, some of the components are volatile (e.g. Pb [73]), and therefore the overall composition of the system can shift during processing, resulting in a corresponding shift in the equilibrium (or metastable) phases. Many of the important details of the 2223 phase formation and stability are

interwined, which make it difficult to separately discuss the individual aspects.

a) Formation mechanism

Most of the formation mechanism models of 2223 phase fall into one of the two broad categories – formation by interaction or by nucleation and growth. Almost all models have a liquid phase in some capacity. It was undoubtedly proved that $\text{Ca}_2\text{PbO}'_4$ phase plays a significant role in the formation of liquid phase during the sintering of Bi-2223 [74-78]. In the nucleation and growth model it was assumed that Bi-2223 is formed by a nucleation and growth process, whereby 2212 reacts with a liquid phase and new 2223 grains are nucleated either at sites on 2212 grains, or directly from the melt. X-ray diffraction studies [79-82] also supported by SEM analysis [83,84] a majority of the researchers have suggested the nucleation and growth model for the formation of Bi-2223.

In the intercalation process 2212 grains are directly transformed into 2223 platelets via insertion of additional Ca/Cu-O layers. TEM studies [85,86] and transmission in X-ray technique conducted by Wang et al. [87], to probe both the phase assemblage and texture of the entire thickness of the tape, have given confirmation of the intercalation process for the formation of Bi-2223.

As the system is bit complex consisting of six components, a multitude of reaction pathways may occur in the processing/heat treatment of Bi-2223. One may get confused on going through literature

by which mechanism Bi-2223 is formed and well designed experiments are required to clarify this point.

b) Stability of 2223 phase

The stability of 2223 phase is very much dependent on the temperature and oxygen partial pressure. Most of the heat treatments for Bi-2223 is done in air wherein some unavoidable secondary phases such as Ca_2PbO_4 were present in the system even after the final stage of heat treatment. But researchers have found that heat treating the tapes in a reduced oxygen atmosphere ($p\text{O}_2 \sim 0.075 \text{ atm}$ (7.5% O_2) [88-91] could favour the formation of Bi-2223 with the widest temperature stability window. In this atmosphere 2223 phase starts to form at $\sim 800^\circ\text{C}$ and is stable upto about 830°C .

1.8.5. Critical current density of (Bi,Pb)-2223/Ag tapes

The critical current density of (Bi,Pb)-2223/Ag tapes is a very sensitive quantity dependent on many factors right from the precursor synthesis route to the final heat treatment stage. For obtaining tapes with reasonably good J_c it is essential to select suitable precursor powder of right composition and phase assemblage and to optimize all the processing parameters. Also the rough handling of the finished tape can reduce transport current due to the fragile nature of the sheath.

Eventhough multiple current limiting mechanisms operate right from the nanometer to millimeter scale, the primary limitations of J_c come from two sources:

- (i) J_c determined by flux pinning and

(ii) J_C determined by the weak links or intergranular current transport

a) Flux pinning and its significance

While the upper limit of the current density is determined by the depairing current density, which is $\sim 10^7 \text{ Acm}^{-2}$ for (Bi,Pb)-2223/Ag at 77 K [91], the practical intrinsic J_C limitation of a conductor is determined by the flux pinning strength. Magnetic flux exists as a lattice of quantized line vortices or fluxons above H_{C1} in HTS [92]. Each fluxon is a tube of radius of the London penetration depth $\lambda(T)$, in which superconducting screening currents circulate around a small non-superconducting core of radius $\xi(T)$, where $\xi(T)$ is the superconducting coherence length. Superconductors can carry bulk current density only if there is a macroscopic fluxon density gradient [93] defined by Maxwell equation $\Delta \times B = \mu_0 J$. This gradient can be sustained only by pinning the vortices (flux pinning) at microstructural defects. Also the fluxon structure is subjected to the Lorentz force $F_L = J \times B$ of the macroscopic current. The critical current density $J_C(T, H)$ is then defined by the balance of the pinning and Lorentz forces, $F_P = F_L$, where F_P is the volume summation of overall microstructural pinning defects in the strongly interacting network of flux lines. Increasing T and H weaken the potential wells at which vortices are pinned, thus reduces $H^*(T)$ and $J_C(T, H)$. Ideally a type II superconductor can carry any non-dissipative current density J smaller than J_C , when J exceeds J_C , a superconductor switches into a dissipative vortex flow state driven by Lorentz force.

This description of flux pinning immediately suggests tailoring the defect structure of the conductor to maximize J_C . But the pinning

interactions in HTS are largely unknown, partly because the coherence length is so small that even atomic-size point defects can pin fluxons. There is strong experimental evidence that point defects such as Zn and Ni impurities [29] or oxygen vacancies [94], or line defects such as edge [95] and screw [96] dislocations, can effectively pin pancake vortices in layered HTSs. These and other forms of defects inherently present in any HTS provide strong flux pinning at low temperature. But the performance of the conductor at or near 77 K is limited by the irreversibility field $H^*(T)$ which is very low for Bi-2223 conductors. Both H^* and J_C can be significantly improved by irradiation which creates effective columnar pinning tracks [97]. For example, neutron irradiation of U-doped Bi-2223 tapes fissions the U and produce heavy-ion tracks that raise $H^*(77K)$ to over 1T while also reducing the anisotropy of J_C [98]. All these cases apply to tapes of very small length (~ 5 cm or less). For long length tapes other type of pinning mechanisms such as doping with nano-size impurities [99,100], tailoring the amount and size of the impurity phases such as Ca_2PbO_4 , Ca_2CuO_3 etc [101,102] inherently present in the system etc have been sought.

b) Weak links and intergranular connectivity

The second intrinsic limitation of critical current comes from the poor connectivity or the weak link nature of the Bi-2223 system. As the coherence length is so small defects along the grain boundaries will deteriorate grain connectivity and lead to weak links. Analysis of the magnetic field dependence on the critical current density conducted by Huang et al. [103] revealed that the transport current is carried through two paths. One is through weakly linked grain boundaries (Josephson junctions); another is through well connected grains. Various kinds of

grain boundaries are observed in Bi-2223/Ag tapes, i.e. the (001) twist boundaries and the resulting colony structure, edge-on c-axis tilt grain boundaries etc. Among these the low angle ab-axis grain boundary is considered to be strongly linked one for transporting current [104-106] and the others may form a weakly linked Josephson junction network. As the conductor is in the polycrystalline form, these grain boundaries are inevitable to remove. But better process control, and thermomechanical treatments can reduce the weak links and enhance the J_C of tapes.

c) Other limitations

While the above said limitations are intrinsic in nature, there are limitations which are extrinsic also. Magneto optical imaging (MOI) studies on BSCCO-2223 tapes conducted by Cai et al. [107] and by Lanbalestier et al. [108] have demonstrated that the transport J_C of very high J_C BSCCO-2223 tapes is more determined by their connectivity than by flux pinning and that an independent and much larger influence on the J_C comes from unhealed cracks produced by deformation during the processing of the tapes. Such cracks, actual or incipient, exist on the sub to several hundred micron scale, producing local variations of current density, depending on the number of such cracks. This has been confirmed by the MOI studies [108] on BSCCO-2223 filaments, where quasi periodic flux-leakage channels were observed which cross the whole filaments transverse to the rolling axis. The presence of such cracks 'incipient' or actual together with other impurity phases and porosity reduce the current carrying cross section of the system and thus reducing J_C .

Finally it can be concluded that there are three simultaneous strategies for raising J_C of (Bi,Pb)-2223/Ag tapes. At the nanoscale, these include (i) improving c-axis misalignment so as to reduce the c-axis current flow; (ii) raising flux pinning and irreversibility field, $H^*(77\text{ K})$, which can improve J_C by at least a factor of 2 in “optimized” composites [109,110], and (iii) raising the effective current carrying cross-section [107-111] by reducing the porosity and effective healing of fabrication damage.

1.8.6. Importance of multifilamentary geometry

Many of the large scale applications of HTS need kilometer lengths of the conductor with sufficiently high J_C . While scaling up from laboratory samples to industrial scale products problems such as global homogeneity and reproducibility of transport J_C are important. It is true that (Bi,Pb)-2223/Ag tapes of monofilament geometry is unable to have the performance needed for industrial application of superconductors. The alternative is the conductors in the multifilamentary geometry like the traditional superconducting wires of NbTi and Nb₃Sn. There are several unique advantages for (Bi,Pb)-2223/Ag tapes in the multifilament configuration and some of them are listed below.

- i) The strain tolerance of the tapes in the multifilamentary configuration is much higher than the corresponding monofilament tapes.
- ii) The silver-superconductor interface is much higher resulting in higher texture and thus I_C .

- iii) Parallel electrical conduction paths to serve as a by-pass in case of local failure.
- iv) Because the silver content is higher multifilament configuration provides.
 - a) better heat sinking and cryostability
 - b) minimal loss of energy by magnetic flux motion
 - c) ac loss reduction (lesser ac loss)
 - d) mechanical protection of the brittle superconductor core against Lorentz force and stress during handling

Tremendous research effort by various groups in the world and by many companies have made defect free wires/tapes exceeding 100A per tape at 77 K in lengths of several hundred meters.

1.9. Achievements and State of the Art Developments of HTS

1.9.1. International Scenario

Over one and half decades have gone after the discovery of high T_C superconductivity and still it is the hot topic of many research laboratories and industries. As a result of the well targeted research efforts made by various groups in the world, several prototypes and some products have been developed. Table 1.3 gives application prototypes developed using Bi-2223 tapes. Fig. 1.10 shows the J_C performance versus length for Bi-2223 tapes made by various manufacturers around the world. In parallel with these wire and bulk applications a spectrum of thin film applications for microwave antennae, filters and superconducting quantum interference devices

(SQUIDS) has also emerged. It is clear from the broad base of applications and their proximity to commercial scale demonstrations that

Table1.3 Application prototypes using Bi-2223 tapes [39,112-113]

Items	Present Status	Features
Current Leads	• 500 A for 400 kJ/SMES	Implemented in 1993
	• 600 A for MAGLEV	Good against vibration
	• 2000 A for Synchrotron	Implemented in 1993
	• 14,500A for ITER	Save 70% power
Transformer	800 kVA	Non-flammable
SMES	100 J Coil at 77 K/ 1 kJ at 35 K	2 Hz operation
Magnets	• 3 T with 40 mm RT bore	Fast cyclic operation
	• 4 T with 50 mm RT bore	4 T in 10 seconds
	• 7 T with 50 mm RT bore	7 T in 1 minute
	• 0.19 T with 280mm RT bore	Active levitation of YBCO
Cables	7m& 1kA 3-phase cable	Magnetic shielding structure
	50 m& 3 kA conductor	Machine stranding
	50 m model	66 kV voltage regulation
	30m, 66kV& 1 kA cable	LN ₂ Cooling system

HTS technologies are on the threshold of the promised superconductor revolution. As manufacturers scale up production prices will inevitably be driven down and the commercial viability will be further enhanced. Add to this voracious appetite of the information technology industry for

faster communication, larger memory capacity and faster processing power, it is clear that the market pull for electronic HTS technologies will grow dramatically in the next few decades.

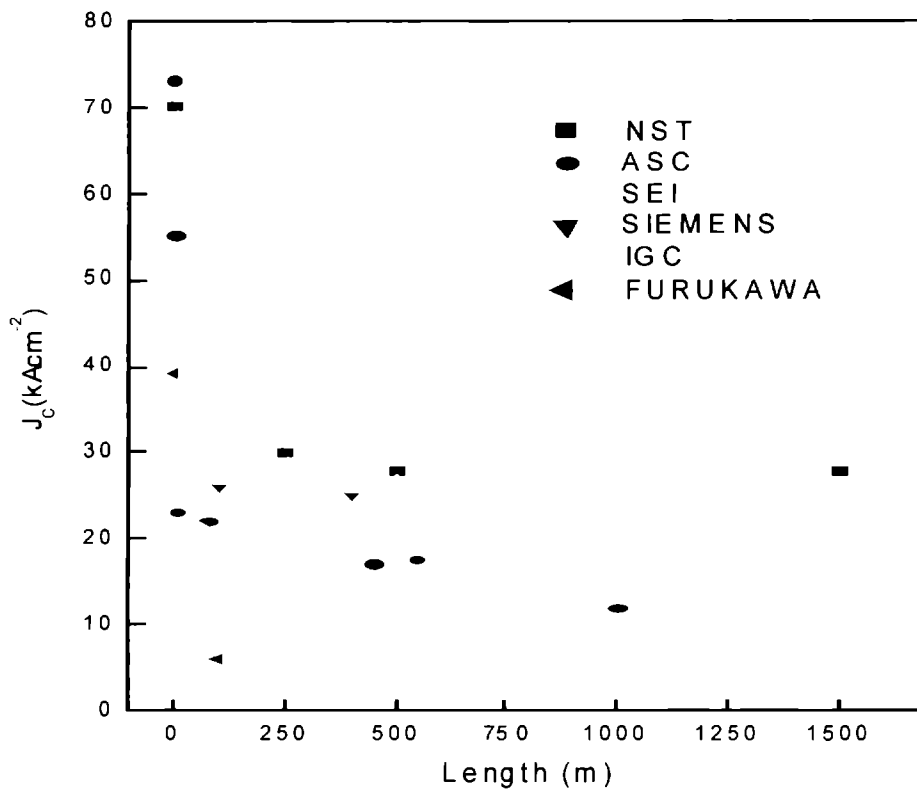


Fig. 1.10 J_c performance versus length for Bi-2223 tapes made by various manufactures around the world [39, 112-113].

NST- Nordic Superconductor Technologies

ASC- American Superconductor Corporation

SEI- Sumitomo Electric Industries

IGC- Intermagnetics General Corporation

1.9.2. National Scenario

Even though, there are some significant development made in the country on LTS magnets and technology using NbTi and Nb₃Sn wires by the dedicated research works of NPL, BARC, IGCAR and BHEL, HTS technology development is no way near to the international scenario. Melt textured YBCO with high J_c has been developed by DMRL. A host of new varieties of rare earth based substrate materials for HTS thin films and the process for making them were developed and patented by RRL, Trivandrum [114-119]. Short lengths of (Bi,Pb)-2223 /Ag tapes of J_c (0T, 77K) ~ 10⁴ Acm⁻² was developed jointly by RRL and BHEL in 1996.

Thereafter by the intense research efforts by RRL, Trivandrum the J_c has been raised to 30 kAcm⁻² (0T,77K). The work done in this thesis is part of HTS wire development program, especially multifilamentary (Bi,Pb)-2223 /Ag tapes and technology developments being pursued at RRL Trivandrum.

1.10 HTS Current Leads

Current leads as the name implies are the connecting leads between a room temperature power source and a power device, a superconducting device, operating at very low temperatures (~4 K). Traditionally the current leads are made of copper with provision for cooling to remove the heat generated by dissipation (Joule heating) and to reduce the low temperature heat load (conductive heat transfer) to the system. Despite adequate cooling and rigorous optimization of these 'all-metal' current leads, there is considerable heat load to the system

which causes either boil off the liquid cryogen (liquid He) or reduced efficiency due to the high power needed to attain and maintain the operating temperature (for systems operating in closed cycle refrigeration with He gas). With the advent of high- T_C superconductors researchers thought of using HTS leads in place of the traditional ‘all-metal’ current leads. If HTS leads are introduced into the system the heat leak from the room temperature can be intercepted at a much higher temperature (usually 60-80K) rather than having to be removed at 4 K.

The properties of HTS leads include zero or no resistance thus eliminating the joule heating and very low thermal conductivity thus reducing the conductive heat transfer to a minimum, making it ideal material for current lead applications. In fact, HTS current leads represent the first large-scale application of high temperature superconductivity. There are three classes of applications where HTS leads are seeing rapid introduction.

- (i) **High current LTS magnets cooled by liquid He:** These include the accelerator and detector magnets for high energy physics (e.g. the large hadron collider (LHC) being developed by CERN, magnets for the International Thermonuclear Experimental Reactor (ITER), detector magnets such as Wendelstein 7-X, Stellarator (W7-X), large helical device (LHD) and high field NMR magnets, SMES etc. All these devices need operating current ranging from 100 A to ~ 60 kA.
- (ii) **Conduction cooled LTS magnets:** The development of conduction cooled LTS magnets solely depends upon the use of HTS current leads. Without the reduction in heat load offered by

HTS leads the realization of these systems will be very difficult or impossible in many cases.

- (iii) **Conduction cooled HTS magnets:** The next generation superconducting magnets will be conduction cooled HTS type. In this case, the magnet would be possible even without HTS leads, but the economics of operation is greatly enhanced by the use of HTS leads, and every HTS magnets developed todate use HTS leads in some part of the system.

1.10.1 Conduction Cooled (CC) and Vapour Cooled (VC) Current Leads

Traditional “all-metal” current leads were all vapour cooled in the sense that the superconducting system will be operating in liquid helium and the current leads used to draw power to the same is extended to the room temperature and will be cooled by He vapour boiling off from the cryogen bath. Usually the vapour will be forced to flow through several holes drilled in the current leads. The low heat of evaporation (20.93 kJ/kg) and large heat capacity (1530 kJ/kg from 4.2 K to 300 K) of He vapour ensure efficient cooling of the current leads. In fact the gas evaporated by one watt at 4.2 K makes available another 70 W of cooling power when it is heated to room temperature. For systems operating in liquid He vapour cooled current leads are a better choice.

In the conduction cooled case, the lead usually has to be installed on a system which will be operating with the help of refrigerators/cryocoolers. The simultaneous implementation of two stage Gifford-Mcmohan refrigerators and HTS current leads paved the way for the development of both LTS and HTS conduction cooled

magnets. In these systems, HTS current leads are used to draw power from a high temperature heat source (60-77 K) to the low temperature system (4K). Thermal conductivity of the lead is a critical problem for the conduction cooled current leads. Eventhough the design aspects are simpler the efficiency of a conduction cooled current lead is much lower compared to the VC case. For example, for a pair of “all-metal” current leads operating in the conduction cooled mode, the heat load is evaluated to be 42 WkA^{-1} , whereas for a vapour cooled current lead it is 1.08 WkA^{-1} [120]. Similarly for a HTS current lead operating in the conduction cooled mode with high temperature heat sink at 80 K, the predicted heat load is 0.24 WkA^{-1} , whereas for a vapour cooled case with same conditions the heat load is only 0.025 WkA^{-1} [120,121].

1.10.2 Material Choices for HTS current leads

Among the HTS compounds discovered to date the systems most studied for bulk applications are BSCCO and YBCO. For the current lead applications also the material choice falls on these two systems as these two compounds can give appreciable amount of transport current under optimized processing conditions. For the BSCCO system the two phases viz. Bi-2212 and Bi-2223 are used as current leads. Other important aspects considered worth for current lead applications are the mechanical and thermal properties of these systems under the operating conditions.

There are two forms of current leads: (i) bulk form and (ii) tape form with a low thermal conductivity sheath. Following gives a comparison of the HTS current leads between the two forms.

1.10.3 HTS current leads in bulk rods or tubes

Both YBCO and BSCCO are used to prepare current leads in the form of a tube or rod [120-136]. YBCO is prepared by melt textured growth (MTG) or by plastic extrusion of the ceramic slurry [122-126]. Bi-2212 is prepared via the melt cast process (MCP), by cold isostatic pressing (CIP) followed by sintering, dip coating on a suitable substrate (DIP) etc [127-136]. Bi-2223 is prepared using cold isostatic pressing and subsequent sintering or by hot isostatic pressing (sinter- forging) [127-131,134,136]. All the above systems have been developed to carry current from ~ 50 A to ~ 14.5 kA. Out of these, the MCP Bi-2212 is far superior compared to the other two types and have been commercialized by companies such as Can superconductors, Nexans superconductors etc and is still under development.

As these systems are intrinsically brittle and hence are mechanically weak considering its integration to the cryogenic system. They are sensitive to mechanical shocks and can easily break. Another difficulty is that these bulk materials require the use of electrical by-pass that has to be resistive during normal operation and to have a very low current response time in case of a “quench”. And lastly these systems need the use of end metal caps/parts that is either coated or mechanically fixed, to establish a good electrical contact at the connecting points.

1.10.4 HTS current leads in tape form

HTS current leads in tape form is prepared using multifilamentary (Bi,Pb)-2223/Ag tapes [136-147]. To reduce the thermal conductivity of the sheath material alternate alloy systems such as Ag-Au, Ag-Mg etc are sought. Many research laboratories around the world are actively

engaged in strategic programs to fabricate current leads using (Bi,Pb)-2223 multifilamentary tapes and to optimize the process parameters needed for the cost effective preparation. Another configuration is AFM on (Accordion Folding Method) coated Bi-2223 current leads. The advantage of AFM coating is that the fill factor (SC/Ag) can be increased which will decrease the effective thermal conductivity of the composite. But this method has the drawback that the preparation procedures are far from being optimized.

Compared to the bulk form of current leads, tape form of current leads have the following advantages:

- (i) low heat leak (for optimized leads)
- (ii) can withstand shock resistance
- (iii) possess high stress tolerance
- (iv) possess high thermal cycling tolerance
- (v) low contact resistance
- (vi) can be easily integrated to the cryogenic system
- (vii) do not need additional by-pass shunt to protect the lead from a possible quench.
- (viii) Small in size and possess high current densities

1.10.5 Operation and Stability of HTS Current Leads

While considering the operation of HTS current leads integrated to a cryogenic or superconductor system they must not only be able to withstand the rated current but also it must be stable in service. The stability of the current leads is determined by the following criteria.

a. Heat leak

The current lead should be designed in such a way that the heat input to the cryogenic system must be as minimum as possible. This will reduce the boil off liquid helium for a vapour cooled system and will enhance the refrigeration efficiency for a conduction cooled system. For the current lead in the tape configuration, thermal conductivity of metallic sheath is the determining factor for the low temperature heat load. It is important to have a sheath material of low thermal conductivity at the temperature range of the operation of the HTS current lead. Ag-Au alloy is a possible candidate and as part of the present work due importance is given to the study of tapes prepared using AgAu alloys in different percentages (Chapter 3). Also it is important to maximize the fill factor (volume ratio of superconductor to the sheath) so as to minimize the metal content as low as possible. A detailed investigation is done to optimize the powder to metal ratio in the preparation of (Bi,Pb)-2223/Ag tapes (Chapter 5).

b. Thermal and Mechanical Stability

Current leads must withstand the shocks and stresses during installation and in service. Also it should be able to withstand the thermal recycling; the current carrying through the lead should not decay after many recycles (during ramp up and ramp down of temperature). Due to the large difference in the coefficient of thermal expansion (CTE) between Ag and Bi-2223 ceramic, thermal stresses during processing and in service may deteriorate the critical current of the tapes. To avoid this, the mismatch of the mechanical strength between the sheath and ceramic has to be reduced and alternate sheath

alloys with improved mechanical strength is the option. A detailed study has been conducted during the thesis work on the superconducting and mechanical properties of tapes prepared using Ag-Cu alloy sheaths (chapter 3)

c. Field tolerance

Current leads have to be anchored to cryogenic systems where magnetic field is present due to the high current carrying superconducting coils or magnets. The current carrying nature of (Bi,Pb)-2223/Ag is highly anisotropic and sensitive towards an applied magnetic field. The reduction of transport I_C is drastic in $B_{||c}$ compared to the field direction $B_{\perp c}$. Enhancing the flux pinning strength of the tapes can reduce this decrease in I_C . Adding nano size impurities having no deleterious effects on the superconducting properties of the system is an option for improving the flux pinning strength of the tapes. As part of the thesis work effect of nano size MgO in (Bi,Pb)-2223/Ag is studied as a candidate for improving the pinning strength of the tapes. Also care must be taken while designing the lead, the c-axis should be arranged favourable for the current flow in presence of a magnetic field.

1.10.6 Design aspects of the current leads

After optimizing the properties of the raw material (i.e. multifilamentary (Bi,Pb)-2223/Ag tapes) with respect to its engineering current density and stability related issues for its use as current leads, the job left is only to design the current lead suitable for specific devices operating at low temperatures. There can be two types of current leads viz. custom

tailored and general purpose. Custom tailored leads are necessary to replace the Cu leads in high field LTS magnets and the leads under development for large projects like LHC, ITER magnets etc. General purpose current leads find application in low or medium field LTS/HTS conduction cooled magnets and NMR devices. Prior to the design of the lead design requirements have to be taken into account; these are the current rating and the operational environment viz. temperature and field. The important design parameters are given below.

- i. Engineering current density (J_E)
- ii. J_C and $J_C(B, T)$
- iii. Anisotropy of critical current ($J_C(B||c)/J_C(B\perp c)$)
- iv. Mechanical issues; strain response and differential contraction
- v. Transient dissipation and quench stability
- vi. Joints and contacts and,
- vii. Piece length and dimensions

1. 11 Scope of the present work

The brief overview presented above highlighted the importance of HTS materials in general and their vast realm of applications on which the country is no way on par with international developments. Presently multifilamentary conductors of (Bi,Pb)-2223 made by the wire – in – tube technique is the raw material required for any kind of HTS power applications. The research work presented in this thesis is a kind of application development of HTS, i.e. HTS current leads, using

multifilamentary (Bi,Pb)-2223 tapes. As required by any kind of HTS power applications, the properties and geometry of the raw material should be optimized for its use as current leads. The investigations conducted mainly focused on the following aspects (i) finding an alternate sheath material with improved mechanical strength and lower thermal conductivity to replace pure Ag. (ii) improving the flux pinning strength by the addition of nanosize impurities, (iii) optimization of geometrical and thermomechanical processing parameters of the multifilamentary tapes, (iv) testing the homogeneity and consistency of the raw material and (v) design, prepare and test the prototype samples for rated current and other mechanical, thermal and electrical properties. As mentioned in the previous section the thermal conductivity of the composite, mainly due to the sheath material is the critical factor causing heat leak to the low temperature system. Investigations were conducted on alternate alloy systems such as Ag-Cu and Ag-Au with an aim to replace pure Ag in the wire-in-tube processing of (Bi,Pb)-2223 multifilamentary tapes. It requires a test of compatibility of the alloy system with the BPSCCO with respect to the superconducting, mechanical, electrical and thermal properties. Results showed that Ag-Cu alloys improve the mechanical strength considerably and Ag-Au alloys reduces the thermal conductivity considerably. For the Ag-Au alloys Cu% in the sheath have to be optimized with the Cu stoichiometry in the precursor. Thus a combination of Ag-Au alloy (for inner sheath) and Ag-Cu alloy (for outer sheath) is the ideal combination for making multifilamentary tapes to be used as current leads. Addition of nano size impurities (nano MgO particles) enhances the self-field J_C and improves the $J_C - B$ characteristics of the tapes, thus enhancing the field tolerance of current leads. The geometrical parameters of the multifilamentary

tapes such as the number of filaments, wire diameter prior to the flat rolling stage and final tape thickness and the thermomechanical processing parameters are optimized for higher J_C s. It is generally observed that for multifilamentary tapes prepared by rolling as the deformation route shows reduced J_C as well as poor J_C homogeneity along the length of the tape. In an attempt to improve the final J_C as well as J_C homogeneity along the length of the tape, studies were conducted on the effect of uniaxial pressing applied prior to the last stage rolling. The results of the optimization studies lead to the development of multifilamentary (Bi,Pb)-2223 /Ag tapes of $I_C > 60$ A for 10cm long tapes at (0T, 77K). The design aspects of conduction cooled current leads are much simpler compared to the vapour cooled one and depend on the current rating and the superconducting system on which it has to be implemented. In this thesis a pair of prototype general purpose current lead of rating > 100 A has been designed fabricated and tested for the rated current, thermal and mechanical stability and quench stability. The thermal compatibility of different types of cryostable glass fibre reinforced epoxy (GFRE) has been studied for its use as housing matrix for better mechanical rigidity. The estimation of the heat leak of the current lead when anchored between 64 K and 20 K is shown to be two orders of magnitude less than that prepared using pure Ag sheath.

References

- [1] H. Kammerlingh Onnes, *Leiden Commn.* **120b**, **122b**, **124c** (1911).
- [2] C.W. Chu, L. Gao, F. Chen, Z.J. Huang, R.L.Meng and Y.Y.Xue, *Nature*, **363** (1993) 323.
- [3] Various Chapters of the book “Practical Superconducting Materials”, *Superconductor Materials Science: Metallurgy, Fabrication and Application*, Ed. S. Toner and B.B. Schwartz (New York, Plenum Press, 1981).
- [4] A. W. Sleight, J. L. Gillson and P. E. Bierstedt, *Solid State Commun.* **17** (1975) 27.
- [5] M. K. Wu, J. R. Ashburn, C. J. Torng, P. H. Hor, R. L. Meng, L. Gao, Z. J. Huang, Y. Q. Wang and C. W. Chu, *Phys. Rev. Lett.* **58** (1987) 908.
- [6] L. F. Mattheiss, E. M. Gyorgy and D. W. Johnson Jr., *Phys. Rev. B* **37** (1988) 3745.
- [7] R. J. Cava, B. Batlogg, J. J. Krajewski, R. Farrow, L. W. Rupp Jr., A. E. White, K. Short, W. F. Peck and T. Kometani, *Nature* **332** (1988) 814.
- [8] D. Pelloquin, M. Caldes, A. Maignan, C. Michel, M. Hervieu and B. Raveau. *Physica C* **208** (1993) 12 1.
- [9] R. Cywinski, Z. P. Han, R. Bewly, R. Cubitt, M. T. Wylie, E. M. Forgan, S. Lee, M. Warden, S. H. Kilarjne, *Physica C* **233** (1994) 273.
- [10] Z. Iqbal, R. H. Baughman, B. L. Ramakrishna, S. Khare, N. S. Murthy, H. J. Bornemann and D. E. Morris, *Science* **254** (1991) 826.

- [11] C. Buzea, T. Yamashita, *Supercond. Sci. Technol* **14** (2001) R115
- [12] J. Bardeen, L.N. Cooper and J.R. Schrieffer, *Phys. Rev. B* **106** (1957) 162; **168** (1957) 1175.
- [13] J. G. Bednorz and K.A. Muller, *Z. Phys. B.* **64** (1986) 189.
- [14] C. Park and R.L. Snyder, *J. Am. Ceram. Soc.* **78(12)** (1995) 3171.
- [15] M.G. Aranda, *Adv. Mater.* **6** (1994) 905 and References therein.
- [16] E. Dagotto and T.M. Rice, *Science*, **271** (1996) 618.
- [17] T.M. Rice, *Physica B*, **5** (1998) 247.
- [18] K.S. Muller, M. Takashige and J.G. Bednorz, *Phys. Rev. Lett.*, **58** (1987) 1243
- [19] Y. Yeshum and A.P.Malozemoff, *Phys. Rev. Lett.*, **60** (1988) 2202.
- [20] Y. Xu, M. Suenaga, Y. Gao, J.E. Crow and N.D. Spencer, *Phys. Rev. B*, **42** (1990) 8756
- [21] M.P.A. Fisher, *Phys. Rev. Lett.*, **62** (1989) 1415.
- [22] J. Bardeen, L.N. Cooper and J.R. Schrieffer, *Phys. Rev.* **108** (1957) 1175.
- [23] N. Bulut and D.J. Scalapino, *Phys. Rev. Lett.* **68** (1992) 706.
- [24] P. Monthoux, A.V. Balatsky and D. Pines, *Phys. Rev. B*, **46** (1992) 14803
- [25] S. Chakravarty, A. Sudbo, P.W. Anderson and S. Strong, *Science*, **261** (1993) 337.
- [26] .D.S.Rokhstar, *Phys. Rev. Lett.*, **70** (1993) 493.
- [27] P. W. Anderson, *Science* **235** (1987) 1196
- [28] S-C. Zhang, *Science*, **275** (1997) 1089.
- [29] S.H. Pan, E.W. Hudson, K.M. Lang, H. Eisaki, S. Uehida and J.C. Davis, *Nature*, **403** (2000) 746.

- [30] J.E. Evetts and B.A. Glowacki, *Supercond. Sci. Technol.* **13** (2000) 443-447.
- [31] M. Murakami, *Supercond. Sci. Technol.* **13** (2000) 448-450.
- [32] P. Komarek, *Supercond. Sci. Technol.* **13** (2000) 456-459.
- [33] V.P. Koshelets and S.V. Shitov, *Supercond. Sci. Technol.* **13** (2000) R53-R69.
- [34] M. Nassi, *Supercond. Sci. Technol.* **13** (2000) 460.
- [35] P. Kummeth, R. Schlosser, P. Masek, C. Albrecht, D. Breitfelder and H-W. Neumuller, *Supercond. Sci. Technol.* **13** (2000) 503.
- [36] T. Ageta, *Supercond. Sci. Technol.* **13** (2000).
- [37] J. Niemeyer, *Supercond. Sci. Technol.* **13** (2000) 546.
- [38] J.L. Duchateau, M. Spadoni, E. Salpietro, D. Ciazynski, M. Ricci, P. Libeyre and A. Dellalorte, *Supercond. Sci. Technol.* **15** (2002) R17.
- [39] Informations published in the website of various companies and laboratories such as
- (i) American Superconductor Corporation (www.amsuper.com);
 - (ii) Los Alamos National Laboratory (www.lanl.gov),
 - (iii) University of Wisconsin Madison (www.asc.wisc.edu)
 - (iv) Argonne National Laboratory (www.anl.gov)
 - (v) Intermagnetics General Corporation (www.igc.com.)
 - (vi) Oxford Instruments, UK, (www.oxfordinst.com)
 - (vii) BICC Cables, UK (www.bicc.com)
 - (viii) Electric Power Research Institute, USA (www.epri.com)
 - (ix) Superconductor Week (www.superconductorweek.com)
- [40] R. Heller, W. Maurer and W-7-X team, *IEEE Trans. Appl. Supercond.* **10** (2000) 614.

- [41] L. D. Cooley, C. B. Eom, E. E. Hellstrom and D. C. Larbalestier, *Proceedings of the 2001 Particle Accelerator Conference*, Chicago
- [42] C. Mechel, M. Hervieu, M.M. Borel, A. Grandin, F. Deslandes, J. Provost and B. Raveau, *Z. Phys. B.: Condens. Matter.* **68** (1987) 421.
- [43] H. Maeda, Y. Tanaka, M.Fukotomi and T. Asano, *Jpn. J. Appl. Phys.* **27** (1988) L209.
- [44] T. Kawai, Y. Egami, H.Tabate and S. Kawai, *Nature*, **349** (1991) 200.
- [45] H. Wang, X. wang, S.Zhang, Z. Lu and M. Jiang, *Appl. Phys. Lett.* **57** (1990) 710.
- [46] M. Onoda, A. Yamamoto, E.T. Muromacha and S. Takekawa, *Jpn. J. Appl. Phys.* **27** (1988).
- [47] T.M. Shaw, S.A. Shivasankara, J.J. LaPlaca, J.J. Guonn, T.R. McGuire, R.A. Roy, K.H. Kelleber and D.S. Yee, *Phys. Rev. B* **37** (1988) 9856.
- [48] H.W. Zanderger, W.A. Green, A. Smil and G. Van Tendeloo, *Physica C*, **168** (1990) 426.
- [49] C.N.R. Rao and B. Raveau, *Acc. Chem. Res.* **22** (1989) 106.
- [50] O. Eibl, *Physica C*, **168** (1990) 215.
- [51] P. Majeswski, B. Hettich, H. Taeger and K. Schulze, *Adv. Mater.* **3** (1991) 67.
- [52] K. Schulze, P. Majewski, B. Hettich and G. Petzow, *Z. Metallkde Bd* **81 H11** (1990) 836.
- [53] U. Endo, S. Koyama and T. Kawai, *Jpn. J. Appl. Phys.* **27** (1988) L 14 76.

- [54] S.A. Sunshine, T. Siegrist, L.F. Schneemeyer, D.W. Murphy, R.J. Cava, B. Batlogg, R.B. Van Dover, R.M. Fleming, S.H. Glarum, S. Nakahara, R. Farrow, J.J. Krajewski, S.M. Zahurak, J.V. Waszczak, J.H. Marshall, P. Marsh, L.W. Rupp Jr. and W.F. Peck, *Phys. Rev. B*, **38** (1988) 893.
- [55] M. Takano, J. Takada, K. Oda, H. Kitaguchi, Y. Miuza, Y. Ikeda, Y. Tomu and H. Mazaki, *Jpn. J. Appl. Phys.* **27** (1988) L 1041.
- [56] P. Strobel, J.C. Toledano, D. Morin, J. Schneck, G. Vaequier, O. Monnereau, J. Primot and T. Fournier, *Physica C*, **201** (1992) 27.
- [57] T. Hatano, K. Aota, S. Ikeda, K. Nakamura and K. Ogawa, *Jpn. J. Appl. Phys.* **27** (1988) 12055.
- [58] J.W. Ekin, D.K. Finnemore, Q. Li, J. Tenbrink and W. Carter, *Appl. Phys. Lett.* **61** (1992) 858.
- [59] Z. Han and T. Freltoft, *Appl. Supercond.* **2** (1994) 201.
- [60] Z. Han, P. Skoo-Hansen and T. Freltoft, *Supercond. Sci. Technol.* **10** (1997) 371.
- [61] R. Navarro, *Supercond. Sci. Technol.* **13** (2000) R147.
- [62] K.H. Sandhage, G.N. Riley Jr. and W.L. Carter, *J. Metals*, **43** (1991) 21.
- [63] M.S. Sarma, U. Syamaprasad, C. Pavithran, P. Guruswamy and P.S. Mukherjee., *Journal of Materials Science Letters (UK)* **16** (1997) 1430
- [64] U. Syamaprasad, M.S. Sarma, P. Guruswamy, V. Prakash Kumar, R. Ragini, K.G.K. Warriar and A.D. Damodaran, *Physica C (NH)* **297**, 85-90 (1998).
- [65] A. Sobha, R. P. Aloysius, P. Guruswamy and U. Syamaprasad, *Supercond. Sci. Technol* **14** (2001) 417
- [66] J Jiang and J S Abell 1998 *Physica C* **296** 13

- [67] Xiao- Dong Su, Jai- Moo Yoo, Jai-Wong Ko, Hai-Doo Kim, Hyung- Sik Chung, Z Q Yang, Gui-We Qiao 2000 *PhysicaC* **331** 285
- [68] Weon-Ju Kim, Sun-Chill kwon, Ho Jin Lee, Hei-Gyoun Lee , Gye-Won Hong, II- Hyun kuk 1998 *PhysicaC* **294** 147
- [69] Q Li, K Brodersen, H A Hjuler and T Fretoft 1993 *PhysicaC* **217** 360
- [70] J.S. Luo, N. Merchant, E. Escorcia-Apricio, V.A. Maroni, D.M. Gruen, B.S. Tani, G.N. Riley Jr. and W.L. Carter, *IEEE Trans. Appl. Supercond.* **3** (1993) 972.
- [71] Y.S. Sung and E.E. Hellstrom, *J. Am. Ceram. Soc.* **78** (1995) 2003.
- [72] Y.E.High, Y. Feng, Y.S.Sung, E.E. Hellstrom and D.C. Larabalestier, *Physica C*, **220** (1994) 81.
- [73] J.S. Luo, N. Merchant, V.A. Maron, S.E. Dorris, M.T. Langan and B.S. Tani, *J. Am. Ceram. Soc.* **78** (1995) 2785.
- [74] T. Uzumaki, K. Yamanaka, N. Kamehara, K. Niwa, *Jpn. J. Appl. Phys.* **28** (1989) L75.
- [75] S.S. Oh and K. Osamura, *Supercond. Sci. Technol.* **4** (1991) 239.
- [76] Y.L. Chen and R. Stevens, *J. Am. Ceram. Soc.* **75** (1992) 1150.
- [77] Y. Yamada, B. Obst and R. Fuikiger, *Supercond. Sci. Technol.* **4** (1991) 165.
- [78] Y. Ikeda, H. Ito, S. Shimomura, Z. Hiroi, M. Takano, Y. Bando, J. Takada and K. Oda, H. Kitaguchi, Y. Miura, Y. Takeda and T. Takada, *Physica C*, **190** (1991) 18.
- [79] J.S. Luo, N. Merchant, V.A. Maroni, D.M. Gruen, B.S. Tani, W.L. Carter, G.N. Riley Jr., *Appl. Supercond.* **1** (1993) 101.
- [80] X-H. Gao, J. Li, S-F. Jiang, D. Gao, G.D. Zheng and S. Gao *Physica C*, **244** (1995) 321.

- [81] Q.Y. Hu, H.K. Liu and S.X. Dou, *Physica C*, **250** (1995) 7.
- [82] Y.D. Chiu, C.H. Kao, T.S. Lei and M.K. Wu, *Physica C*, **255-240** (1994) 485.
- [83] P.E.D. Morgan, R.M. Houseley, J. R. Porter and J.J. Ratto, *Physica C*, **176** (1991) 279.
- [84] J.C. Griewel and R. Flukiger, *Supercond. Sci. Technol.* **9** (1996) 555.
- [85] S. Ikeda, H. Ichinose, T. Kimura, T. Matsumoto, H. Maeda, Y. Ishida and K. Ogawa, *Jpn. J. Appl. Phys.* **27** (1988) L999.
- [86] W. Bian, Y. Zhu, Y.L. Wang and M. Suenaga, *Physica C*, **248** (1995) 119.
- [87] Y-L. Wang, W. Bian, Y. Zhu, Z.X. Cai, D.O. Welch, R.L. Sabatini, M. Suenaga and T.R. Thurston, *Appl. Phys. Lett.* **69** (1996) 580.
- [88] W. Zhu and P.S. Nicholson, *J. Appl. Phys.* **73** (1993) 8423.
- [89] M. Xu and D.K. Finnemore, *J. Appl. Phys.* **76** (1994) 1111.
- [90] J.A. Parrell, D.C. Larbalestier a and S.E. Dorris, *IEEE Trans Appl. Supercond.* **5** (1995) 1275.
- [91] Q. Li, M. Suenaga, T. Hikata and K. Sato, *Phys. Rev. B*, **46** (1992) 5957.
- [92] G. Blatter, M.V. Feigelman, V.B. Geshkenbein, A.I. Larkin and V.M. Vinokur, *Rev. Mod. Phys.* **66** (1994) 1125.
- [93] A.M. Campbell and J.E. Evetts, *Adv. Phys.* **21** (1972) 194.
- [94] P. Kes, *Physica C*, **185** (1991) 288.
- [95] A. Diaz, L. Mechin, P. Berghuis and J.E. Evetts, *Phys. Rev. Lett.* **80** (1998) 3855.
- [96] B. Dam et al. *Nature* **399** (1999) 439.
- [97] L. Civale, *Supercond. Sci. Technol.* **10** (1997) A11.

- [98] Tonis et al., *Appl. Phys. Lett.* **78** (2001) 3851.
- [99] B. Zhao, X. Wan, W. Song, Y. Sun, J. Du, *Physica C*, **337** (2000) 138
- [100] Y.C. Guo, Y. Tanaka, T. Kuroda, S.X. Dou, Z.Q. Yang, *Physica C* **311** (1999) 65
- [101] B. Zhao, W. Song, X. Wan, Y. Sun, J. Du, *Physica C*, **337** (2000) 145
- [102] M. H. Pu, W. H. Song, B. Zhao, X. C. Wu, Y. P. Sun and J. J. Du *Supercond. Sci. Technol* **14** (2001) 299
- [103] Y.K. Huang, B. ten Haken, H.H.J. Ten Kate, *Physica C*, **309** (1998) 197.
- [104] M. Dhalle, M. Cuthbert, M.D. Johnston, J. Everett, R. Flukiger, B.X. Don, W. Goldaiker, T. Beales, A.D. Caplin, *Supercond. Sci. Technol.* **10** (1997) 721.
- [105] A.E. Pashitski, A. Polyanski, A. Gurevich, J.A. Parrell, D.C. Larbalestier, *Physica C*, **246** (1995) 133.
- [106] Y. H. Li, J. A. Kilner, M. Dhalle, A.D. Caplin, G. Grasso, R. Flukiger, *Supercond. Sci. Technol.* **8** (1995) 764.
- [107] X.Y. Cai, A. Polyanski, Q. Li, G.N. Riley Jr., D.C. Larbalestier, *Nature*, **392** (1998) 906.
- [108] D.C. Larbalestier, J.W.A. Anderson, S.E. Babcock, X. Y. Cai, S. E. Dorris, M. Feldmann, J. Jiang, Q. Li, J.A. Parrell, R. Parella, M. Polak, A. Polyanski, G.N.Riley Jr., M. Rupich, Y.Wu, *Presented at the International Symposium on Superconductivity*, Japan, November 1998.
- [109] J. W. Anderson, J. A. Parrell, M. Polak, D.C. Larbalestier, *Appl. Phys. Lett.* **71** (1997) 3892.

- [110] J.W. Anderson, J.A. Parrell, D.C. Larbalestier, *J. Mater. Res.* (1999).
- [111] J.W. Anderson, X.Y. Cai, M. Feldmann, A. Polyanski, J.Jiang, J.Parrell, D.C. Larbalestier, *Supercond. Sci. Technol.* (1998).
- [112] Y. Aiyama, T. Ageta, *Cryogenics* **41** (2001) 179
- [113] T. Matsushita, *Supercond. Sci. Technol* **13** (2000) 51
- [114] J. Koshy, J. Kurian, P.K. Sajith, K.S. Kumar, R. Jose, A.M. John and A.D. Damodaran, *U.S. Patent* No. 5741747 dated 21.4.1998.
- [115] J. Koshy, J.K. Thomas, J. Kurian, Y.P. Yadava and A.D. Damodaran *U.S. Patent* No. 5856276 dated 5.1.1999.
- [116] J. Koshy, J.K. Thomas, J. Kurian, Y.P. Yadava and A.D. Damodaran *U.S. Patent* No. 6040275 dated 21.3.2000.
- [117] J. Koshy, J.K. Thomas, J. Kurian, Y.P. Yadava and A.D. Damodaran *U.S. Patent* No. 6121206 dated 19.9.2000.
- [118] J. Koshy, J.K. Thomas, J. Kurian, Y.P. Yadava and A.D. Damodaran *European Patent* No. EP 0 679 615 B1 dated 21.7.1999.
- [119] J. Koshy, J. Kurian, P.K. Sajith, K.S. Kumar, R. Jose, M.J. Asha and A.D. Damodaran *European Patent* Appl. 96308464.5-2208 dated 22.11.1996.
- [120] P.F. Hermann, *Hand Book of Applied Superconductivity*, ed. B. Seeber (Bristol: Institute of Physics p801)
- [121] A.J. Rodenbush, D. Aized and B.B. Gamble, Conduction and Vapour Cooled HTS Current Leads (ASC, USA).
- [122] D. Ponnusamy, Z. Li and K. Ravi Chandar, *IEEE Trans. Appl. Supercond.* **5(2)** (1995) 769.
- [123] M.A. Daugherty, F.C. Prenger, D.D.Hill, D.E. Daney and K.A. Woloshun, *IEEE Trans. Appl. Supercond.* **5(2)** (1995) 773.

- [124] J.R.Hull *Cryogenics*, **29** (1989) 1116.
- [125] A. Ballarino, *IEEE Trans. Appl. Supercond.* **9(2)** (1999) 523.
- [126] M. Teng, A. Ballarino, R. Herzog, A. Jspeert, Present at the Applied Superconductivity Conf., July 1997.
- [127] J.L.Wu, *IEEE Trans. Appl. Supercond.* **5(2)** (1995) 777.
- [128] R. Heller, G. Friesinger, A.M. Fuchs, T. Mito, S. Satoh, K. Takahata, M. Tasca, M. Vogel, *Cryogenics*, **41** (2001) 539.
- [129] A. Hobl, D.Krischel, M. Schillo, P. Schafer, J.Bock, S. Gauss, *IEEE Trans. Appl. Supercond.* **9(2)** (1999) 495.
- [130] R. Heller, G. Friesinger, W. Goldacker, M. Quilitz, M. Tasca, A.M. Fuchs, W. Pfister, M. Vogel, *IEEE Trans. Appl. Supercond.* **9(2)** (1999) 507.
- [131] P.F. Herrmann, C. Cottevjelle, A. Leriche and M. Quemener and J. Bock, *IEEE Trans. Appl. Supercond.* **7(2)** (1997) 359.
- [132] S.M. Ting, K.R. Marken Jr., L. Cowey, W.Dai, S. Hong, S.nelson, *IEEE Trans. Appl. Supercond.* **7(2)** (1997) 700.
- [133] J. Le Bars, T. Dechambre, P. Regnier, K. Gagnant, *IEEE Trans. Appl. Supercond.* **9(2)** (1999) 503.
- [134] R.Heller, G. Friesinger,W. Goldacker, H.Kaltiol, B.Ullmann, A.M. Fuchs, B. Jakob, G. Pasztor, G. Vecsey, R.Wesche, *IEEE Trans. Appl. Supercond.* **7(2)** (1997) 692 (60 kA modules).
- [135] J.A. Selvaggi, J.L.Wu, J. Bock, *IEEE Trans. Appl. Supercond.* **5(2)** (1995) 782.
- [136] J.L. Wu, *IEEE Trans. Appl. Supercond.* **5(2)**, (1995) 777.
- [137] A. Ballarino, L. Serio, *Presented at the Particle Accelerator Conference NewYork 1999.*

- [138] A. V. Gavrilin, V. E. Keilin, I. A. Kovalev, S. L. Kruglov, V. I. Scherbakov, I. I. Akimov, D. K. Rakov, A. K. Shikov, *IEEE Trans .Appl. Supercond.* **9(2)** (1999) 531
- [139] R. Heller, J. R. Hull, *IEEE Trans on Appl. Supercond.* **5(2)** (1995) 797
- [140] T. Isono, K. Hamada, T. Ando, H. Tsui, Y. Yasukawa, A. Tomioka, M. Nozawa, M. Konno, K. Sakaki, *IEEE Trans . Appl. Supercond.* **9(2)** (1999) 519
- [141] X. K. Fu, V. Roussac, Y.C. GUO, P.N. Mikheenko, H. K. Liu, S. X. Dou, *Physica C* **320** (1999) 183.
- [142] D. M. Spiller, C. Beuz, M. K. Al-Mosawi, C. M. Friend, P. Thacker, A. Ballarino, *Supercond. Sci. Technol.* **14** (2001) 168
- [143] L. martini, F. Barberis, R. Berti, G. Volpini, L. Bigoni, F. Crucio, *Physica C* **341 - 348** (2000) 2513.
- [144] A. Ballarino, *IEEE Trans Appl. Supercond.* **9(2)** (1999) 523.
- [145] S. Odaka, S. B. Kim, A. Ishinama, Y. Sato, S. Honjo, Y. Iwata, S. Shingo, *IEEE Trans . Appl. Supercond.*
- [146] B. Zeimetz, S. X. Dou, H. K. Liu, *Supercond. Sci. Technol.* **11** (1998) 1091.
- [147] X. Fu, Y. Zhou, W. Lin, P. Hua, R. Zeng, X. Wang, S. Chang, N. Song, P. Ye, G. Yuan, L. Lin, *Physica C* **282 - 287** (1997) 2651.

CHAPTER 2

PREPARATION AND CHARACTERIZATION TECHNIQUES

2.1. INTRODUCTION

Processing of ceramic products with controlled properties is an area where a variety of techniques and instrumental characterization should be made use of. Especially in the case of HTSC tape processing, the stringent demands on phase purity, high degree of grain alignment/microstructure and fragile nature of superconductors make it necessary to monitor the process carefully right from the selection of reactants to the final characterization by employing appropriate techniques. In this chapter, a brief description of various techniques applied during the tape fabrication both in mono and multifilament configuration and characterization are given.

2.2. Preparation of Mono and Multifilamentary tapes

2.2.1 Monofilament tapes

Superconducting BPSCCO/Ag tapes were fabricated using the standard powder-in-tube (PIT) technique. For this, the precursor powder of appropriate phase assemblage and particle size was filled to appropriate packing densities in seamless high purity (99.99%) silver tubes (Pyromet Inc., Pa, USA) of OD = 10 mm and ID = 7-8 mm. These powder filled tubes were closed with silver plugs and sealed. These tubes were then annealed in air at 500°C for 1 h to remove the moisture and adsorbed gases. Mechanical deformation operations were

started with groove rolling of the tubes. A reduction per pass upto 10% was used for rolling the wires to a final diameter of ~ 1.5 mm. Apart from the roller draft (gap between the rollers), the speed of the roller also could be varied. After the groove rolling the wires were flat rolled into tapes. The thickness reduction in the tape rolling stage was upto 5% per pass. Also intermediate annealing was performed at 500°C for 10 to 20 min after every six or seven passes to relieve the stress of the work-hardened sheath. The heat treatment process was started by loading small pieces (2-5 cm) of tapes on high purity alumina substrates. The temperature of the furnace was controlled using programmable temperature controllers (ATHENA XT18/XT16). All the heat treatments were done in the temperature $830\text{-}840^{\circ}\text{C}$ in muffle furnace.

2.2.2. Multifilamentary tapes

For the preparation of BPSCCO/Ag multifilamentary tapes the raw material used was monocoil wires of dia $\sim 0.8\text{-}1.5$ mm. Short pieces of these wires were filled in Ag tubes of diameter I.D. 8.5 mm, O.D. 10 mm. Groove rolling and tape rolling process was applied with intermittent annealing at 500°C for 10-20 min. The heat treatment procedures were similar to that used for the monofilament tapes.

2.2.3. Preparation of Current leads

Current leads were prepared using fully reacted multifilamentary tapes of length >10 cm, width 3-4 mm and thickness ~ 0.3 mm. Sufficient numbers of multifilamentary tapes were housed in a cryostable glass fibre reinforced epoxy for better mechanical rigidity. Ni coated Cu end terminals were soldered to both ends as the interconnectors for ease of integration with superconducting systems.

2.3. Analytical Methods

In the present study, different analytical methods have been adopted for characterizing the samples after various stages of processing. X-ray diffraction technique was employed for phase analysis as well as texture evaluation. Microstructural analysis of the samples was carried out by scanning electron microscopy and optical microscopy. Differential thermal analysis was employed to study the thermal characteristics of the precursor powder.

2.3.1. X-ray diffraction technique

In the present study, X-ray diffraction technique (XRD) [1] was utilized for identifying various crystalline phases formed in the reaction mixture, after various heat treatment conditions. Monitoring the phase assemblage is an important step in optimizing the reaction conditions such as atmosphere, temperature, duration etc. The X-ray diffraction technique was employed to study phase conversion aspects during the powder processing stages and also *in situ* conversion of filled powder to the desired high- T_C phase in the PIT tape processing. Apart from phase analysis, XRD measurements have also been used to assess the texture information (from the sharpness of the basal plane reflections).

In a typical experiment, the powder samples were filled in aluminium sample holders. Care was taken to minimize the preferred orientation/stacking of crystallites which is important owing to the basal plane growth exhibited by the grains of (Bi,Pb)-2212 or (Bi,Pb)-2223 phases. The powder filled sample holder were kept at the centre of a vertical goniometer cell of a PW1710 model Philips Automated Powder Diffractometer with a coupled θ - 2θ mode of Bragg Brentano Geometry.

Step or continuous scans could be made from 3° onwards in 2θ usually at 0.01 degree/step. Most of the scans have been done applying 40kV tube p.d. and 20 mA tube current. Cu K_α radiation (wavelength = 1.5418 Å) β -filtered by Ni has been used for all measurements.

In the case of tapes, the powder was taken out by chemical etching off the sheath by a solution containing 30 vol% H_2O_2 and 50 vol% NH_4OH in equal volumes. The chemical etching was applicable only in the case of pure Ag sheath. For alloy sheathed tapes mechanical peeling off the sheath is done. As the amount of powder thus obtained was less it required the use of an appropriate sample holder and the entry slit width was to be reduced for restricting the beam on the sample area. This caused a decreased overall intensity count that was compensated by performing slower scans. The phase analysis was done by comparing the patterns with those given in JCPDS (Joint Committee for Powder Diffraction Standards) as well as literature.

2.3.2. Microstructural analysis

While XRD is a powerful method to assess the average phase assemblage within the reacting mixture, specific properties like transport J_c are more dependent on the inter and intra-granular structural details. Grain morphology, orientation, size and size distribution are all important parameters in gaining an understanding on the process dependence of properties of materials in general. When second phase materials either desirable in small amounts or are difficult to eliminate completely, often XRD methods fail in detecting them especially when such phases are not constituted by electron dense atoms. On the other hand, the distinct morphology, size and reflectivity characteristics of

different phases get manifested under microscopic examination thereby aiding not only the identification but also quantification of such small fractions of impurity phases.

2.3.3. Scanning Electron Microscopy (SEM)

In the present study, the scanning electron microscopy (SEM), in the back-scattered mode, has been performed mainly on superconducting core of Ag/BPSCCO tapes. A JEOL JSM 5600LV is used for this purpose. The operating voltage generally used was 15 kV and the magnification range to 500-15000. The features sought during SEM examination were (a) differences in grain morphology, suggesting the nature and growth of second phase grains and (b) the size and alignment of grains in superconducting core of the tapes. Samples were prepared by fixing fresh fractured as peeled core material of the tape using silver paste on brass stud. After curing the paste, a thin gold coat was given on the surface using vacuum coating unit.

2.3.4. Optical Microscopy

While SEM was used for the analysis of microstructure including the grain morphology and texturing optical microscope was used for the analysis of the morphology of the mono and multifilamentary tape as a whole. Factors such as filament breaking, non-uniformities occurred during the mechanical deformation process (sausaging etc) can be obtained with the help of a low magnification optical microscope (Olympus SZPT). Samples were prepared by mounting the tape samples on a mould of polyester resin. After curing the samples were polished using a polishing machine and the polished surface was viewed under the microscope.

2.3.5. Thermal Analysis

Differential thermal analysis was conducted for studying the reactions taking place in the precursor powder and to fix the heat treatment temperature of the tapes [3-5]. Supported by XRD phase analysis DTA can help both in establishing the reaction pathway and in optimizing the heat treatment temperature for the formation of a desired phase.

In the present study, DTA was employed in determining the relevant temperature ranges required for the processing. DTA analysis of the precursor powders was carried out in air from room temperature (RT) to 900°C at a heating rate of 10°C/min. The DTA instrument used was Shimadzu DTA 50.

2.4. Superconductivity Measurements

Superconducting state of the samples was characterized by resistance temperature measurements for determining the critical temperature and width of transition. The other characterization techniques involved were measurements of critical current density and its dependence on applied magnetic fields and orientation, voltage current characteristics etc. Also the strain tolerances of the tapes both in axial and bend strains were studied. In the present study, all the superconductivity measurements were done at liquid nitrogen temperature (77 K).

2.4.1. J_C Measurement

Traditionally two different types of J_C have been defined and studied in superconductivity measurements. The magnetic J_C is to be

calculated from DC magnetization of hysteresis measurements of a fixed temperature and slow field sweep. The formula connecting the hysteresis loop opening ΔM and J_C involves assumptions on $J_C(H)$ dependencies collectively known as critical state models. Also geometry of sample comes into the formula. A more meaningful measurement from application side is the measurement of *transport* J_C . The measurement method is *four probe method* as described below.

The basic principle behind critical current measurements is the same as that for four terminal resistance measurements. The current is applied to the sample by means of current contacts at both ends, and the voltage is measured across a pair of taps positioned along the length of the sample. The current is slowly increased from zero and the voltage across the taps is monitored. Eventually a $V - I$ (or equivalently and $E - J$) characteristic is measured. After getting the $V - I$ plot at the required temperature, a criterion is used for defining J_C . In the electric field criterion, J_C is defined as the current density which develops a fixed value of electric field (usually $1\mu\text{Vcm}^{-1}$) on the surface of the superconductor. Sometimes, the resistivity criterion viz. defining J_C to be that current density which causes a pre-fixed resistivity (usually around $10^{-12} \Omega\text{cm}$) developed in the tape is also used. Moreover it is also important to state that whether the J_C measurement is done in a pulsed configuration or continuous configuration.

In the present study, the schematic diagram of the set up used for J_C measurement is given in Fig.2.1.

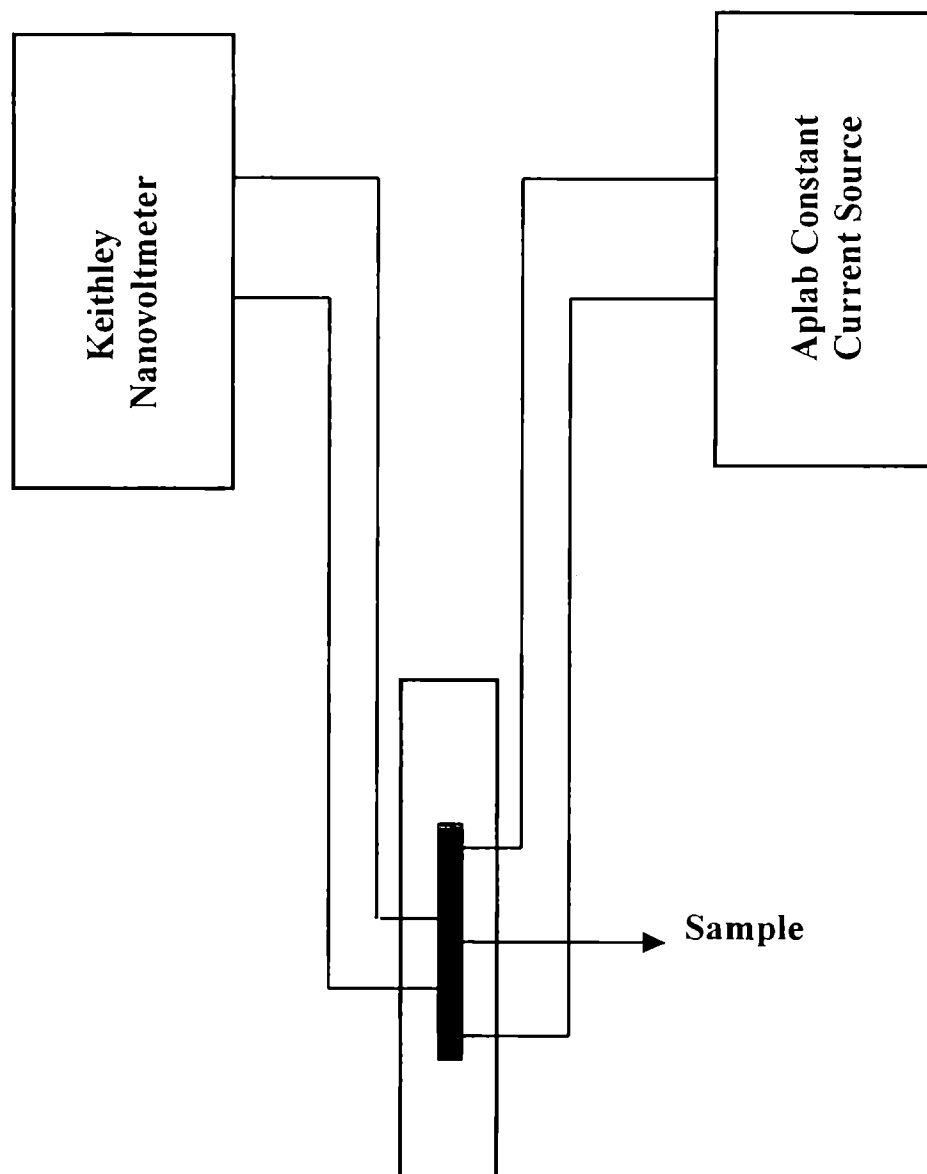


Fig. 2.1 Schematic Diagram showing the four probe connection used for J_C measurements. The samples were immersed in liquid nitrogen and the measurements were taken using appropriate software and are fully automated.

Current was driven from an Aplab (India) programmable current source. Voltage across the voltage tapes was measured using a Keithley 181 nanovoltmeter. Measurements were carried out using appropriate

software and interfaced to a computer with GPIB (National Instruments, USA) interface card.

Current leads and voltage taps were directly soldered on to the sample being tested for I_C . Currents were applied in intervals of 10 sec, samples being short in length, steady state attainment followed quickly without complication like equilibration time which is important in long length characterization.

2.4.2. V-I. or E-J. characteristics

The voltage versus current (V-I) or electric field versus current density (E-J) characteristics is an important measurement for superconductor characterization. The non-linear relationship between V and I in high- T_C superconductors has been studied in detail by many groups using power law dependence of the form

$$V = KI^\alpha$$

where K is a constant and α is a function of applied magnetic field and temperature.

The occurrence of power law behaviour has been ascribed to the collective mixture of strongly correlated fluxoids under a large thermal disorder and pinning potential [4]. The strongly pinned conventional superconductors such as NbTi and Nb₃Sn showed a nearly power law V-I behaviour with α varying from 15 to 70 [5]. For HTSC, α ranges from 30 at 77 K up to 70 at 4.2 K in low magnetic fields [4, 6-8]. The higher values of α , the sharper the take off in the V – I characteristics at the critical current.

2.4.3. J_c -B measurement

Dependence of critical current density on applied magnetic field is a very important characteristic. At low field strengths, the measurements may yield information on weak links. At intermediate strengths information on intragranular flux pinning and in slurry fields (which is the most important aspect in magnet applications) information on flux lattice melting can be obtained. The set up used for the measurements of $J_c - B$ characteristics are shown schematically in Fig.2.2. Magnetic field is produced using a pair of electromagnets cored with iron. The field generated was calibrated using a hall probe (Lakeshore – Gauss meter). Fig. 2.3 shows the photograph of the magnets used for the set-up.

2.4.4. Measurement of $I_c - \sigma$ and $I_c - \varepsilon$ (Mechanical properties)

The stress tolerance and strain of BPSCCO/Ag composite tapes are two important parameters considering the applications of long length BPSCCO/Ag tapes for high current cables or in magnet applications. In the present investigation I_c dependence on tensile stress (tensile loading) was studied using a home designed set-up with the provision for holding the sample in the vertical mode (Fig. 2.4). Suitable guide bushes were provided in the vertical shaft (stainless steel rod); from which the stress is transferred to the sample; to avoid lateral stresses. Sample is soldered to the sample holder (copper blocks) and the current terminals were insulated using teflon blocks. The flexibility of the design is that I_c

measurements can be done in the on load condition with the sample in the liquid nitrogen bath.

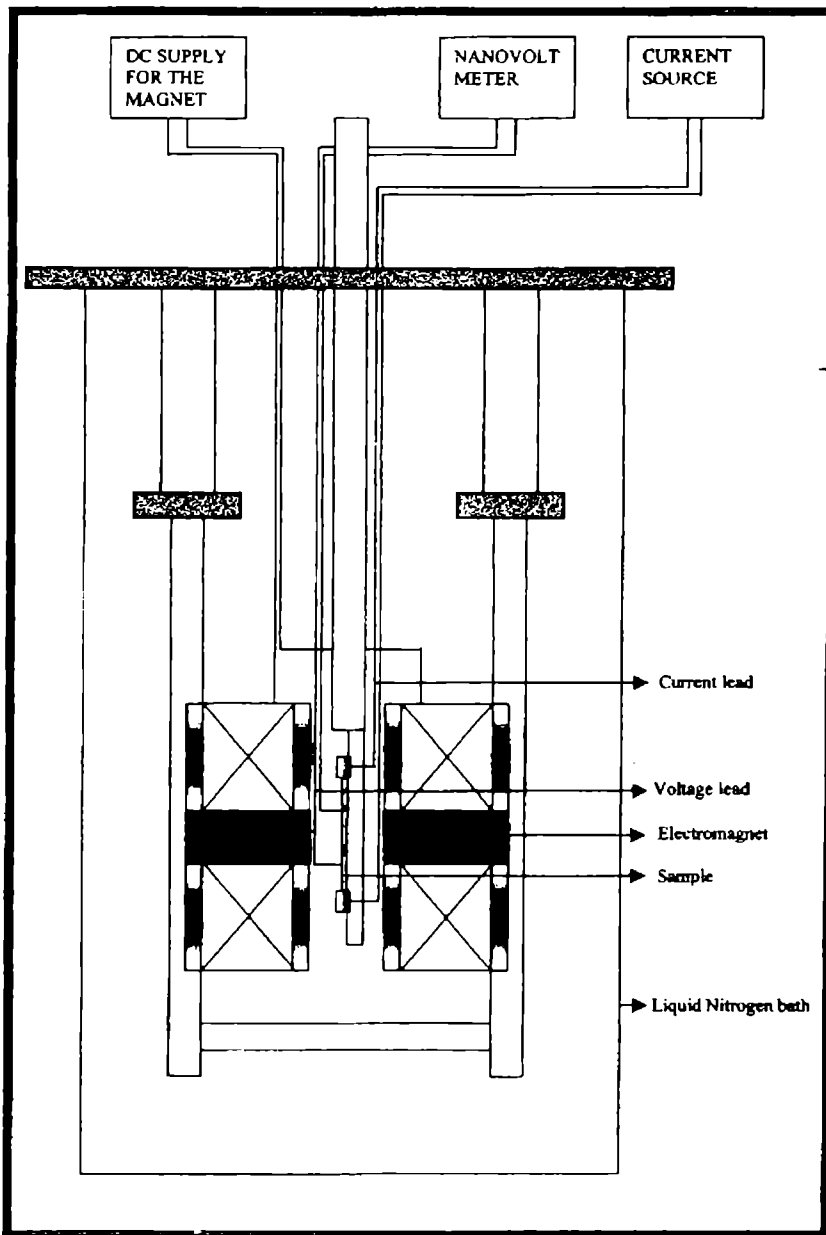


Fig. 2.2 Schematic diagram of the set-up used for J_c -B measurement

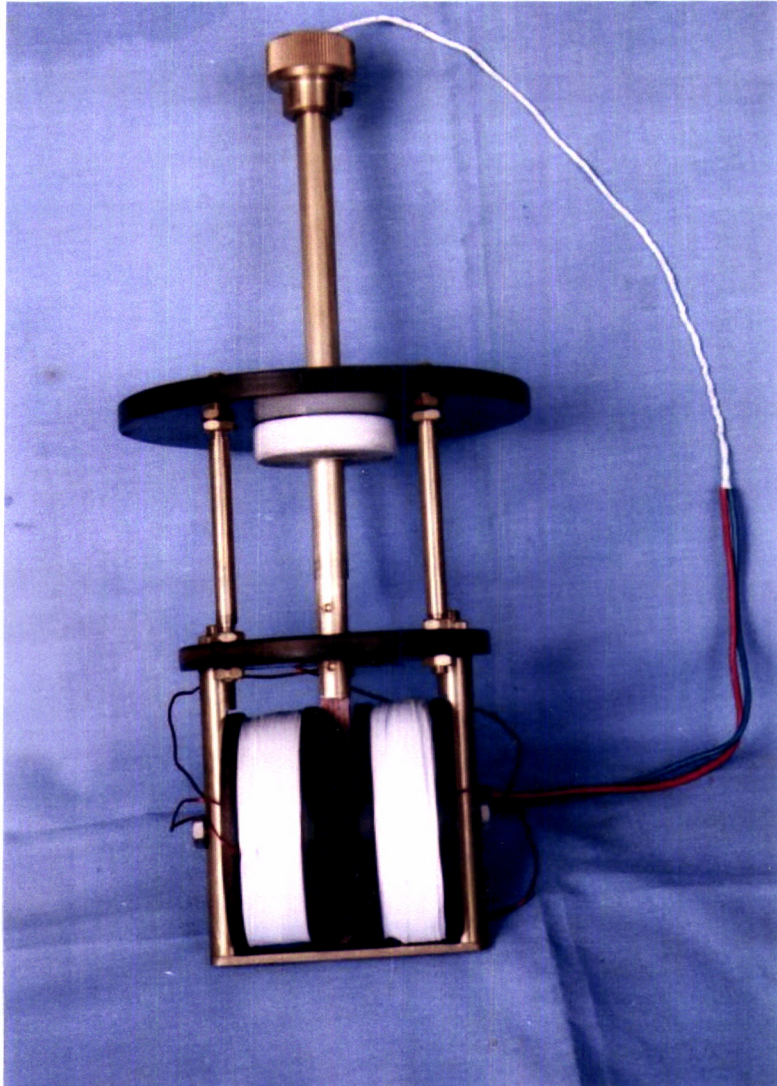


Fig. 2.3 Photograph of the magnets used for the J_C -B measurement

I_C dependence on bending strain was studied by bending the samples onto different cylindrical mandrels of predetermined radii and measuring the I_C in the bend state. I_C measurements were done at 77 K, 0 T with $1 \mu\text{Vcm}^{-1}$ criterion. The bending radii were selected from lower strain percentages to values above ϵ_r .

1. Guide bushes
2. Stainless steel rod
3. Insulating Teflon block
4. Current terminal
5. Sample holder
6. Space for sample
7. Liquid nitrogen bath
8. Load

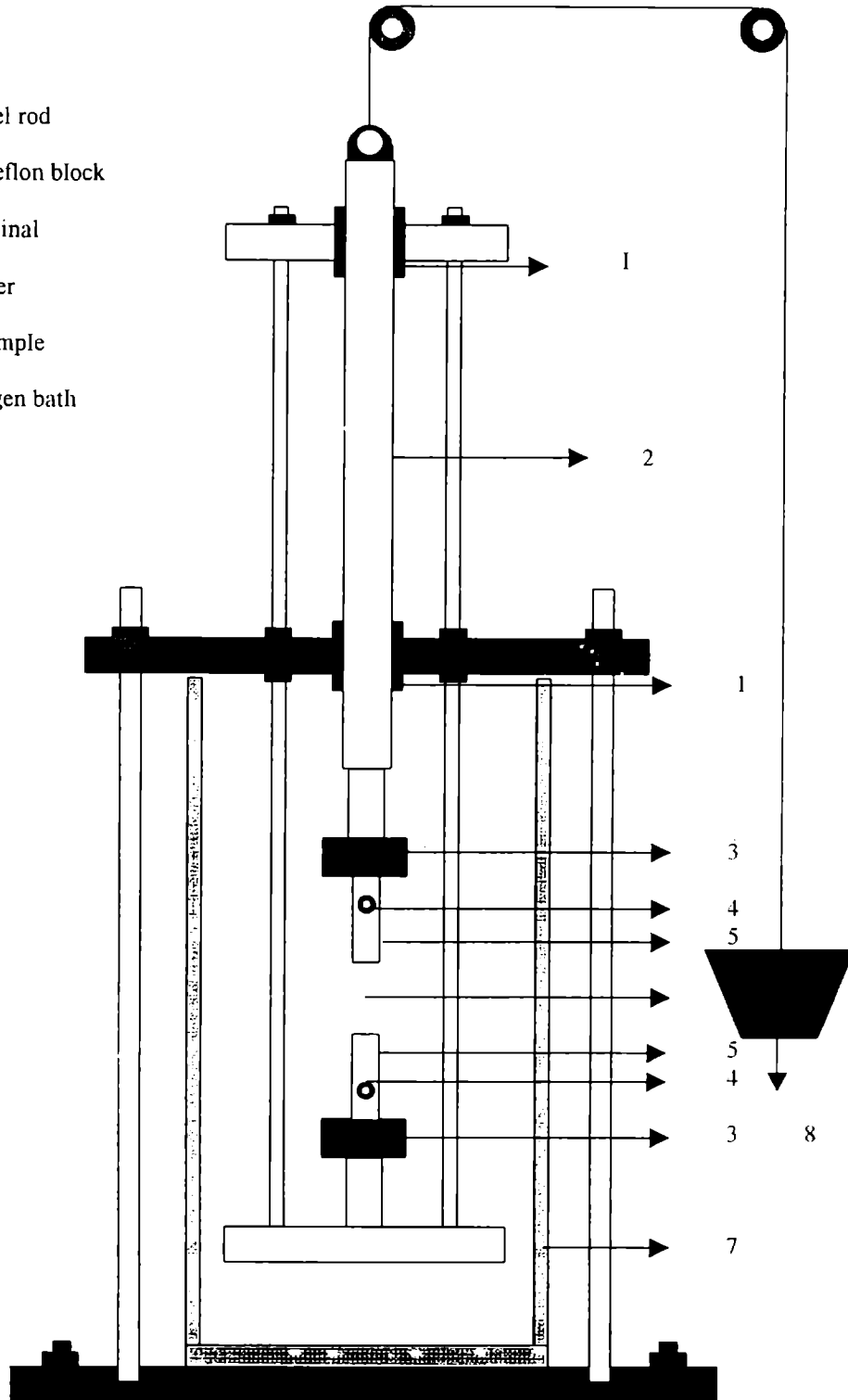


Fig.2.4. Schematic diagram of the I_c - σ measurement

2.5. Conclusions

The major experimental facilities and techniques used for the preparation of mono and multifilamentary (Bi,Pb)-2223/Ag tapes have been reviewed in the present chapter. Like any other modern ceramic system targeted for controlled properties, a rigorous analysis of phase, morphology and reaction kinetics is demanded by the system under investigation. The present study utilized techniques such as x-ray diffraction, electron microscopy and thermal analyses for studying these fundamental aspects. On the other hand the final product, viz. the superconducting tapes have been characterized employing J_C , J_C -B, J_C - σ , J_C - ε measurements.

References

- [1] H.P. Khrhg and L.E. Alexander, “*X-ray Diffraction Procedures*” (John Wiley & Sons, New York, 2nd edn., 1974).
- [2] W.W. Wendlandt, “*Thermal Methods of Analysis*” (Interscience Publishers, New York, 1964).
- [3] T. Onogi, T. Ichiguchi and T. Aido, *Solid State Commun.*, **69** (1989) 991.
- [4] E. Evetts and B.A. Gloacki, *Cryogenics* **28** (1998) 641.
- [5] M. Ban, T. Ichiguchi and T. Onogic, *Phys. Rev. B* **40** (1989) 4419.
- [6] J.W. Ekin, H.R. Hart Jr. and A.R. Gaddipati, *J. Appl. Phys.*, **68** (1990) 2285.
- [7] T. Fukami, T. Yamamoto, T. Nishizaki, Y. Horie, F. Ichikawa, T. Somine, E. Hulguin and L. Rinderes, *Solid State Commun.*, **83** (1992) 605.
- [8] A. Oota, H. Matsui, M. Funakura, J. Iwaya and K. Mitsuyama, *Physica C*, **210** (1993) 489.

CHAPTER 3

STUDIES ON ALTERNATE SHEATH ALLOYS FOR THE PREPARATION OF (Bi, Pb)-2223/Ag TAPES

3.1. Introduction

Ag is used as the sheath material for fabrication of (Bi,Pb)-2223/Ag tapes due to its advantageous roles such as having no detrimental effect on the superconducting properties [1-7], promotion interfacial (superconductor-silver) grain growth and grain alignment. But while considering the application of (Bi,Pb)-2223/Ag tapes into devices such as coils, magnets, cables, current leads etc. the mechanical and electrical properties of Ag are the origin of many disadvantages. The strength and stiffness of the sheath material, which are very low for pure Ag, especially after long duration sintering stages, are insufficient to withstand the large Lorentz forces (in magnet applications).. The low electrical resistivity causes eddy current losses in a.c. applications. Also the high thermal conductivity of Ag is a crucial problem for application of (Bi,Pb)-2223/Ag tapes as current leads.

In order to encounter the drawbacks of pure Ag researchers have been trying the feasibility of using several silver rich alloys as sheath materials. To list some of them are Ag-Cu, Ag-Mg, Ag-Au, Ag-Mn, Ag-Mg-Pd, Ag-Au-Mg [8]. Despite the serious efforts made by various groups on Ag-alloys the J_C of the tapes using these alloys are found to be lower than those using pure Ag [9]. This may be due to the interaction between alloying elements and superconducting phases as

well as the difficult compromise to keep features of silver, whilst simultaneously improving the electrical and mechanical properties.

The present chapter gives the results on our investigation on Ag-Cu and Ag-Au alloys as alternate sheath materials. For the Ag-Cu system the investigation is concentrated to find the optimum doping percentage of Cu in the alloy with respect to the Cu stoichiometry in the precursor powder.

3.2. Superconducting Properties

3.2.1. Experimental

(a) Alloy Preparation

Both Ag-Cu and Ag-Au alloys were prepared by the melt cast process. The Cu% was varied from 0 to 12 at% while the Au% was varied from 0 to 6 at%. In order to ensure homogeneity of alloys a master alloy of each was prepared first with 20 wt% Cu and Ag was added to the master alloy to obtain Ag-Cu alloys of composition: Ag-3 at% Cu, Ag-6 at% Cu, Ag-9 at% Cu, Ag-12 at% Cu and Ag-Au alloys of composition: Ag-1 at% Au, Ag-3 at% Au, Ag-6 at% Au. The alloy ingots were cold worked and machined to obtain Ag-Cu and Ag-Au alloy tubes of 6.8/4.8 mm OD/ID. The purity of all the metals used was 99.99%.

(b) Tape preparation

The tape preparation procedures are the same as described in Chapter 2. In order to study the effect of Cu alloying on the Cu composition in the precursor it has been decided to use two precursors

of slightly lower and higher Cu contents compared to the optimum for pure Ag sheath. Our experience with BPSCCO system has shown that a stoichiometry of $\text{Bi}_{1.8}\text{Pb}_{0.4}\text{Sr}_2\text{Ca}_{2.2}\text{Cu}_{3.1}\text{O}_x$ is the optimum for pure Ag sheath with regard to the final phase purity and J_c . Thus the stoichiometries selected for Ag-Cu alloy system were $\text{Bi}_{1.8}\text{Pb}_{0.4}\text{Sr}_2\text{Ca}_{2.2}\text{Cu}_{3.0}\text{O}_x$ (designated as copper deficient – CD), and $\text{Bi}_{1.8}\text{Pb}_{0.4}\text{Sr}_2\text{Ca}_{2.2}\text{Cu}_{3.2}\text{O}_x$ (designated as copper rich – CR). For Ag-Au alloys precursor with the optimum composition was only used. The list of samples prepared together with their labeling (for further discussion) is given in Table 3.1. Precursor powders were filled in Ag-Cu and Ag-Au alloy tubes with a packing density of 3.2 g cm^{-3} . The final tape thickness prior to the first stage sintering is $280 \mu\text{m}$.

Table 3.1. List of samples prepared for Ag-Cu and Ag-Au alloys

Doping level of Cu in alloy (at%)	Tubes	Labeling for samples	
		CD (Cu: 3.0)	CR (Cu: 3.2)
12	AgCu12	CD12	CR12
9	AgCu9	CD9	CR9
6	AgCu ₆	CD6	CR6
3	AgCu ₃	CD3	CR3
0	Ag	CDAG	CRAG
Doping level of Au in alloy (wt%)			
6	AgAu6	Au6	
3	AgAu3	Au3	
1	AgAu1	Au1	
0	Ag	Au0	

(c) Heat treatment and temperature optimization

As two Cu stoichiometries were used for Ag-Cu alloy tapes, the optimum heat treatment temperatures will be different for the two

precursors. Differential thermal analysis (Shimadzu DTA 50) of the two precursors were carried out to estimate the difference in sintering temperature. However, a preliminary experiment was conducted to determine the actual sintering temperatures for both the precursors using the undoped samples CDAg and CRAg. For this purpose the samples were heat treated at temperatures from 828 to 840°C with an interval of 2°C. The total duration was 250 h, divided into five stages each being 50h and three intermittent rolling steps. The final tape thickness was 130-140 μm . To ensure temperature accuracy, heat treatment was performed in a pre-calibrated gradient furnace.

The same heat treatment schedule and rolling procedure was performed for the CD and CR series of Ag-Cu alloy sheathed samples except that CD and CR series samples were heat treated in separate batches at 833°C and 829°C (judging from the preliminary experiment) respectively in a large volume muffle furnace with a flat temperature profile and with a temperature stability and accuracy better than $0\pm 1^\circ\text{C}$.

The Ag-Au alloy sheathed samples were heat treated in the same furnace but at a temperature of 831°C. All other conditions remain the same.

The phase evolution of the samples at each stage of heat treatment was studied by an automated powder X-ray diffractometer (Philips PW 1710) using Cu $K\alpha$ radiation. Samples for the XRD were prepared by peeling off the sheath and grinding the core material taken from the tape. The volume percentages of the different phases were estimated from the integrated peak intensities of the respective phases such as Bi-2223 ($2\theta = 28.8$), Bi-2212 ($2\theta = 27.5$), Bi-2201 ($2\theta = 29.8$), Ca_2PbO_4 (2θ

=17.8), CuO ($2\theta = 38.8$) and Ca_2CuO_3 ($2\theta = 36.4$). The four probe method with a criterion of $1 \mu\text{Vcm}^{-1}$ was used to measure I_c of the samples at 77 K, 0 T.

3.2.2. Results and discussion

I. Ag-Cu alloy system

(a) Optimization of sintering temperature for the precursors CD and CR

Fig 3.1 shows the DTA plots of the precursors. The DTA plots have been taken at a heating rate of $10^\circ\text{C}/\text{min}$ in static air atmosphere. Two endotherms are visible for both the precursors at temperatures of 858.1°C and 876.0°C for CD and 854.6°C and 872.8°C for CR. These endotherms correspond to the formation of the liquid phase and melting of the (Bi,Pb)-2212 phase [10,11]. From this, it can be adjudged that the reaction temperature of the two precursors differs by about 4°C and is lesser for the CR precursor. This can be attributed to the higher Cu content in the CR powder.

The J_c values at different stages of heat treatment for the CD_{Ag} and CR_{Ag} samples as a function of temperature are plotted in Fig.3.2. After 150 h of heat treatment, peak J_c values are visible for CR_{Ag} at 834°C and CD_{Ag} at 838°C . But after 200h of heat treatment, the peak J_c values shift to 832°C for CR_{Ag} and 836°C for CD_{Ag}. A maximum J_c of $34.3 \text{ kA cm}^{-2}/832^\circ\text{C}$ for CR_{Ag} and $30.6 \text{ kA cm}^{-2}/836^\circ\text{C}$ for CD_{Ag} was observed after the last stage (250 h) of heat treatment. This suggests that the optimum sintering temperature for CR_{Ag} is somewhere around 832°C and for CD_{Ag} is 836°C . This very well agrees with the DTA result that the reaction temperature of CR powder is lesser by about 4°C .

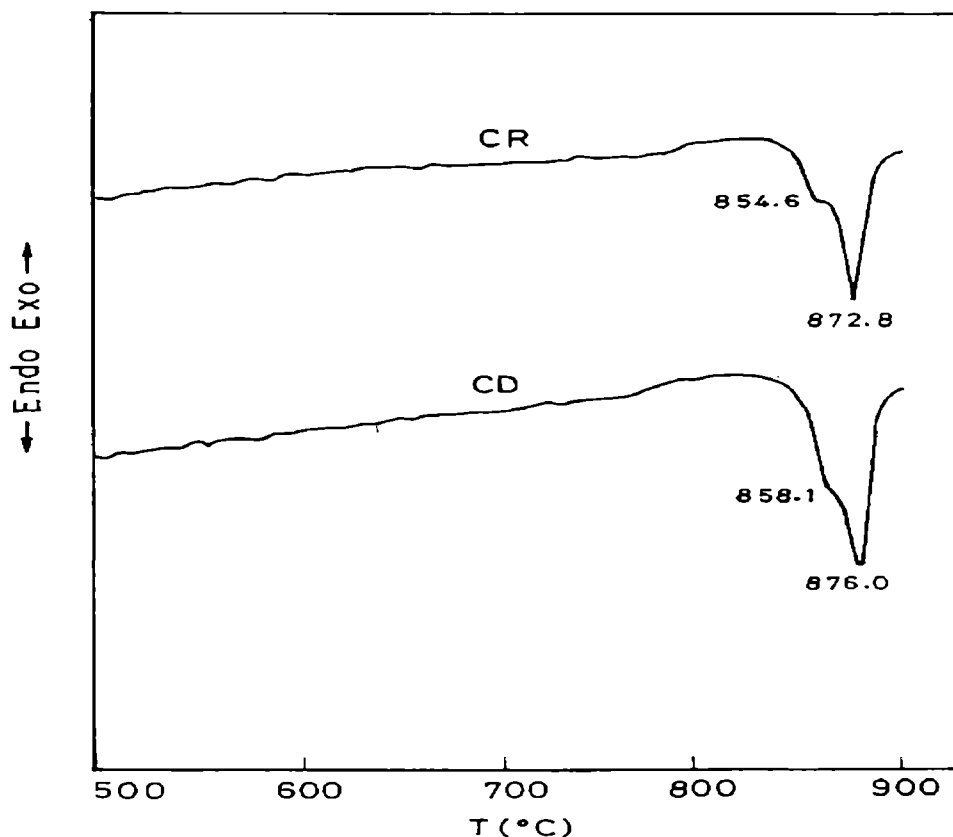


Fig. 3.1 DTA plot of the precursors CD and CR

Nevertheless, presence of Cu in the sheath can cause slight changes in the sintering temperatures of the alloy-sheathed tapes. Based on the fact that low Cu fractions reduces the melting point of Ag in the Ag-Cu binary alloy system (M.P. of Ag: 961°C, M.P. of Cu: 1083°C, eutectic temperature of Ag-Cu: 779°C and eutectic composition: 28.1 wt% Cu) we have chosen two common optimum sintering temperatures, viz. 829°C for CR and 833°C for CD series, which are 3°C less than the optimum temperatures determined for pure Ag sheathed tape samples.

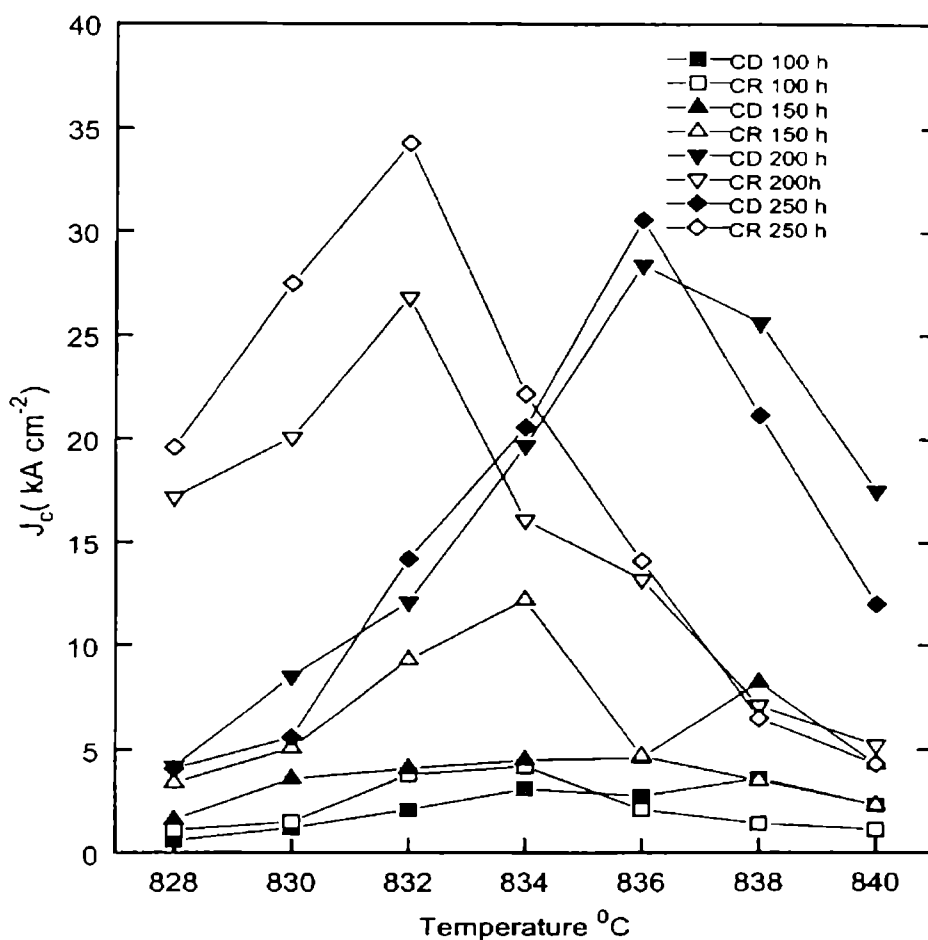


Fig. 3.2. J_c variation as function of sintering temperature for CDAg and CRAg samples for different durations of heat treatment

b. Phase evolution study

The phase fraction calculations were based on the relation

$$F_x = I_x / \Sigma I$$

where F_x , is the phase fraction of the phase x , I_x , the integrated peak intensity of x and ΣI is the sum of the integrated peak intensities of all the phases present. The integrated peak intensity of a particular phase was measured by selecting a representative peak of the phase (as described earlier under Section 2) from the XRD pattern using appropriate software [12,13].

Table 3.2. Phase assemblage of the precursor with Cu stoichiometries of 3.2 (CR) and 3.0 (CD)

Phases	Volume percentage	
	CR	CD
Bi-2223	0	0
Bi-2212	55.9	55.7
Bi-2201	19.4	12.6
Ca ₂ PbO ₄	19.1	31.7
CuO	5.6	-

Table 3.2 gives the phase fractions in the two precursors CD and CR. The volume percentage of Bi-2212, which is the main phase, is almost same in both the precursors while the level of Ca₂PbO₄, which is the next significant phase, is higher in CD (31.7%) than in CR (19.1%). Correspondingly, the level of Bi-2201 is higher in CR (19.4%) compared to CD (12.6%). CuO in CR precursor is estimated to be 5.6%, whereas that in CD is below the detectable limits.

Table 3.3 gives the volume percentage of all the phases in CR samples at the different stages of heat treatment. The phases detected are Bi-2223, Bi-2212, Ca₂PbO₄, CuO and Ca₂CuO₃. In pure Ag sheathed sample (CRAg) Bi-2201 was detected (2.94 vol%) after 50 h of sintering.

The volume percentage of Bi-2223 as a function of sintering time is plotted in Fig.3.3. The Bi-2223 fraction formed after 50h of sintering is found to increase with increase of Cu content in the sheath. At this stage, the formation of Bi-2223 in CR12 sample is almost double (30.45%). However, as the heat treatment progresses the trend slowly

get reversed as can be seen from the plots in Fig.3.3. At the 150 h stage, the fraction of Bi-2223 is found to be the highest in pure Ag-sheathed

Table 3.3. Phase assemblage of CR series samples at different stages of heat treatment. Bi-2201 was detected at 50 h duration (2.94 vol%)

Sample	Phases	Volume percentage of different phases				
		Duration of heat treatment				
		50 h	100 h	150 h	200 h	250 h
CR12	Bi-2223	30.42	36.50	59.00	69.09	72.30
	Bi-2212	48.32	40.83	21.56	10.27	11.07
	Ca ₂ PbO ₄	15.86	14.87	10.24	13.09	8.43
	CuO	3.40	5.60	6.20	6.40	6.80
CR9	Bi-2223	24.04	31.55	62.50	70.51	75.50
	Bi-2212	56.22	45.40	20.80	10.45	10.46
	Ca ₂ PbO ₄	12.40	18.35	9.00	10.14	8.51
	CuO	4.89	3.40	5.4	8.01	4.54
CR6	Bi-2223	20.56	34.35	66.25	73.20	78.25
	Bi-2212	66.04	48.96	16.78	11.28	6.52
	Ca ₂ PbO ₄	6.53	2.41	1.67	1.09	1.25
	CuO	-	2.58	3.20	3.93	5.22
	Ca ₂ CuO ₃	6.53	2.41	1.67	1.09	1.25
CR3	Bi-2223	16.89	37.50	68.6	75.72	82.61
	Bi-2212	61.00	45.06	13.00	9.18	5.13
	Ca ₂ PbO ₄	12.28	10.62	15.60	9.68	7.0
	CuO	4.57	4.02	2.70	4.46	3.80
	Ca ₂ CuO ₃	5.26	2.80	1.60	0.96	1.46
CRAg	Bi-2223	15.45	33.4	70.4	80.96	85.76
	Bi-2212	61.91	52.19	17.74	8.09	8.08
	Ca ₂ PbO ₄	11.47	10.3	7.30	5.30	3.23
	CuO	4.41	1.89	2.46	3.14	1.63
	Ca ₂ CuO ₃	3.81	2.22	2.10	2.51	1.30

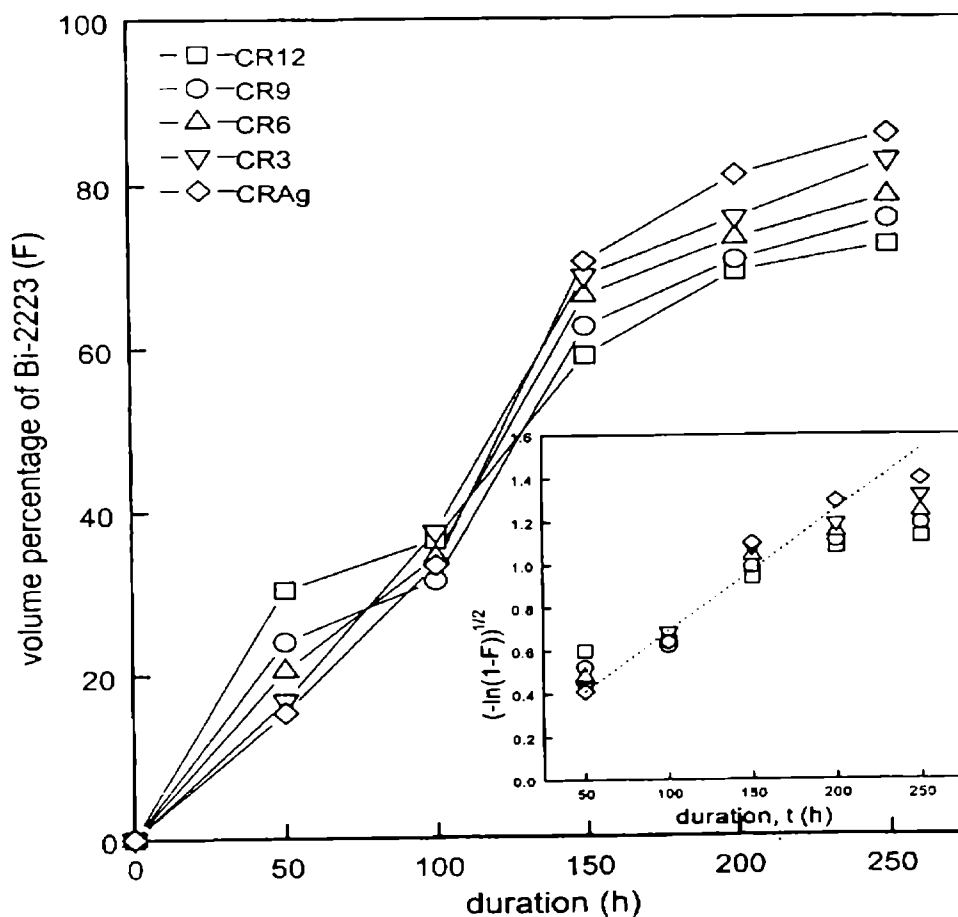


Fig. 3.3 Variation of the volume fraction of Bi-2223 as a function of sintering time for CR series samples

tape (70.4%), whereas that in CR12 sample is only 59.0%. This trend continues in the subsequent heat treatment stages and after 250 h the pure Ag sheathed sample, i.e. CRAg yields the highest volume percentage of Bi-2223 fraction (82.6%). It should be noted that none of the samples in CR series shows any deterioration of Bi-2223 phase growth even up to the last stage of heat treatment.

It is noticeable that CuO and Ca_2CuO_3 are detected in pure as well as the Cu doped samples but the amount of these secondary phases is more in Ag-Cu alloy sheathed samples. The highest percentage of CuO

after 250 h is seen in CR12 which is 6.8% while the CRAg shows only 1.63% of CuO. The increased amount of CuO seen in Ag-Cu samples may be due to the diffusion of Cu from the sheath into the core.

The volume percentage of all the phases at the different stages of heat treatment for the CD samples is given in Table 3.4. The phases present in this series are Bi-2223, Bi-2212 and Ca_2PbO_4 . CuO is detected in CD12 sample from the 100 h stage onwards. The volume fraction of Bi-2223 as a function of sintering time is plotted in Fig. 3.4.

Table 3.4. Phase assemblage of CD series samples at different stages of heat treatment

Sample	Phases	Volume percentage of different phases				
		Duration of heat treatment				
		50 h	100 h	150 h	200 h	250 h
CD12	Bi-2223	45.45	63.55	72.40	80.21	74.6
	Bi-2212	44.92	19.54	16.90	12.1	6.00
	Ca_2PbO_4	9.63	13.10	8.20	5.62	13.2
	CuO	-	3.81	4.20	4.40	6.2
CD9	Bi-2223	42.50	68.55	74.30	84.21	75.6
	Bi-2212	43.66	22.47	16.48	9.59	13.58
	Ca_2PbO_4	13.84	8.98	9.22	5.20	10.82
CD6	Bi-2223	24.56	70.94	83.40	87.8	81.61
	Bi-2212	65.50	13.96	7.67	5.90	10.19
	Ca_2PbO_4	9.94	15.11	8.93	6.30	8.20
CD3	Bi-2223	20.49	69.82	84.50	86.5	85.76
	Bi-2212	68.59	15.09	6.18	4.88	7.30
	Ca_2PbO_4	10.97	15.09	6.18	4.88	7.30
CDAg	Bi-2223	19.6	40.4	67.5	77.4	83.4
	Bi-2212	66.00	47.16	22.27	14.2	6.78
	Ca_2PbO_4	14.40	12.44	10.23	8.40	9.82

As in the case of CR samples, the fraction of Bi-2223 after the 50 h of sintering in CD12 sample is more than double compared to CDAg

sample and there is a significant increase in the content of Bi-2223 as the Cu content in the sheath increases (Table 3.4). After 100 h of heat treatment, a peak Bi-2223 percentage of 70.94 is obtained for CD6 and

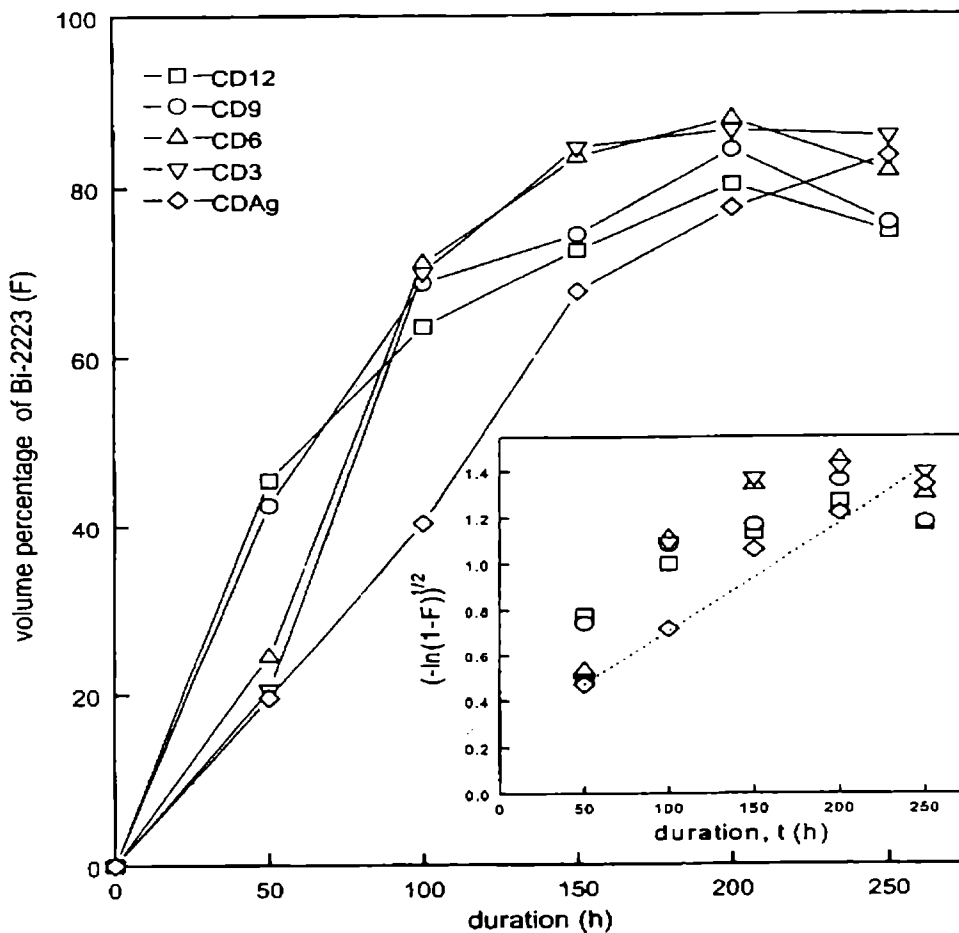


Fig. 3.4. Volume percentage of Bi-2223 at different stages of heat treatment for CD series samples

comparable percentages are also seen for CD9 and CD3 samples (68.55% for CD9 and 69.82% for CD3). The pure sample CDAg shows only 40.4% of Bi-2223 which is far less than the least for the Ag-Cu sample (63.55% for CD12 sample). After the 150 h stage, the peak percentage of Bi-2223 (84.5%) is seen for the CD3 which is the least Cu doped one and a similar result for CD6 is also seen where the volume

percentage of Bi-2223 is 83.4. After 200 h of heat treatment, the peak percentage of Bi-2223 is seen for CD6 (87.8%) and CD3 shows 86.5% of Bi-2223. At this stage also, the least volume fraction of Bi-2223 is yielded by the undoped sample (77.4%) and the highest Cu doped sample shows 80.21% of Bi-2223. After 250 h of heat treatment, the phase growth of Bi-2223 in all the Ag-Cu samples shows a degrading trend. The ultimate volume percentage in CDAg is 83.4, which is comparable with the peak percentage seen at this stage (85.76% for CD3). It is noticeable that 6.2% of CuO is detected in CD12 after 250 h of heat treatment. This can be attributed to the excessive diffusion of Cu from the sheath to the core.

It is observed that the rate of formation of Bi-2223 in all the Ag-Cu sheathed samples (both in CD and CR) during the initial stages of heat treatment (0-50 h) is much higher than the pure Ag sheathed samples and the rate increases with Cu content in the sheath. The higher rate of conversion of Bi-2223 from Bi-2212 and other secondary phases can be due to the higher Cu content in the sheath. Cu atoms available in the sheath can diffuse into the core creating excess Cu sites in the system and can promote the conversion of the double Cu-O layers in Bi-2212 to triple Cu-O layers (Bi-2223), which is assisted by the liquid phase formed during the sintering process.

A notable point at this stage is that despite higher Cu content in CR series samples, the rate of growth of Bi-2223 is slower in CR compared to CD series samples (0-200 h). This can be explained by taking into account the fraction of Ca_2PbO_4 present in the precursors, which is the main ingredient for the formation of the liquid phase [14].

The level of Ca_2PbO_4 in CR precursor is much less than that of CD powder (Table 3.2) but both having approximately the same amount of Bi-2212. A higher fraction of Ca_2PbO_4 in the CD precursor facilitates a larger fraction of the liquid phase at the initial stages of heat treatment, which will ease the diffusion of Ca^{2+} and Cu^{2+} ions favouring the reaction rate.

The insets shown in Figs.3.3 and 3.4 are the plots of $[-\ln(1 - F)]^{1/2} = kt$, the proposed rate equation for the formation of high-Tc phase in (Bi,Pb)-2223/Ag tapes by Hu et al. [15], for CR and CD series of samples. They have suggested a two-dimensional nucleation (random) growth model, $F = 1 - \exp(-k^2t^2)$ where F is the conversional fraction of Bi-2223, t is the sintering time and k is the rate constant. It is clear from these figures that the reaction kinetics of the undoped samples CDAg and CRAg follow the two-dimensional nucleation growth model, whereas deviations from this model can be observed for the entire Ag-Cu alloy sheathed samples.

c. Critical current density of the tapes

The critical current densities of the CR and CD samples as a function of Cu composition in the sheath are plotted in figs.3.5 and 3.6 for the sintering time from 100 to 250 h. It is thought that the volume percentage of Bi-2223 is the main factor that determines the amount of critical current density [15] of Bi-2223/Ag tapes. This is very evident if we observe the figures 3.5 and 3.6, i.e., as the sintering time precedes the critical current density increases suggesting a direct correlation of the latter with the amount of Bi-2223. In the discussion to follow, we

will attempt to analyze the observed J_c results with regard to the volume fraction of Bi-2223 and its dependence on the Cu doping in the sheath.

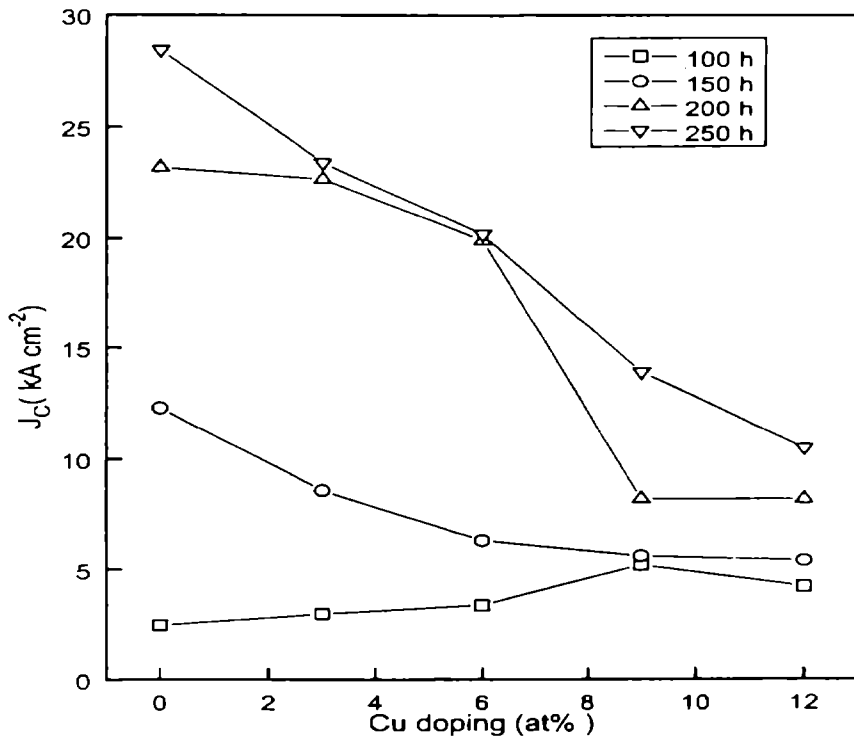


Fig. 3.5 Variation of J_c as function of Cu doping percentage in the sheath

After 100 h of heat treatment the highest J_c among the CR series samples is observed in CR9 (5.2 kA cm^{-2}) and for the CD series in CD6 (12.3 kA cm^{-2}); in both cases the least J_c is shown by the undoped sample. It is clear from Figs.3.5 and 3.6 that the J_c s of the CD series samples are higher than the CR series at the 100 h stage. This is obviously due to the higher amount of Bi-2223 formed at this stage in the CD samples ($> 60\%$) compared to the CR samples ($< 40\%$).

At 150 h stage, peak J_c s of 12.3 kA cm^{-2} for CRAg and 15.6 kA cm^{-2} for CD6 are observed, respectively for the CR and CD series samples. From this stage onwards, J_c values of the CR samples

decreases significantly as the Cu content in the sheath increases (Fig.3.5).

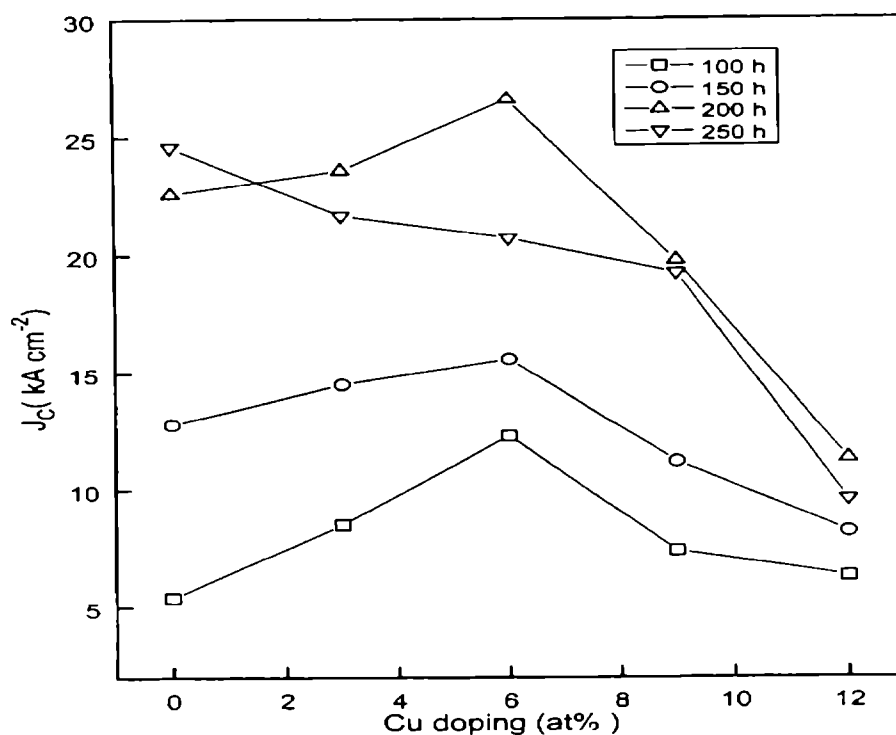


Fig 3.6 Variation of J_c as function of Cu doping percentage in the sheath

A rapid degradation of J_c is observed for the samples doped with Cu beyond 6 at. %, after the 200 h of heat treatment. This is because of the amount of Bi-2223 present in the samples doped with Cu beyond 6 at.% is lesser and the amount of non-superconducting secondary phases such as CuO and Ca_2CuO_3 is higher (Table 3.3). These non-superconducting secondary phases act as inhibitors in the path of transport current. A maximum J_c of 28.5 kA cm^{-2} is observed for the CRAg sample after 250 h of heat treatment. Comparable values are obtained for the sample CR3 (23.4 kA cm^{-2}) and CR6 (20.18 kA cm^{-2}).

For the CD series samples, up to 200 h of heat treatment, the maximum J_c is observed in CD6 sample (26.6 kA cm^{-2}). At this stage, CD3 sample shows a J_c of 23.6 kA cm^{-2} . The J_c values of all the CD series samples except the undoped sample, are higher than the CR series samples because of the higher amount of Bi-2223 present in these samples. After 250 h of heat treatment, the undoped sample CDAg shows the highest J_c (24.6 kA cm^{-2}), and the Cu doped samples show lower J_c values than the previous stage.

Taking into account the J_c results and the volume percentage of Bi-2223 observed in CD samples, the optimum Cu doping level in this series is around 6 at.% and a doping level up to 9 at.% can be tolerated with a slight sacrifice of J_c . In the case of CR samples it seems that a doping level up to 3 at.% can be considered, even though these samples show relatively lower performance compared to the undoped sample.

II. Ag-Au alloy system

The J_c values of Ag-Au alloy sheathed tapes after 200 h of heat treatment is plotted in Fig. 3.7. The J_c values of all the samples are more or less identical except for some minor scattering observed for Au3, where the J_c is slightly lower (31.5 kA cm^{-2}). Figure 3.8 is the XRD pattern of the samples after the final stage of sintering. XRD patterns of all the samples appear to be identical with same phases and approximately in equal amounts. (Bi,Pb)-2223 is the major phase, Bi-2212 and Ca_2PbO_4 are also observed as minor secondary phases, Fig.3.9 illustrates the J_c -B characteristics of the samples. It is noteworthy that there is a slight improvement in the J_c -B characteristics of Ag-Au alloy

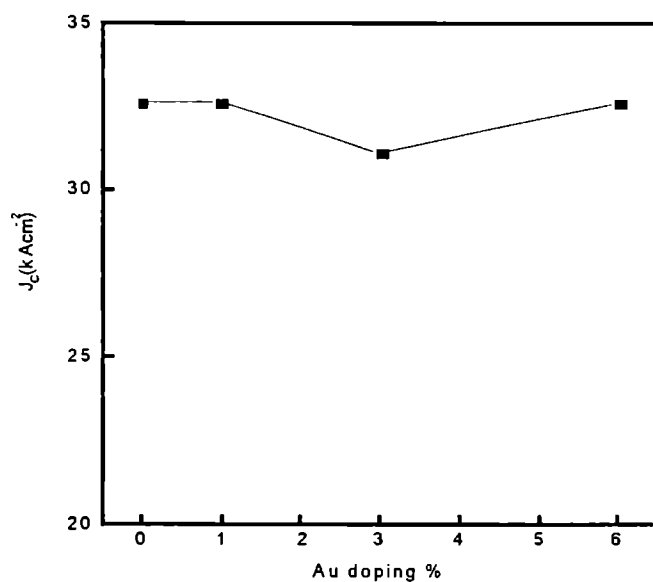


Fig. 3.7 Variation of J_c as a function of Au doping

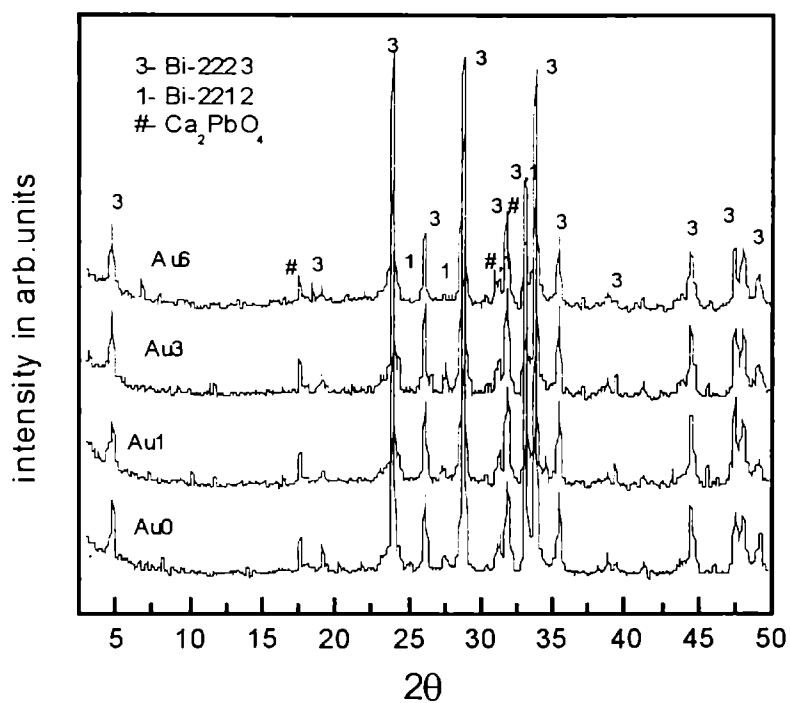


Fig. 3.8 XRD patterns of the samples after the final stage sintering (180 h)

sheathed tapes over pure Ag sheathed ones, the best being the highest Au doped sample. The SEM picture of the surface morphology of samples Au0, Au1 and Au6 are given in Fig.3.10. It is observed that surface morphology of the samples are also the same. SEM picture of the transverse section of Au0 and Au6 are shown in Fig.3.11. Fully grown and well connected grains with nearly the same orientation is seen in both the samples. The XRD and SEM results suggest that the critical current density of the Au doped samples should not differ considerably from that of the undoped sample and the observed J_c values (Fig.3.7) confirm this point.

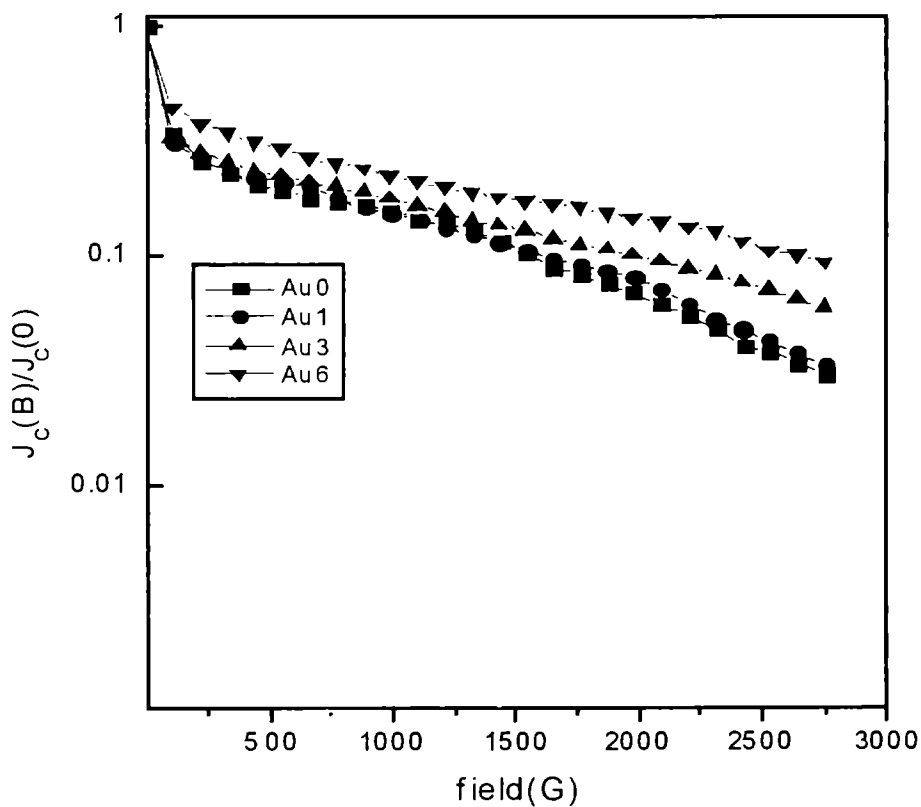


Fig. 3.9 Variation of normalized J_c as function of applied field for AgAu samples.

Our results are consistent with the results reported in the literature [16] where the Au doping % was varied up to 31 at.% and observed no

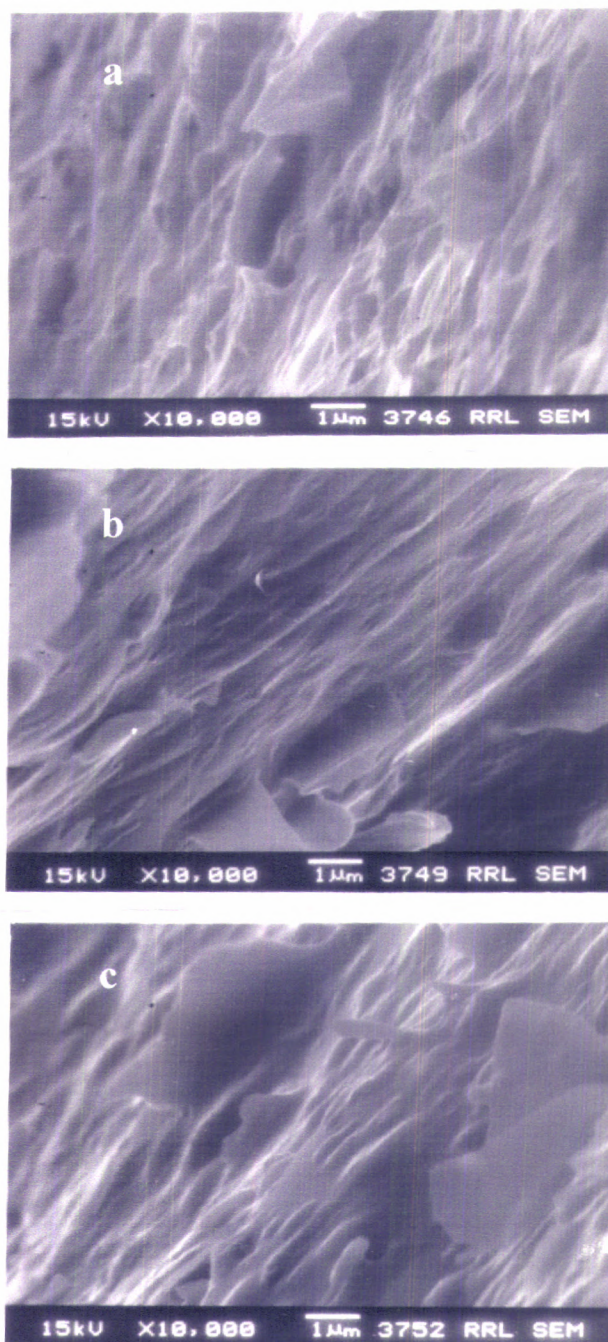


Fig. 3.10 SEM micrographs of the surface morphologies of AgAu sheathed and pure Ag sheathed samples: (a) Au0, (b) AgAu1, (c) AgAu6

degradation of critical current density. This suggests that Au can be an ideal candidate for making silver alloys for BPSCCO tapes. Further they have higher melting temperature and lower oxygen affinity compared to pure Ag. Moreover they are not chemically reactive in oxidizing atmospheres and allow enough oxygen diffusivity for *in situ* conversion of (Bi,Pb)-2223 from the precursor phases.

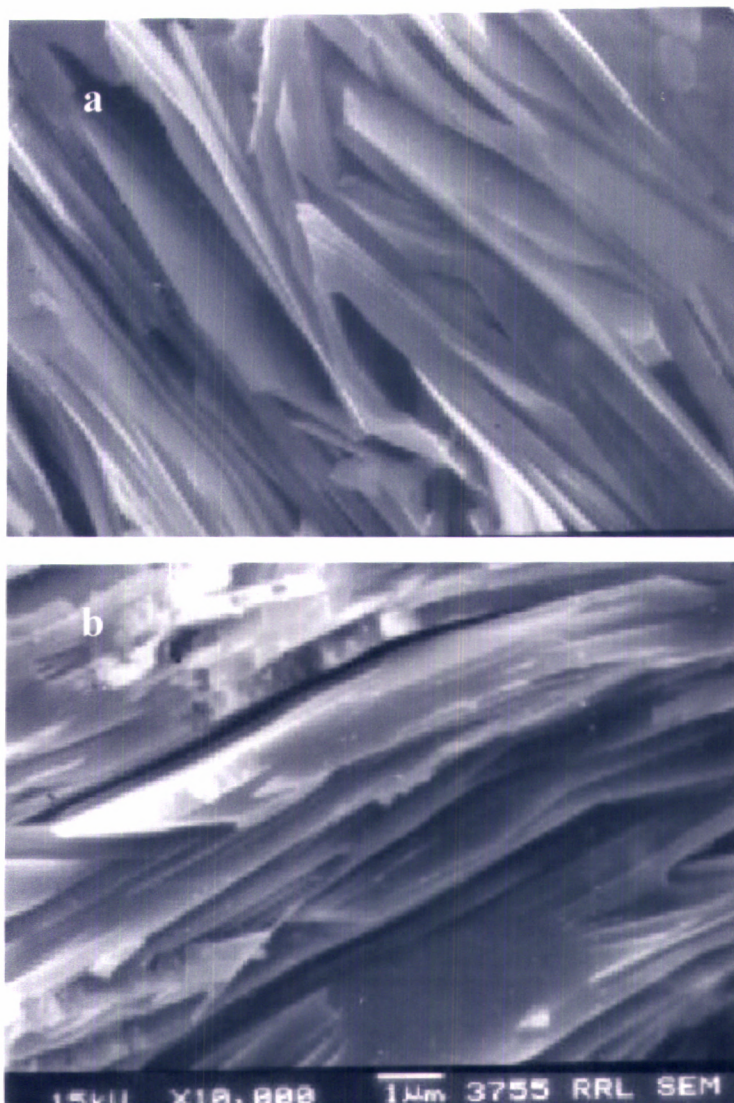


Fig. 3.11 SEM micrographs of the transverse sections of (a) AgAu6 and (b) pure Ag tapes after the final stage heat treatment

Now coming to the Fig. 3.9, what causes the better J_c -B characteristics (showing a lesser reduction of J_c in an applied field) of Au doped samples? There can be a minor diffusion of Au particles from the sheath to the ceramic core. These gold particles can act as flux pinners improving the flux pinning potential or pinning strength of the samples. The concentration/distribution of Au particles is less than sufficient for an enhanced flux pinning suggesting that there is only a minor diffusion of gold particles to the core of superconductor.

3.3. Mechanical Properties

3.3.1. Mechanical behaviour of BPSCCO composite tapes

The mechanical behaviour of these composites is very sensitive to the distribution and geometry of the components, as well as to the direction of the applied stresses. Considering the tensile stresses along the tape, the approximation of equal strain of the metallic sheaths and ceramic core is valid when describing the behaviour of both monocoil and multicore tapes with untwisted filaments. Neglecting residual stresses, the elastic modulus of the tape, E_t , may be written as

$$E_t = (1 - f) E_s + E_{sc} (p) \quad (1)$$

Here f is the superconductor filling factor E_s and E_{sc} being the Young's modulus of the metallic sheaths and textured BPSCCO core with porosity p , respectively.

The stress-strain curves, $\sigma_t(\epsilon)$, of composite BPSCCO tapes fabricated by the PIT and WIT process, after yield, shows a multiple cracking behaviour [17], with in most cases, the metallic sheaths

completely debonded from the cores prior to the initial fracture. Therefore, for mechanical design, the behaviour of tapes was approached by a composite of ductile metallic sheaths and brittle ceramic cores [17]. For tensile stresses along the tape, the rule of mixtures gives

$$\sigma_t(\varepsilon, p) = (1 - f) \sigma_s(\varepsilon) + f \sigma_{sc}(\varepsilon, p) \quad (2)$$

The stress level of superconducting core, $\sigma_{sc}(\varepsilon, p)$, is obtained by assuming a linear variation with external strain ε [17].

$$\sigma_{sc}(\varepsilon, p) = (\varepsilon_{r,sc} + \varepsilon) E_{sc}(p) \quad (3)$$

where $\varepsilon_{r,sc}$ is the average of residual strains in the cores.

Assuming for the metallic sheath after yielding, a linear strain hardening coefficient [17]

$$\omega = \partial(\sigma_s)/\partial\varepsilon [(E_s \varepsilon)] \quad (4)$$

the stress of the yielded sheath is

$$\sigma_s(\varepsilon) = (1 - \omega) \sigma_{0.2,S} + \omega E_S (\varepsilon_{r,S} + \varepsilon) \quad (5)$$

where $\varepsilon_{r,s}$ is the residual strain and $\sigma_{0.2,s}$ is the yielding point of the metallic sheath..

According to the above model, the improvement in $\sigma_{0.2,S}$ and E_S are directly related to the final tape strength, which, in turn, is dependent on the type of alloy selected. Moreover, equations (2)–(5) correspond to isothermal conditions and the variations for different temperatures should be considered when present.

3.3.2. Experimental

The stress-strain (load-elongation) characteristics of both Ag-Cu and Ag-Au alloys were obtained by a tensile testing machine (Instron). Annealed samples (800°C/30 min) of identical dimensions were used for this purpose. The effect of bend strain and tensile stress on the superconducting properties was studied only for Ag-Cu alloy sheathed tapes. Both mono and multicore were selected for this purpose. The doping level of Cu was varied from 0 to 9 at % and a precursor stoichiometry of $\text{Bi}_{1.8}\text{Pb}_{0.4}\text{Sr}_{2.0}\text{Ca}_{2.2}\text{Cu}_{3.0}\text{O}_x$ (both judging from the previous experiment) was used. Monofilament tapes were prepared by the same procedure as described in the previous experiment. For the multifilament tapes pure Ag sheathed wires of diameter 1.45 mm were inserted into Ag-Cu tubes, which were further groove rolled to a diameter of 2.1mm and then flat rolled to 400 μm . In both cases, a pure Ag sheathed sample was taken as the reference. Heat treatment was performed in three stages at 833°C with two rolling steps in between for a total duration of 200 h. The final thickness of the monofilament tape is 150 μm and that of multifilament tapes is 250 μm . The fill factors of the superconductor core in the mono and multifilament tapes are estimated to be 25 and 16.7 respectively.

I_c dependence on bending strain was studied by bending the samples onto different cylindrical mandrels with predetermined radii and measuring the I_c in the bent state. The bending radii were selected from lower strain percentages to values above ϵ_r . I_c dependence on tensile stress (tensile loading) was studied using the set up, as described in Chapter 2.

Sample identification

We label the samples as Ag, AgCu3, AgCu6, AgCu9 for monofilament samples of Cu compositions 0, 3, 6 and 9 at% respectively in the sheath. Similarly MAg, MAgCu3, MAgCu6, MAgCu9 denote the corresponding multifilament samples.

3.3.3. Results and Discussion

(a) Tensile properties

Fig.3.12 illustrates the stress, elongation characteristics of Ag-Cu alloys. It is clear from the figure that the tensile strength of Ag-Cu alloys are considerably higher than pure Ag. UTS of AgCu12 is 156% (262.8 MPa) of that of the pure Ag (168.2 MPa).

Fig.3.13 illustrates the stress-elongation characteristics of Ag-Au alloys. The strength of Ag-Au alloys are comparable to that of pure Ag. The UTS of AgAu6 is only 107.6% (181.8 MPa) of that of the pure Ag. Another notable point is that Ag-Au alloys produce more elongation compared to Ag-Cu alloys. This clearly indicates that the strain hardening mechanism in Ag-Au alloys is different from that of Ag-Cu alloys. Also the strengthening mechanisms are different for the two types of alloys. To get a clear picture of the strength of Ag-Cu and Ag-Au alloys UTS is plotted as a function of the % of doping for the two alloys in Fig. 3.14. While 6 at% Cu doping increases the UTS to 147.5%, 6 at% of Au doping causes only an increase of 107.6%.



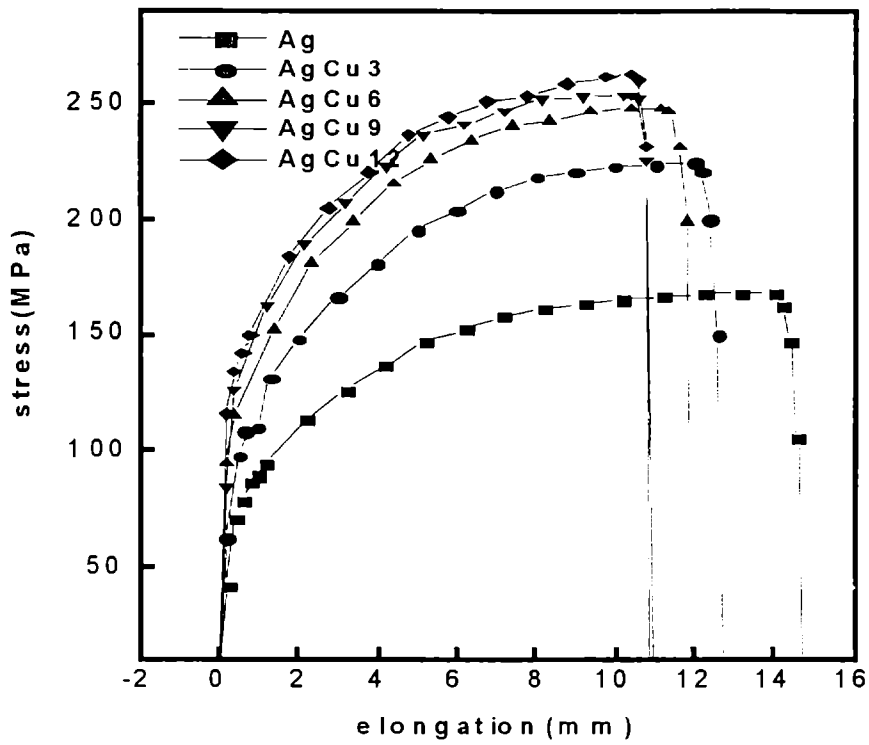


Fig. 3.12 Stress elongation curves of Ag-Cu alloys

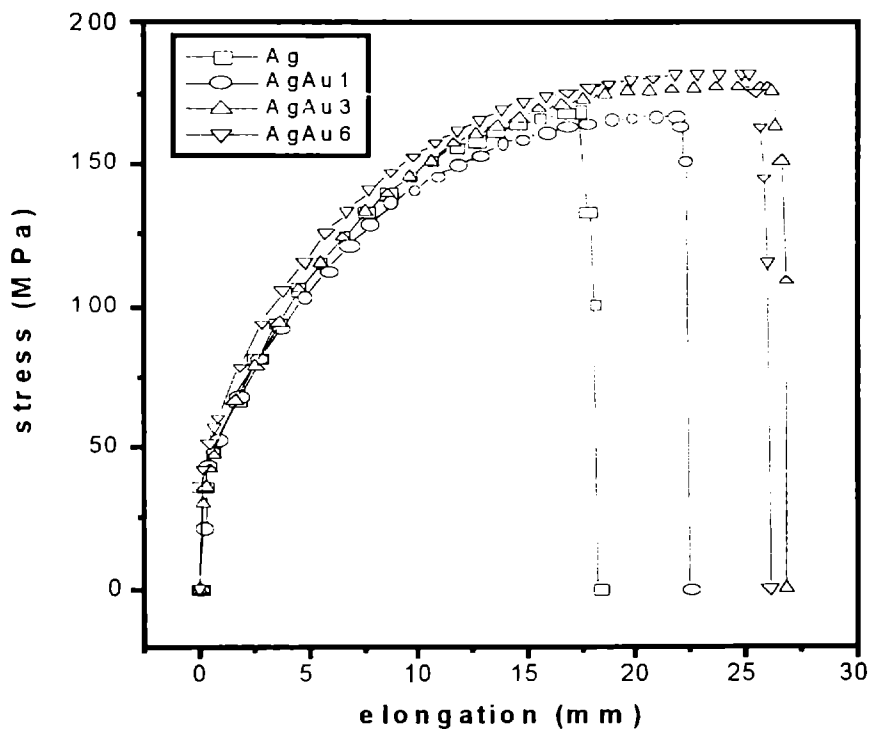


Fig. 3.13 Stress elongation curves of Ag-Au alloys

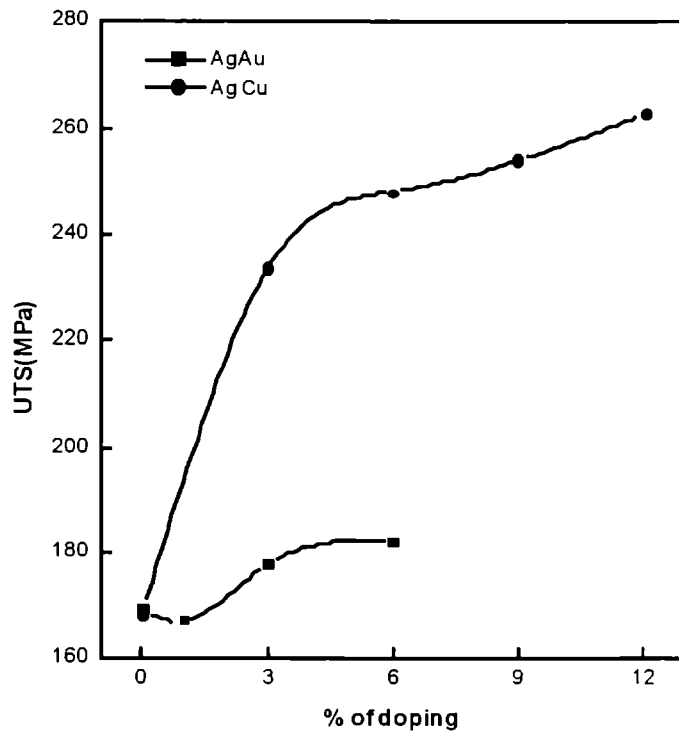


Fig. 3.14 Variation of UTS as a function of doping percentage for AgCu and AgAu alloys

The random substitution of silver by alloying atoms (solid solution) is the common hardening mechanism of the cast alloys. But for alloyed elements with solubility in silver decreasing with temperature (for example Cu and Mn), ageing, annealing or slow solidification process may produce metallic aggregates, yielding heterogeneous materials with improved strength. In addition, the nucleation of oxide precipitates during preparation is also very likely and would certainly present when annealing in oxidizing atmospheres. Also the oxidation of dissolved elements produces oxide precipitates with very different kinetics and final sizes, enhancing the strength of the alloy. But for the AgAu alloys hardening mechanism other than solid solution effects are

absent and the mechanical properties improve moderately with respect to those of pure silver.

Table 3.5 J_C values of mono and multifilamentary tapes

Sample	J_C (kAcm ⁻²)
P	24.7
AgCu3	26.5
AgCu6	29.8
AgCu9	23.4
MP	14.5
MagCu3	16.1
MagCu6	17.4
MagCu9	13.8

As the tensile strength of Ag-Au alloys do not improve considerably on Au doping it was decided that further studies on the effect of both tensile and bend strains on the superconducting properties will be conducted only for Ag-Cu alloy sheathed tapes.

(b) Superconducting Properties

Table 3.5 gives the J_C values of mono- and multifilamentary tapes after the final stage of heat treatment. The J_C measurements were performed on samples of lengths of about 3 cm cut from the sintered tapes. The highest J_C value is shown by the 6 at% Cu doped sample in

both mono- and multifilamentary cases, showing its suitability for practical applications in windings.

The variation of I_C as a function of the bend strain applied to the mono- and multifilamentary samples are plotted in Figs.3.15 and 3.16 respectively. The strain percentages were calculated using the relation $\varepsilon = t/(2R + t)$ [18], where t is the thickness of the tape and R is the bending radius. The irreversible strain (ε_r) and the strain level for a 10% I_C degradation along with the corresponding bending radii are given in Table 3.6.

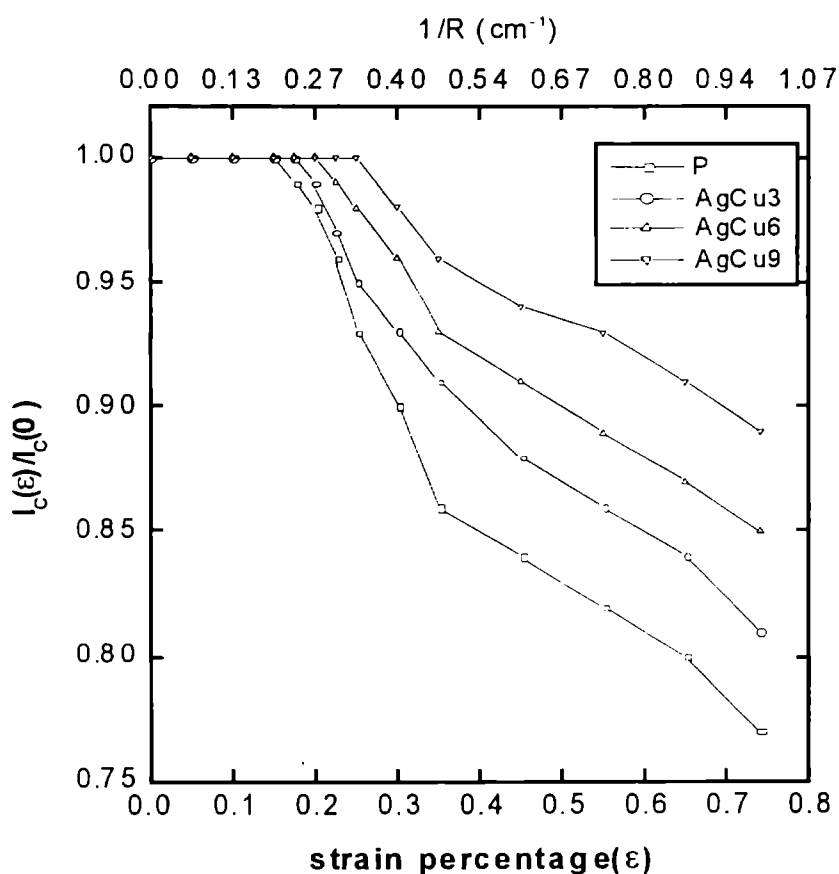


Fig. 3.15 Variation of normalized I_C as a function of strain percentage for Ag-Cu monofilamentary tapes

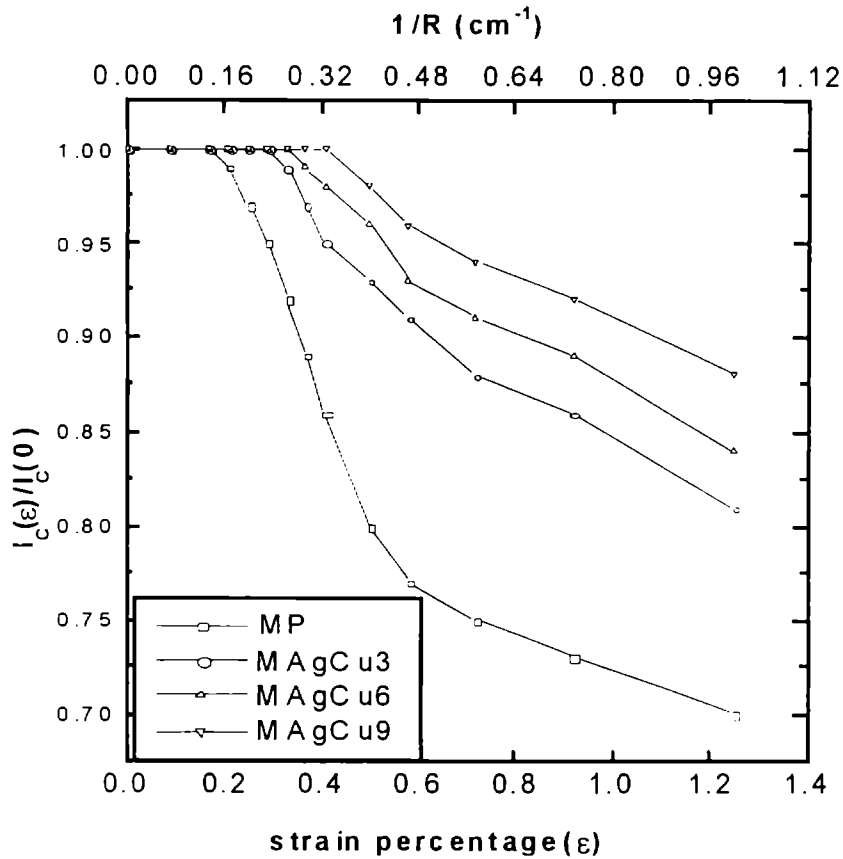


Fig. 3.16 Variation of normalized I_C as a function of strain percentage for Ag-Cu multifilamentary tapes

From the figures it is clear that the strain tolerance of all the Ag-Cu alloy sheathed tapes is superior to the undoped sample and it improves monotonically as the level of Cu doping in the sheath increases. The irreversible strain (ϵ_r) and the strain level for the 10% I_C degradation are found to be higher by about twice for the highest Cu doped sample of the mono- and multifilamentary tapes compared to the pure sample.

The amount of I_C retained after the strain level of 0.74% ($>\epsilon_r$) for the monofilamentary tapes is significant (76% for P and 88% for AgCu9) and it decrease as the Cu doping in the sheath decreases. Similar results are found in the case of multifilamentary tapes, except

for a marked difference between the pure and Ag-Cu alloy sheathed samples. For the pure sample the degradation of I_c above ϵ_r is rapid upto $\epsilon = 0.58$ and the reduction gradually levels off. The percentage of I_c retained after a strain level of 1.25% for the pure sample is 70, whereas it is 88% for MAgCu9.

Table 3.6 Irreversible strain and strain level for 10% I_c degradation

Sample	Irreversible strain (ϵ_r) (%)	bending radii (mm)	Strain level for a 10% I_c degradation (%)	Bending radii (mm)
P	0.163±0.01	46.5±3.5	0.33±0.03	23±2.0
AgCu3	0.190±0.01	40.0±3.0	0.40±0.05	19±2.0
AgCu6	0.210±0.01	35.0±2.0	0.50±0.05	16±1.5
AgCu9	0.275±0.03	27.0±2.0	0.70±0.05	11±1.5
MP	0.19±0.02	67±7.0	0.35±0.02	36±2.0
MAgCu3	0.31±0.02	41±2.0	0.65±0.07	20±2.0
MAgCu6	0.35±0.02	36±2.0	0.82±0.10	16±2.0
MAgCu9	0.46±0.04	28±3.0	1.10±0.17	12±2.0

It is well accepted that the crack development in the ceramic core of the superconductor is the main cause for the degradation of I_c due to applied strain [18-25]. Also it should be reckoned that for a tape sample in the bent state, it is at the metal-core interfacial area where the maximum stress is exerted. A smooth interface region ensures that the stress is distributed throughout the interface. The interfacial region of a pure Ag sheathed sample usually develops a sausaging or wavy surface, which arises due to the large difference in the mechanical properties between the ceramic superconductor and the sheath. Sausaging can be minimized by making Ag alloy sheathed tapes [25]. As the Cu doping

level increases, the Ag-Cu alloy acquires a better yield strength and reduces the roughness in the interfacial area, which are the sites where stress concentrates. Moreover in the pure Ag sheathed sample the sheath deforms plastically under the applied strain, which allow small cracks to develop is not longer defects. On the other hand the plastic deformation of the sheath is partly stabilized by the better yield strength of the alloy. Therefore crack propagation in the Ag-Cu alloy sheathed tapes only begins at comparatively higher strain levels.

Thus better strain tolerance observed in the Ag-Cu alloy sheathed tapes is due to the enhanced sheath strength of the alloy, which reduces the roughness in the interfacial area and the partial stabilization of the plastic deformation of the sheath, which inhibits crack propagation at lower strains levels.

In the multifilamentary geometry the cracks in each ceramic core are independent of each other and are limited to the particular filament as the silver boundary acts as a crack arrester. The subdivision of the core into finer cases in addition to the enhanced sheath strength of the Ag-Cu alloys make the multifilamentary tapes able to endure more strain.

The variation of I_C as a function of the applied tensile stress for the mono- and multifilamentary tapes is plotted in figures 3.17 and 3.18 respectively. The critical stress σ_c (stress level above which I_C degrades irreversibly), and the stress limit for 10% I_C degradation are given in table 3.7.

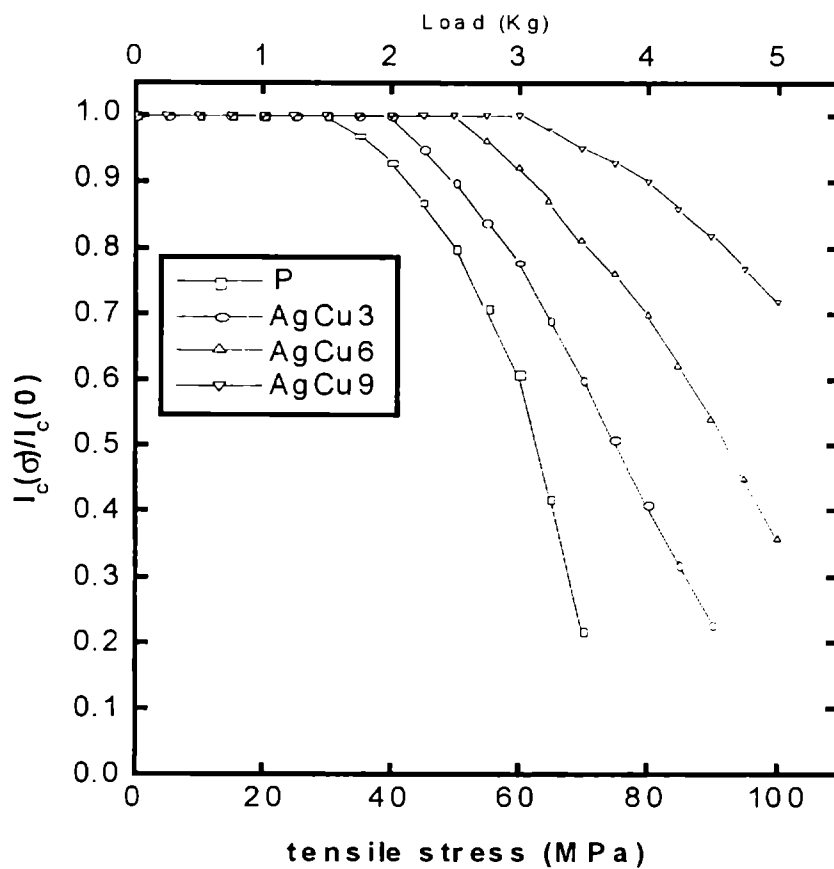


Fig. 3.17 Variation of normalized I_c as a function of stress for Ag-Cu monofilamentary tapes

Table 3. 7 Critical stress and stress limit for 10% I_c degradation

Sample	Critical stress (σ_c) (MPa)	Stress limit for a 10% I_c degradation (MPa)
P	33 \pm 2	43 \pm 2
AgCu3	43 \pm 2	53 \pm 2
AgCu6	53 \pm 2	63 \pm 2
AgCu9	63 \pm 2	83 \pm 2
MP	53 \pm 1.5	63 \pm 1.5
MAgCu3	72 \pm 1.5	85 \pm 1.5
MAgCu6	85 \pm 1.5	95 \pm 1.5
MAgCu9	104 \pm 1.5	114 \pm 1.5

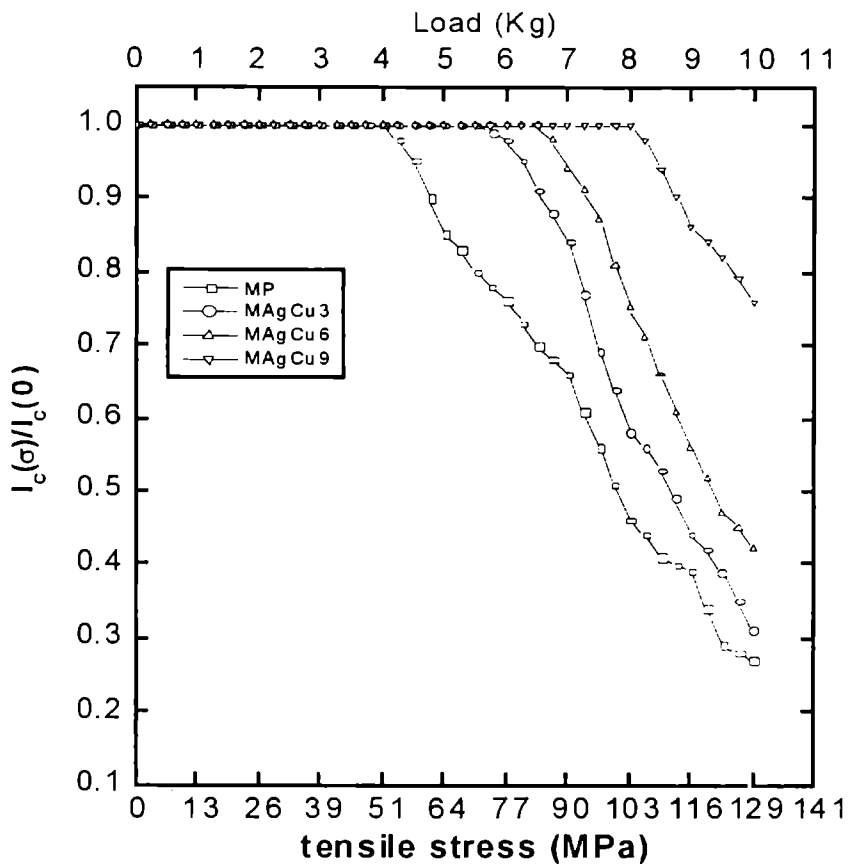


Fig. 3.18 Variation of normalized I_c as a function of stress for Ag-Cu multifilamentary tapes

The stress tolerance characteristics of both the mono- and multilayer tapes to the applied stresses seem to be the same. Improvement of the critical stress value (σ_c) can be observed for the Cu doped samples in both the mono- and multifilamentary tapes. Also the critical stress values of the multifilamentary tapes are significantly higher than the corresponding monofilamentary values. The critical stress values and the stress limit for a 10% I_c degradation have improved by nearly two times for the highest Cu doped sample in mono-

and multifilamentary cases. The I_C degradation beyond the critical stress value is more rapid compared to the bend strain characteristics.

The improved yield strength provided by the Ag-Cu alloy sheathed tapes causes the critical stress levels to increase in accordance with the level of Cu doping in the sheath. Also, the low fill factor of the superconductor present in the multifilamentary configuration further increases the critical stress values

The ceramic core in a tape loaded in the tensile mode will break more rapidly soon after the strain attains its critical value because the same strain is experienced throughout the cross sectional area. This is not the case with bending, where the strain is distributed equally from the neutral axis; the layers above the neutral axis will experience tensile strains towards the bending direction while those below it experience compressive strains opposite to the bending direction. For the monofilament tapes the number of cracks and the crack depth in the core can be higher on the application of tensile stresses above σ_c , whereas on the application of bend strain above ϵ_r crack initiation begins at the tensile side while the compressive side can withstand still higher strains. Similarly for the multifilamentary tapes only a fraction of filaments which experience the maximum strain will break abruptly for stresses above σ_c . This explains the higher percentage of retained I_C values and the slow degradation of I_C on the application of bend strains above ϵ_r compared to the I_C degradation characteristics due to tensile stresses above σ_c .

3.4 Electrical and Thermal Properties

The electrical and thermal properties of Ag-Cu and Ag-Au alloys from room temperature (RT) to 77 K are deduced from the resistivity measurements conducted on these alloy samples. In order to get a comparison with the electrical and thermal properties of the sheath after different heat treatment cycles, the samples used for the resistivity measurements were also given a heat treatment for 100 h (50+50 h) with one intermediate rolling at the same temperature used for the tape heat treatment.

a) Electrical conductivity

The variation of electrical conductivity of Ag-Au and Ag-Cu alloys as function of alloy doping percentage is shown in Figs. 3.19 and 3.20 respectively. It is obvious that the conductivity values at 77 K are higher than that of the room temperature values for both alloys and pure silver. But the interesting point is that the electrical conductivity values of Ag-Au alloys are considerably lower than that of the Ag-Cu alloys. For example the ratio of conductivity values at 77 K and RT ($\sigma_{77\text{ K}}/\sigma_{\text{RT}}$) for pure Ag is ~ 5.7 , for AgAu6 is ~ 2 and that for AgCu12 is ~ 4 .

b) Thermal Conductivity

The variation of thermal conductivity of Ag-Au and Ag-Cu alloys as function of alloy doping percentage is shown in Figs. 3.21 and 3.22 respectively. Thermal conductivity values are deduced from the corresponding electrical conductivity values using the *Wiedemann-Franz* law, which links the thermal conductivity to electrical

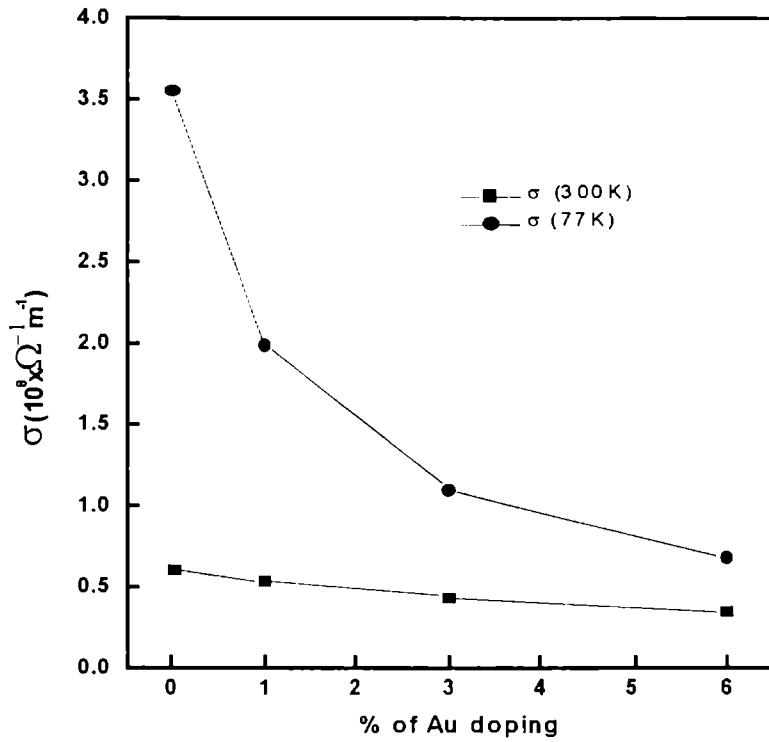


Fig. 3.19 Variation of electrical conductivity as function of Au doping in Ag

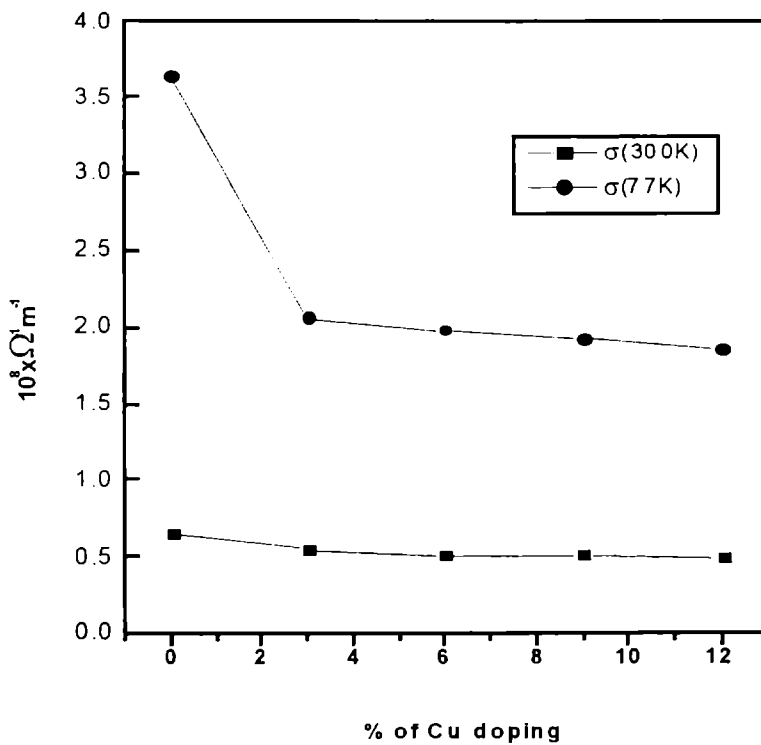


Fig. 3.20 Variation of electrical conductivity as function of Cu doping in Ag

conductivity according to the relation:

$$\kappa / \sigma = L.T,$$

where 'L' is the Lorenz number($L = 2.45 \times 10^{-8} \text{ W}\Omega\text{K}^{-2}$) and 'T' is the temperature in K. κ and σ are the thermal conductivity and electrical conductivity values of the alloys.

Thermal conductivity values of both Ag-Au and Ag-Cu alloys at 77 K are lower than that of the corresponding room temperature values. Moreover the reduction of thermal conductivity by Au doping is very much significant compared to that caused by Cu doping. For example 6 at% Au doping reduces the thermal conductivity of pure Ag to about 20%, while 12 at% Cu doping reduces it only to 50%.

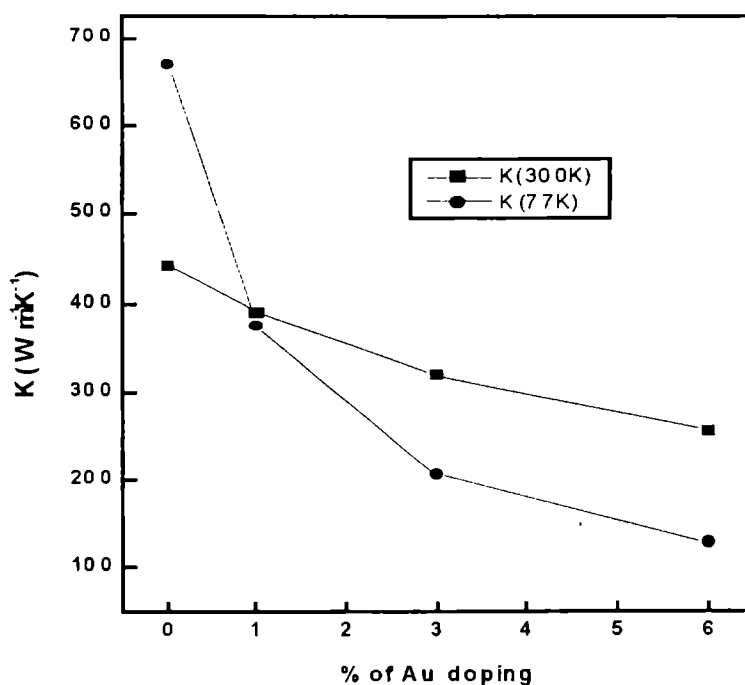


Fig. 3.21 Variation of thermal conductivity as function of Cu doping in Ag

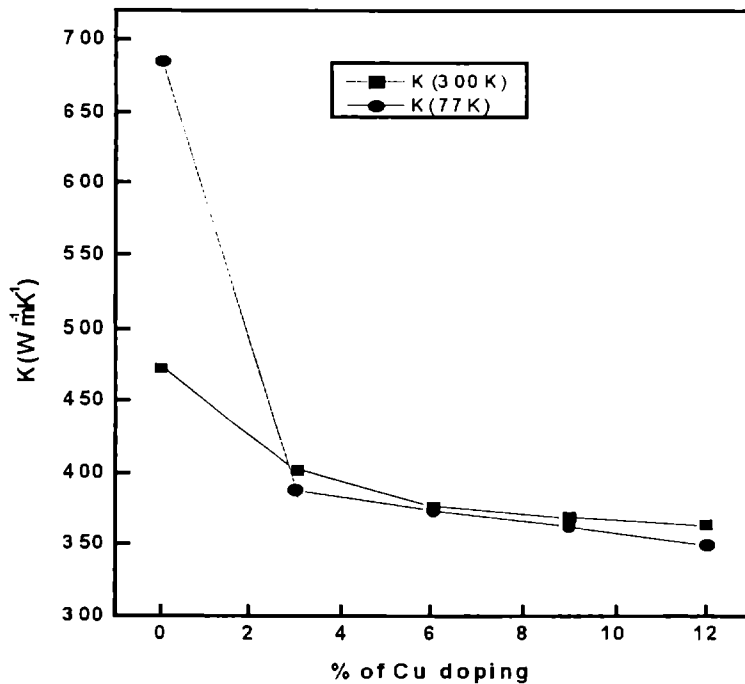


Fig. 3.22 Variation of thermal conductivity as function of Cu doping in Ag

3.5 Conclusions.

The conclusions drawn from the present investigation can be summarized as follows.

- i) The optimum level of Cu doping in the sheath in the process of making Bi-2223/Ag-Cu alloy sheathed tapes is dependent on the Cu stoichiometry in the system.
- ii) A copper deficient precursor is preferred for making Ag-Cu alloy sheathed tapes with superior properties. Cu atoms from the alloy sheath diffuse into the core and thereby supplement the Cu

- deficiency. A stoichiometry of $\text{Bi}_{1.8}\text{Pb}_{0.4}\text{Sr}_{2.0}\text{Ca}_{2.2}\text{Cu}_{3.0}$ (CD) allows use of Cu up to 6 at.% in the sheath without any deterioration either in the Bi-2223 phase fraction or transport J_c .
- iii) Use of copper rich precursors in Ag-Cu alloy sheaths, in general, reduces the rate Bi-2223 formation, ultimate Bi-2223 fraction and leads to the formation of non-superconducting secondary phases such as Ca_2CuO_3 and CuO thereby results in tapes with inferior J_c .
 - iv) Eventhough both the CD and CR precursors follow the two-dimensional nucleation (random) growth model in pure silver sheath, they show deviations from the model in Ag-Cu alloy sheath.
 - v) For the AgAu alloy system, Au doping in the sheath does not affect the superconducting properties and the microstructure of the samples. However there is a slight improvement in the J_c -B characteristics of the Au doped samples compared to the pure one, may be due to the minor diffusion of Au atoms from the sheath to the core and acting as extra flux pinners.
 - vi) Tensile strength of AgCu alloys are considerably higher than that of AgAu alloys. The difference in the strength of the alloys is due to the different hardening mechanisms involved.
 - vii) The bend strain tolerance and stress tolerance of the (Bi,Pb)-2223/Ag-Cu alloy sheathed tapes improve remarkably as the level

- of Cu doping in the sheath increases. The enhanced resistance towards mechanical damage and the consequent improvement in the transport current retention are attributed to the enhanced sheath strength provided by the Ag-Cu alloys, which in turn provide a smooth interface area between the superconductor core and the sheath and due to the partial stabilization of the plastic deformation of the sheath towards applied strains compared to the undoped samples.
- viii) Multilayer tapes can withstand higher mechanical strains and stresses due to their fine filament structure with a lower superconductor fill factor.
 - ix) The degradation of I_C is more rapid for tensile stresses above σ_c , whereas it is gradual for bend strains above ε_r . This behaviour is explained by taking into account the type of strain experienced by the core in the two cases: for tensile loading the whole cross sectional area experiences the same strain, while it is distributed equally from the neutral axis for bend strains.
 - x) The mechanical properties of the Ag-Cu alloy sheathed tapes are as good as those reported for other types of alloy sheathed tapes [24-26]. The critical stress values (σ_c) of the AgCu9 and AgCu6 samples are 104 and 84 MPa, respectively, while that of the AgMgNi tape [26] is 102 MPa. This shows that the Ag-Cu alloy can be considered as alternative candidates for the fabrication of long-length (Bi,Pb)-2223 tapes.
 - xi) The electrical and thermal conductivities of Ag-Au alloys are considerably lower than Ag-Cu alloys which in turn are lower than pure Ag at 77 K. 6 at% Au in Ag reduces the electrical and

thermal conductivities to about 20% and 12 at% Cu reduces them only to about 50%.

References

- [1] W. Gao, S.C. Li, D. A. Rudman, G. J. Yurek, J. B. Vander Sande, *Physica C* **161** (1989) 71.
- [2] P. S. Mukherjee, A. Simon, J. Koshy, P. Guruswamy, A. D. Damodaran, *Solid State Commun.* **76** (1990) 659
- [3] C. J. Kim, M. S. Halm, D. S. Suhr, K. B. Kim, H. J. Lee, H. G. Lee, G. W. Hong, D. Y. Won, *Mater Lett.* **11** (1991) 79
- [4] J. C. Griewel, R. Flukiger, C. Benz, Y. Yang, R. G. Surlock, *Physica C* **229** (1994) 177
- [5] H. K. Liu, R. K. wang, S. X. Dou, *Physica C* **229** (1994) 39
- [6] Z. Yi, I. law, S. Fischer, C. beuz, Y. Yang, R. G. Surlock, *Physica C* **254** (1995)193
- [7] S. Li, W. gao, y. Hu, H. K. Liu, s. X. Dou, *Physica C* **276** (1997) 229
- [8] R. Nararro, *Supercond. Sci. Technol.* **13** (2000) R147 and the reference therein.
- [9] P. vasc, R. Flukiger, M. Leghissa, B. Glowacki, *Supercond. Sci. Technol.* **13** (2000) R71
- [10] T. Hatano, K. Aota, S. Ikeda, K. Nakamura, K. Ogawa, *Jpn. J. Appl. Phys.* **27** (1988) L2055
- [11] J. C. Grivel, A. Jeremie, B. Hensel, R. Flukiger, *Supercond. Sci. Technol.* **6** (1993) 725
- [12] A. Sobha, R. P. Aloysius, P. Guruswamy, K. G. K. Warriar, U. Syamaprasad, *Physica C* **307** (1998) 277
- [13] A. Sobha, R. P. Aloysius, P. Guruswamy, K. G. K. Warriar, U. Syamaprasad, *Physica C* **316** (1999) 63
- [14] S. Nhien, G. Desgardin, *Physica C* **272** (1996) 309.

- [15] Q. Y. Hu, H. K. Liu, S. X. Dou, *Physica C* **250** (1995) 7.
- [16] K. nomura, T. Sasaoka, J. Sato, S. Kuma, H. Kumakura, K. Togano, N. Tomita, *Appl. Phys. Lett.* **64** (1994) 112
- [17] K. Osamura, S. Nonaka, Y. Katsumura, s. Ochiai 1995 *Advances in Superconductivity VIII ed* H. Hagawa and Y. Enomoto (Berlin: Springer) p 859.
- [18] J. K. F. Yau, N. Savvides, C. C. Sorrell, *Physica C* **266** (1996) 223
- [19] S. Salib, C. Vipulanandan, *Mater. Res. Bull.* **32** (1997) 1333.
- [20] M. rabra, N. Sekimura, H. Kitaguchi, P. Kovac, K. Demachi, K. Miya *Supercond. Sci. Technol.* **12** (1999) 1129.
- [21] M. Polak, J. A. Parrell, A. A. Polyanaskii, A. E. Pashitski, D. C. Larbelestier, *Appl. Phys. Lett.* **70** (1997) 1034
- [22] M. S. Sharma, U. Syamaprasad, C. Pavithran, P. Guruswamy, P. S. Mukherjee, *J. Mater. Sci. Lett.* **16** (1997) 1430
- [23] M. Labtinen, J. Passi, Z. Han, J. Sarkeniem, *Physics C* **277** (1997) 238
- [24] M. T. Malachevsky, D. A. Esparza, *Physica C* **324** (1999) 153
- [25] Y. tanaka, T. Asano, T. Yangiya, M. Fukutomi, K. Komori, H. Maeda, *Jap. J. Appl. Phys.* **31** (1992) L235
- [26] L. Martini, *Supercond. Sci. Technol.* **11** (1998) 231.

CHAPTER 4

EFFECT OF NANO SIZE MgO ADDITION: ENHANCED FLUX PINNING IN (Bi, Pb)-2223/Ag TAPES

4.1. Introduction

The ability of HTS to carry high current under high magnetic field and high temperature is utmost important when considering its application for practical devices. For this, the flux pinning strength of the system must be enhanced. Improving the flux pinning strength of HTS is a tricky job as the coherence length (ξ) is very small. Further it depends upon the system under consideration. For example, (Bi,Pb)-2223/Ag tapes are inherently weak in its flux pinning capability and as a result the irreversibility field (H^*) is very low. Many research efforts are going on around the world to improve the flux pinning strength of Bi-2223 tapes as the system is promising for its high current carrying capacity at 77 K. One of the effective method is irradiation which will create columnar defects of ~ 30 nm as artificial pinning centers [1-4]. But this method has the drawback that it is very expensive and is not suitable for large scale applications. Alternative approach is to dope the system with nanosize impurities or to create nanosize defects in the system by adjusting the processing/heat treatment conditions. The choice of external impurity must be so made that it should not deteriorate the superconducting properties and its doping percentage should be critically adjusted. Several candidates are reported in the literature such as carbon nanotubes [5], SiC nanoparticles [6], Ca_2PbO_4 [7], etc. Also slight Pr substitution for Ca and excess doping of Pb [8,9] act as flux pinners. MgO particles added to Bi-2212 [10,11] and

YBCO bulk materials [12] showed considerable enhancement of the critical current density. As a result, the effect of nanosize MgO particles and MgO nanorods in (Bi, Pb)-2223/Ag tapes have been the subject of detailed investigation [13-16] around the world, and the reported results are widely varying regarding the optimum percentage of MgO doping. In this study, we have conducted a systematic investigation on the effect of MgO doping on the superconducting properties of (Bi,Pb)-2223/Ag tapes.

4.2. Experimental

Precursor powder was prepared by a sol-gel route [17]. Nanosize MgO particles (average particle size: 30 nm) were added to the precursor powder in different percentages viz 0, 0.1, 0.3 and 0.6 wt%. In order to ensure a homogeneous dispersion of MgO particles in the precursor a master dopant was made first by adding 2 wt% MgO in the precursor and grinding it in acetone for 2 h. Then the requisite amount of master and precursor were mixed and ground in acetone for another 1 h. Precursor powders were filled in Ag tubes of ID/OD: 8/10 mm with a packing density of 3.2 gcm^{-3} . Usual procedure for the preparation of PIT (Bi,Pb)-2223/Ag tapes were adopted and the heat treatment was done at the optimum conditions. The tapes were characterized at 77 K for its transport I_C and J_C -B behaviour. XRD and SEM analysis were carried out to study the phase purity and microstructure.

Sample identification

We label M0, M1, M3 and M6 respectively for the samples doped with 0 (pure), 0.1 wt%, 0.3 wt% and 0.6 wt% MgO.

4.3. Results and discussion

Figure 4.1 shows the XRD pattern of all the samples after the 90 h of heat treatment. The phases detected are Bi-2223, Bi-2212 and Ca_2PbO_4 . There is a slight retardation in the growth of Bi-2223 as the amount of MgO increases. This is obvious from the reduced intensity of XRD peaks of Bi-2223 compared to Bi-2212 in the MgO added samples. Figure 4.2 is the XRD pattern of all the samples after final heat treatment (180 h). Bi-2223 is detected as the major phase with Bi-

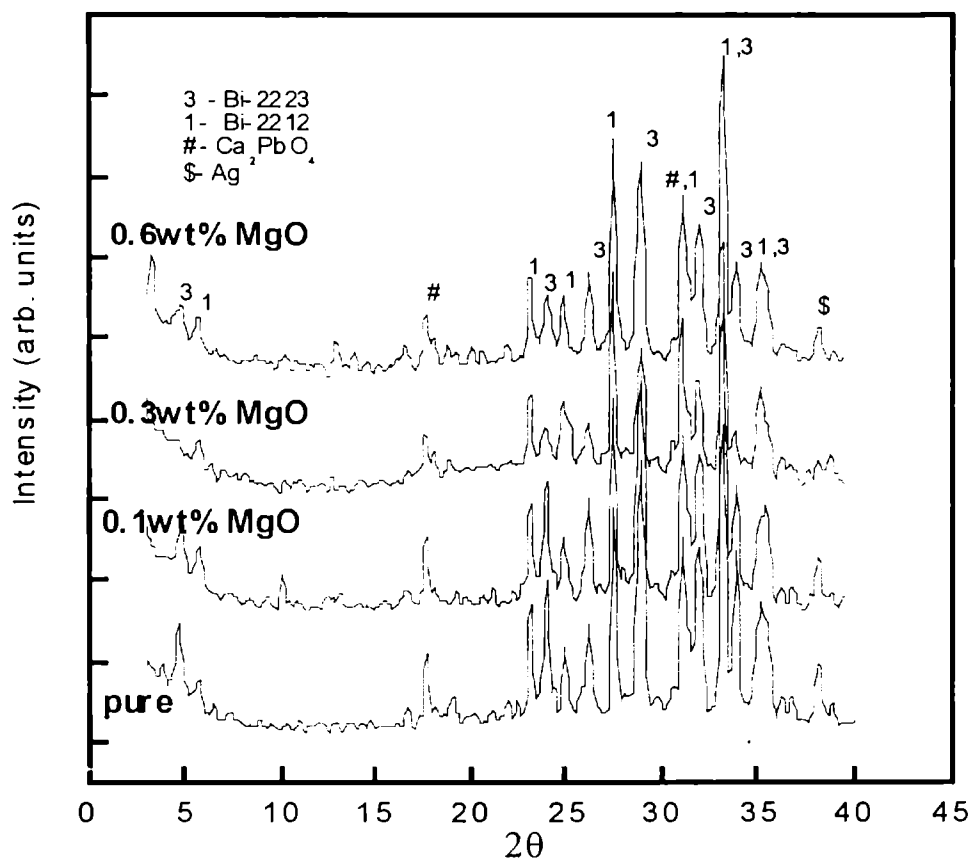


Fig. 4.1 XRD patterns of the MgO added samples after 90 h heat treatment

2212 and Ca_2PbO_4 as the secondary phases. Here also the fraction of Bi-2223 decreases as the amount of MgO in the precursor increases. This is obvious from the increased intensity of XRD peaks of Bi-2212 in MgO doped samples compared to the pure one.

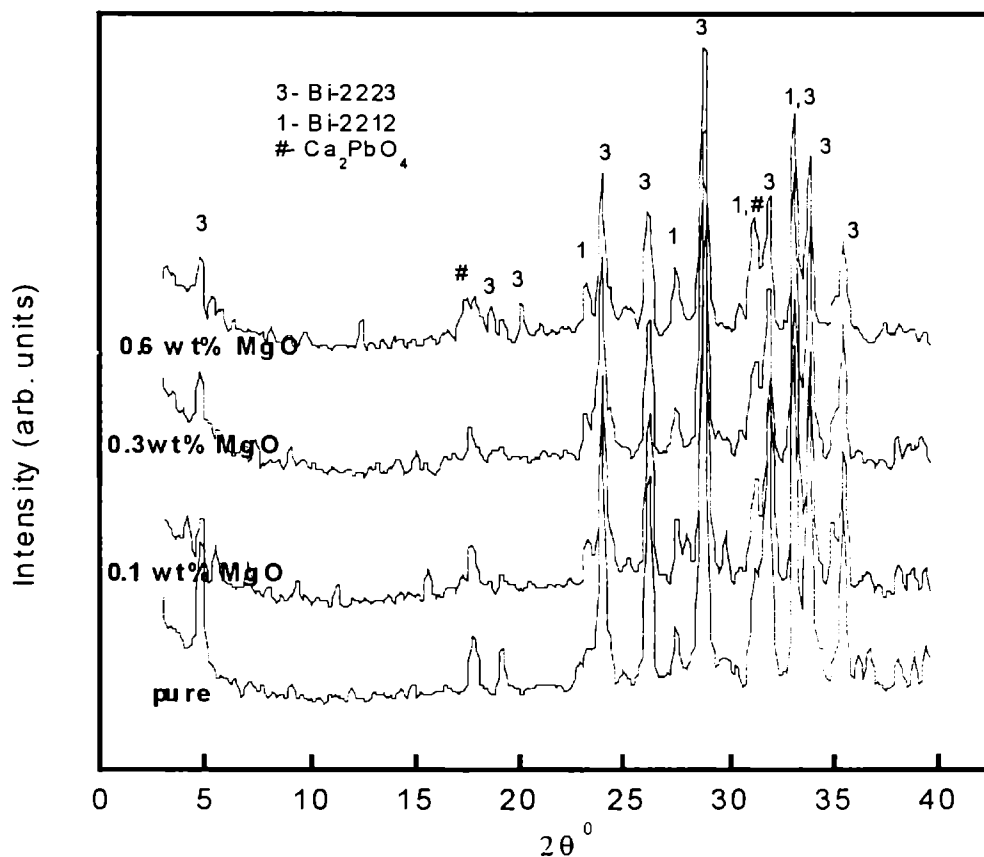


Fig. 4.2 XRD patterns of the samples after the final stage heat treatment

Figure 4.3 illustrates the variation of J_c as a function of the percentage of MgO doping. M3 shows the highest J_c value (38.7 kA cm^{-2}) and pure sample M0 shows the least J_c value (30.5 kA cm^{-2}). Figure 4.4 is the SEM picture of the transverse section of the samples taken in the back scattered mode. Samples for the SEM analysis were

prepared by etching the sheath metal off by a solution containing 50

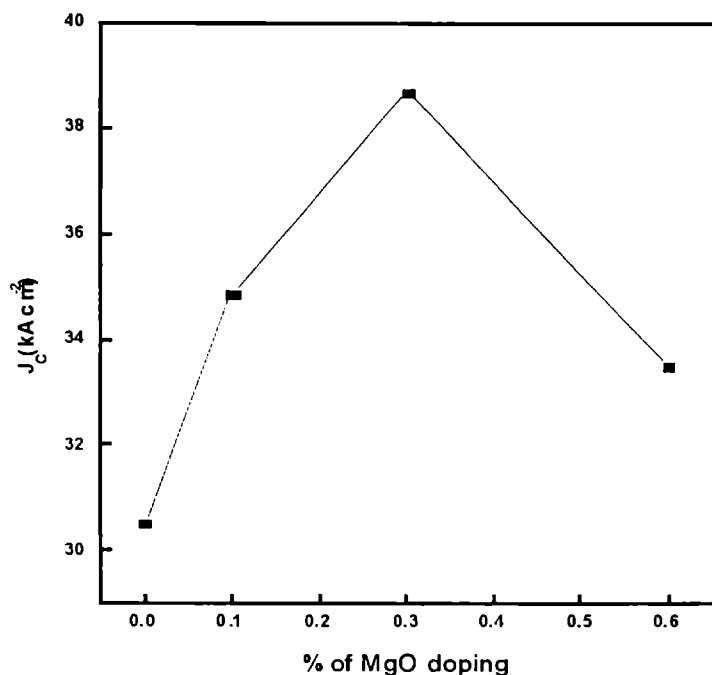


Fig. 4.3 Variation of J_c as function of MgO doping in the precursor powder

vol% H_2O_2 and 50 vol% NH_4OH . The sectional morphology of all the samples seems to be the same with nearly the same level of texture and phase purity. MgO particles are found embedded into large grains of Bi-2223 in the M6 sample. No such particles were observed in M1 and M3, may be due to the lower percentages of MgO. Moreover in M6 the size of MgO particles embedded in the matrix varies from nanometer to the micrometer scale indicating possible agglomeration of nanosize MgO particles when added in higher percentages.

Figure 4.5 shows the variation of normalized J_c ($J_c(B)/J_c(0)$) as a function of applied field, which is parallel to the c-axis of the tape. It is obvious from the figure that M3 shows a better behaviour, i.e. less

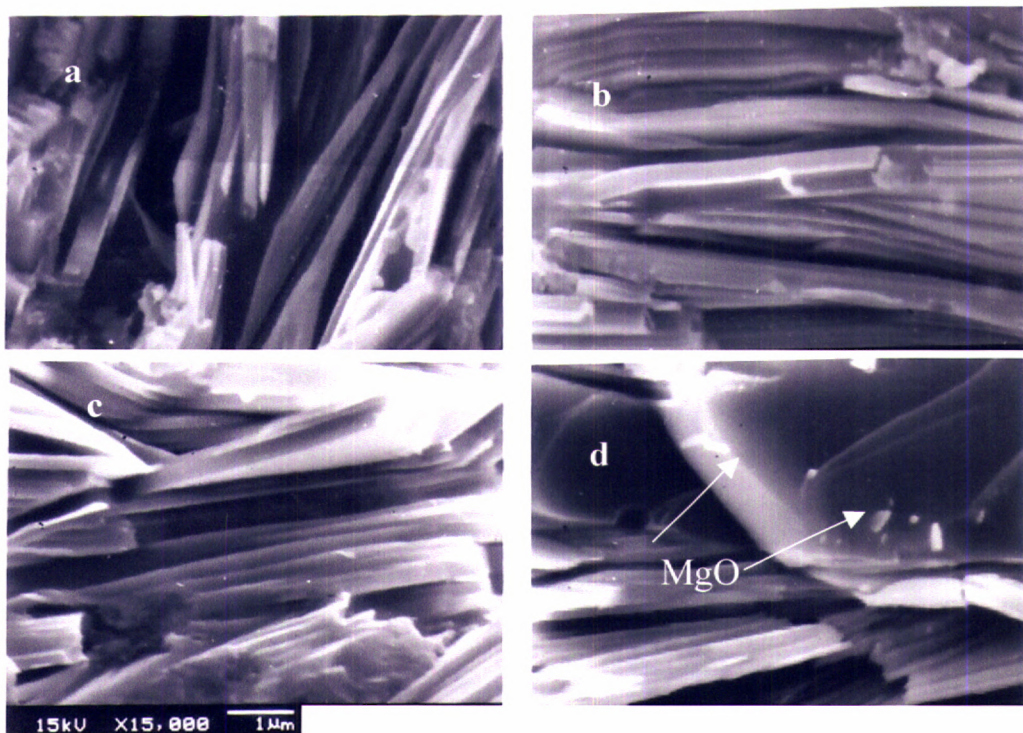


Fig. 4.4 SEM Micrograph of the transverse section of the MgO added samples, (a) M0, (b) M1, (c) M3, (d) M6

reduction of J_C on applied field compared to other samples. Moreover, the behaviour of all the MgO added samples are better than the pure sample. Among the MgO added samples M6 shows the worst characteristics, which is closer to the characteristics of pure sample.

Higher self field J_C s and the improved J_C -B characteristics of MgO added samples originated from the enhanced flux pinning strength of these samples. This is obvious when we analyze the XRD and SEM results. XRD results clearly showed a slight retardation in the growth of high- J_C phase (Bi-2223) and the SEM results did not show any significant improvement in the microstructure and texture in MgO added tapes. This shows that the J_C enhancement in MgO added samples is

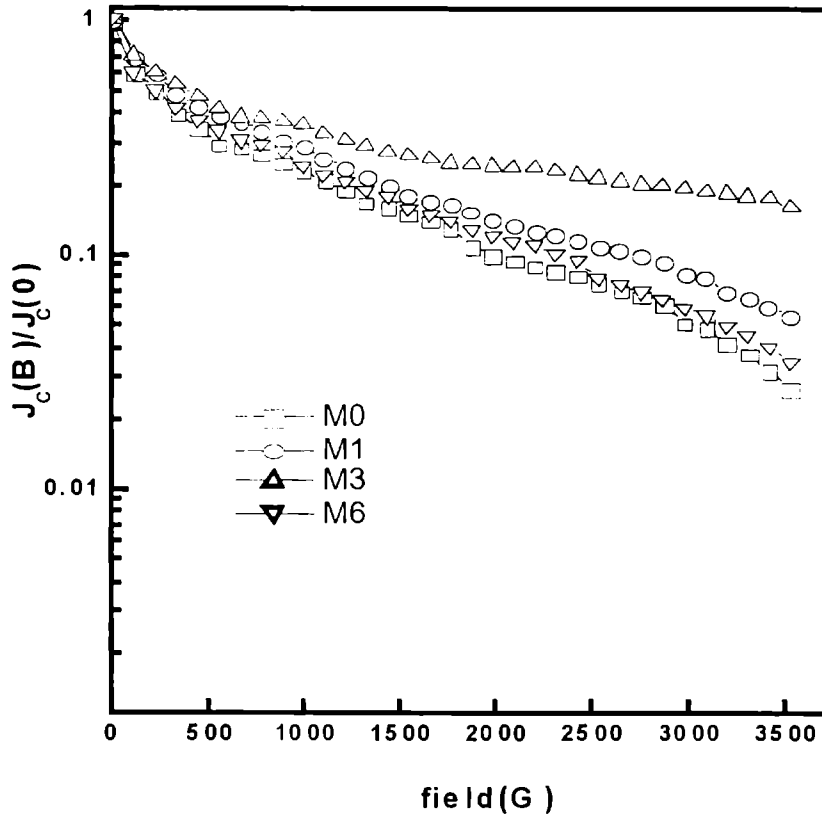


Fig. 4.5 Variation of normalized J_c ($J_c(B)/J_c(0)$) as a function of applied field perpendicular to the tape's surface

neither due to increased phase purity nor because of better microstructure, but can only be due to the enhanced flux pinning strength provided by the nanosize MgO particles embedded in the superconducting matrix.

It is widely accepted that a very fruitful tool with which one can investigate the pinning properties in superconductors is the determination of the pinning force density $F_p = J_c \times B$. For both conventional and high- T_c superconductors a scaling of F_p is defined. For example, Koblichka et al. [18,19] presented an analysis of the scaled

F_p in NdBCO based on the description by Dew-Hughes [20,21] in order to prove that the pinning is by composition fluctuations. In high- T_C superconductors there are two fundamentally different pinning mechanisms [22] describing the interaction of a vortex core with a pinning site: the δl -pinning, which is due to a scatter of electron mean free path, and the δT_C - pinning, which is associated with a spatial scatter of the superconducting transition temperature, T_C , throughout the sample. A third mechanism, which played some role in conventional superconductors, wherein the magnetic interaction between a flux line and a defect can be considered inactive in high- T_C materials with their large values of κ . In this case, the core interaction ' $F_{p, \text{core}}$ ' dominates the magnetic interaction, ' $F_{p, \text{max}}$ ' by a factor of $\kappa/4 \ln \kappa$, where κ denotes the Ginzburg-Landau parameter [23]. The δl -pinning is caused by non-superconducting (normal or conducting) particles of the size of the order of coherence length (ξ) embedded in the superconducting matrix and δT_C pinning is caused by other superconducting phases causing fluctuations in T_C .

For the present case, the pinning force density ($F_P = J_c \times B$) normalized with respect to its maximum value ($F_P/F_{P \text{ max}}$) is plotted in Fig. 4.6 as a function of applied field. It is clear from the figure that for M3 the peak position ($F_{P \text{ max}}$) appears at higher fields compared to other samples. Moreover all other samples except M3 show multiple peaks suggesting that different pinning mechanisms acting simultaneously. The appearance of a single peak in M3 suggests that for this sample only one pinning mechanism is dominant and as we noticed earlier this is caused by nanosize MgO particles (δl pinning caused by normal particles) embedded in the superconducting matrix. For other

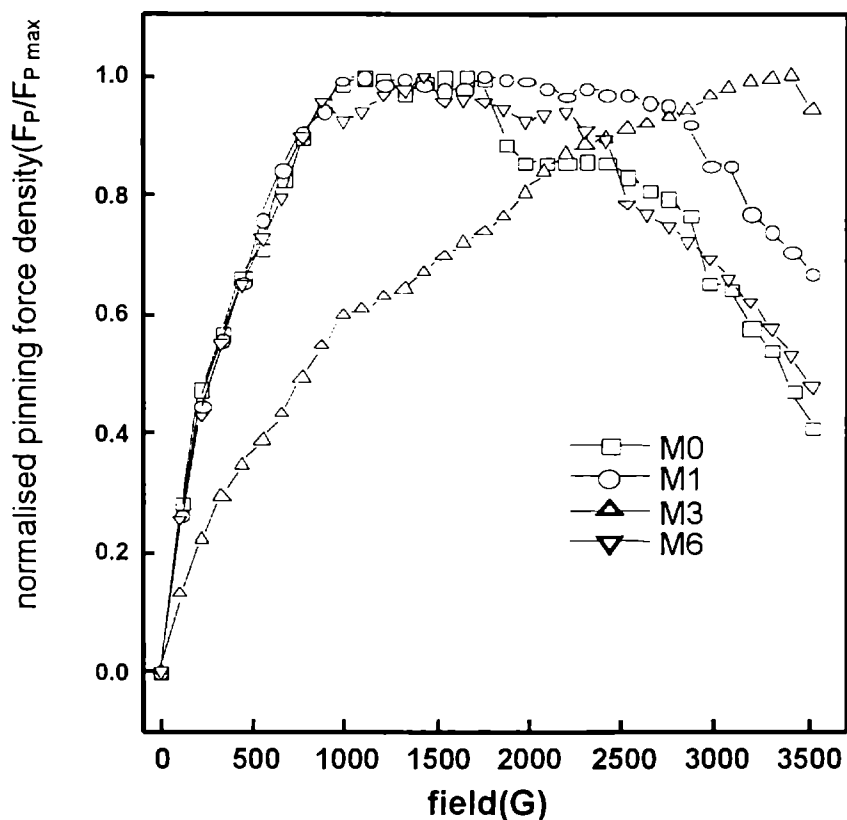


Fig. 4.6 Variation of the normalized pinning force density ($F_p/F_{p \max}$) as function of the applied field

samples including the pure one, M0, other secondary phases and crystal defects such as grain boundaries are acting as flux pinners and are active for comparatively lower fields.

4.4. Conclusions

The following points can be concluded from the above study.

1. MgO addition in (Bi, Pb)-2223/Ag tapes does retard the phase growth to a slight extent and the effect is significant at higher percentages of MgO doping.

2. Eventhough the Bi-2223 phase growth retards by MgO addition, there is no significant reaction between Bi-2223 and MgO at the doping percentages ($1 < \text{wt}\%$).
3. Nanosize ($\sim 30 \text{ \AA}$) MgO particles when added in optimum percentages ($\sim 0.3 \text{ wt}\%$) does enhance the flux pinning strength of (Bi, Pb)-2223/Ag tapes. The essential pinning mechanism is the δl pinning, where the pinning is caused by the interaction of flux lines with normal cores (here MgO) of the size of the order of the coherence length of the system.

References

- [1] H. Safar et al. *Appl. Phys. Lett.* **67** (1995) 130.
- [2] A. Wisniewski, C. Czurda, H.W. Weber, M. Baran, M. Reissner, W. Steiner, P.X. Chang and L. Zhou, *Physica C*, **266** (1996) 309.
- [3] Y. Fukumoto, Y. Zhu, Q. Li, H.Z. Weismann, M. Suenaga, T. Kaneko, K. Sato, K. Shibutani, T. Hase, S. Hayashi and C.H. Simon, *Phys. Rev. B*, **54** (1996) 10210.
- [4] Y. Zhu, Z.X. Cai, R.C. Budhani, M. Suenaga and D.O. Welch, *Phys. Rev. B*, **48** (1993) 6436.
- [5] K. Fossheim, E.D. Tuset, T.W. Ebbesen, M.M.J. Treacy and J. Schwartz, *Physica C*, **248** (1995) 195.
- [6] Y.C. Guo, Y. Tanaka, T. Kuroda, S.X. Dou and Z.Q., Yang, *Physica C*, **311** (1999) 65.
- [7] B. Zhao, W. Song, X. Wan, Y. Sun and J. Du, *Physica C*, **337** (2000) 145.
- [8] M.H. Pu, W.H. Song, B. Chao, X.C. Wu, T. Hu, Y.P. Sun and J.J. Du, *Supercond. Sci. Technol.*, **14** (2001) 305.
- [9] M.H. Pu, W.H. Song, B. Chao, X.C. Wu, Y.P. Sun and J.J. Du, *Supercond. Sci. Technol.* **14** (2001) 299.
- [10] S.L. Huang, D.D. Hughus, D.N. Cheng and R. Jenkins, *Supercond. Sci. Technol.*, **9** (1996) 368.
- [11] W. Wei, J. Schwartz, K.C. Goretta, U. Balachandran and A. Bhargava, *Physica C*, **298** (1998) 279.
- [12] Q.H. Chen, M.H. Fang, Z.K. Jiao, Q.R. Chang, H.H.Wen, Z.X. Chao, *Physica C*, **277** (1997) 113.

- [13] X.G. Wan, Y.P. Sun, W.H. Song, K.Y. Wang, L.D. Jiang, J.J. Du, *Physica C*, **307** (1998) 46.
- [14] X.G. Wan, Y.P. Sun, W.H. Song, L.D. Jiang, K.Y. Wang, J.J. Du, *Supercond. Sci. Technol.* **11** (1998) 1079.
- [15] B. Chao, X.G. Wan, W.H. Song, Y.P. Sun and J.J. Du, *Physica C*, **337** (2000) 138.
- [16] W.D. Huang, W.H. Song, T. Lui, B. Zhao, M.H. Pu, X.C. Wu and T.Hu, *Supercond. Sci. Technol.* **13** (2000) 1499.
- [17] M.S. Sarna, U.Syamaprasad, C. Pavithran, P.Guruswamy and P.S. Mukherjee., *Journal of Materials Science Letters (UK)* **16** (1997) 1430
- [18] M.R. Koblishka, A.J.J. Van Dalen, T. Higuchi, S. Yoo and M. Murakami, *Phys. Rev. B*, **58** (1998) 2863.
- [19] M.R. Koblishka and M. Murakami, *Supercond. Sci. Technol.* **13** (2000) 738.
- [20] E.J. Kramer, *J. Appl. Phys.* **44** (1973) 1360.
- [21] D. Dew-Hughes, *Phil. Mag*, **30** (1974) 293.
- [22] G. Blatter, M.V. Feigel'man, V.B. Gashkenbein, A.I. Larkin and V.M. Vinokur, *Rev. Mod. Phys.* **66** (1994) 1125.
- [23] R.P. Hubener, *Magnetic flux structures in superconductors* (New York, Springer) 1979.

CHAPTER 5

STUDIES ON THE OPTIMIZATION OF PROCESS PARAMETERS FOR THE PREPARATION OF MULTIFILAMENTARY (Bi,Pb)-2223/Ag TAPES

5.1. Introduction

Studies in the preceding sections were mainly devoted for identifying a suitable sheath material for the use of (Bi,Pb)-2223/Ag tapes as current leads and to improve its field tolerance or enhancing the flux pinning strength of the tapes. For many of the practical applications of HTS, multifilamentary tapes are considered to be the state of the art conductors due to the advantages such as (i) provides parallel electrical conduction to serve as a bypass in case of local failure, (ii) better heat sink, (iii) improves strain tolerance and mechanical strength, (iv) reduced ac losses and (v) better protection from atmospheric environment. Eventhough several methods such as wire-in-tube [1,2], tape-in-tube [2,3], jelly roll [4,5], accordion folding [6] and wire drawing of a billet having serial bores packed with the precursor [7] have been attempted by different groups, the former one, i.e. the wire-in-tube (WIT) method has been widely accepted as the most viable process for making multifilamentary HTS tapes. But the conductor layout as well as the layout of the tape itself should be tailored and the processing parameters should be optimized so as to suit specific applications. In the present case, the multifilamentary tape layout should be optimized for the current lead application. With an aim to

maximize the fill factor (ff: ratio of superconductor to silver), so as to reduce the silver content, the present chapter begins with an optimization study conducted in monofilament tapes. The influence of starting packing density (SPD) and tape width on the final superconducting properties are investigated.

The second part of this chapter deals with the optimization of the geometrical parameters of the multifilament tapes. The parameters selected for optimization are the wire diameter in the filling stage, number of filaments, wire diameter prior to tape rolling as well as the final tape thickness.

After the optimization of fill factor and the geometrical parameters of the multifilamentary tapes a study is conducted to optimize the heat treatment schedule and thermomechanical processing for obtaining higher transport current densities. Thermomechanical processing has vital importance in the processing of (Bi,Pb)-2223/Ag tapes as the conversion reaction from precursor phases to Bi-2223 is of a reaction- sintering type, requires long duration heat treatments and has to take place *in-situ*. On going through literature, one can see that current densities of the order of $10^5 - 10^6 \text{ Acm}^{-2}$ are achievable at 77K in Bi-2223 thin films [8-12] whereas practical conductors of multifilamentary configuration has J_{CS} in the range 20-25 kAcm^{-2} [12] and J_{CS} of the order of 70 kAcm^{-2} (0 T, 77 K) have been achieved in short length R&D samples [13]. Also recent magneto optical imaging (MOI) studies conducted on Bi-2223 tapes [14-17] have proved the presence of large number of “incipient cracks” in the finished tapes which severely obstruct the supercurrent flow. The critical problems

which limit the current flow are inherent with the system, which contains five cations and the thermodynamic instability with respect to temperature and atmosphere and the processing which requires intermittent rolling or mechanical deformation to enhance the texture and density of finished tapes. Intermittent rolling will produce filament cracking which if remained unhealed [incipient cracks] after the final sintering stage will reduce the current density. The liquid phase formed during the reaction-sintering will effectively heal the cracks produced during the mechanical deformation. But the amount of liquid phase decreases as the sintering proceeds and will be insufficient to heal the cracks if a significant amount of conversion had taken place prior to the last stage mechanical deformation. So it is important and necessary to optimize the thermomechanical processing and heat treatment schedules in the processing of (Bi,Pb)-2223/Ag tapes.

5.2. Optimization of powder packing density in monofilamentary tapes.

The influence of starting packing density (SPD) and tape width on the final core density and J_C of PIT processed (Bi,Pb)-2223/Ag tapes are dealt within this section.

5.2.1. Experimental

(Bi,Pb)-2223/Ag tapes were made by the PIT technique. The precursor powder was synthesised by the sol-gel route with a nominal cation ratio Bi:Pb:Sr:Ca:Cu = 1.8:0.4:2:2.2:3.2. The powder was filled in high purity (99.99%) silver tubes (OD – 10.0 mm, ID – 7.5 mm) with three different packing densities viz. 3.30 g cm^{-3} [powder fraction p (40 wt%), High (H)], 2.80 g cm^{-3} [p (33.5 wt.%), medium (M)], 2.30 g cm^{-3}

[p (27 wt.%), low (L)]. The end sealed tubes were then groove rolled. In order to optimize the tape width the starting wire diameters for the subsequent flat rolling were selected as 3, 2, 1.3, and 1.0 mm. A three-stage heat treatment schedule was performed [(50 + 50 + 80) h/830°C] with intermittent rolling. A thickness reduction of around 5% per pass was used during both groove rolling and tape rolling. The heat treatment of all the samples was carried out in a large volume muffle furnace to ensure uniform temperature to all the samples. The final thickness of all the tape samples was in the range 130-140 μm .

Core density and J_c measurements, powder XRD and optical microscopy were used to study the effect of packing density and tape width at various stages of processing. The core densities of the wires and tapes at various stages of processing were determined by measuring the density of the composite wire/tape by a modified hydrostatic weighing method employing a high sensitivity Mettler's microbalance. A natural oil (specific gravity: 0.908 g cm^{-3}) was used as the hydrostatic medium in order to minimize the error due to vaporization. The method is based on the assumption that during rolling uniform elongation occurs both for the core and the silver sheath. In other words, the superconductor to silver mass ratio was assumed constant over the whole length of the wire/tape under low rates of deformation used in the experiment. The core density (ρ_{SC}) was calculated from the density of the composite wire/tape (ρ_{C}) by using the formula [14].

$$\rho_{\text{SC}} = \frac{X\rho_{\text{C}} \rho_{\text{Ag}}}{\rho_{\text{Ag}} - \rho_{\text{C}} + X\rho_{\text{Ag}}}$$

Where x = superconductor to silver mass ratio; ρ_{Ag} = density of silver; ρ_c = density of superconductor and silver composite.

It was possible to obtain accurate density values with a maximum deviation of $\pm 1\%$ for tape samples of overall mass above 150 mg. Critical current measurements at 77 K were done using liquid nitrogen by the standard four probe technique with $1 \mu V cm^{-1}$ criterion. Optical microscope was used to study the morphology of the tape sections and to estimate the area of cross-section.

Sample identification

We label H3, H2, H1.3 and H1 for the high density (H) packed samples which are flat rolled down from 3, 2, 1.3, and 1 mm wire diameters, respectively. Similarly M3, M2, M1.3 and M1 are for the medium density (M) samples and L3, L2, L1.3 and L1 for the low density (L) samples.

5.2.2. Results and discussion

Fig.5.1 shows the XRD pattern of the precursor powder used for filling the tubes. The dominant phase in the precursor is 2212 with minor fractions of 2201, Ca_2PbO_4 , CuO, etc. This is an optimized phase assemblage [8] suitable for fabrication of (Bi,Pb)-2223/Ag tapes and was obtained by vacuum calcination of the pyrolysed gel at $750^\circ C$ for 10 h in reduced oxygen partial pressure followed by calcination at $800^\circ C$ for (10 + 10) h in free flowing oxygen in two stages with intermittent grinding. In Fig.5.2, a typical XRD pattern of the tapes after the final heat treatment is shown. It can be seen that the core contains mainly the

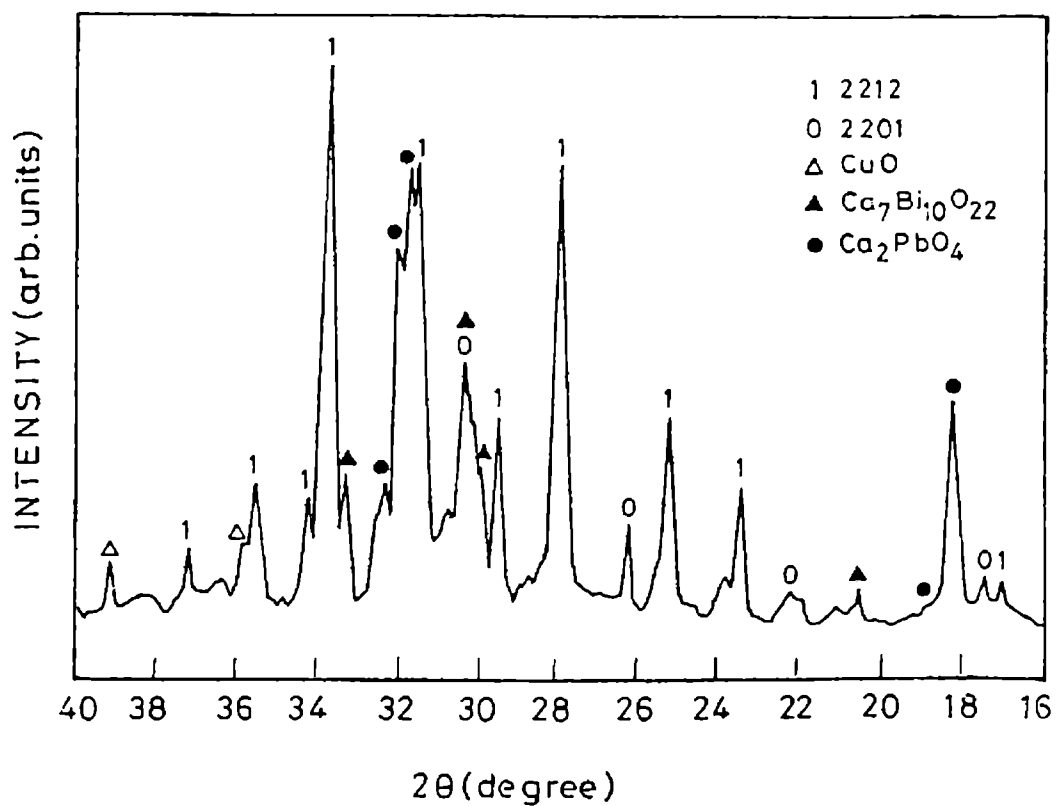


Fig. 5.1 XRD pattern of the precursor powder at the filling stage

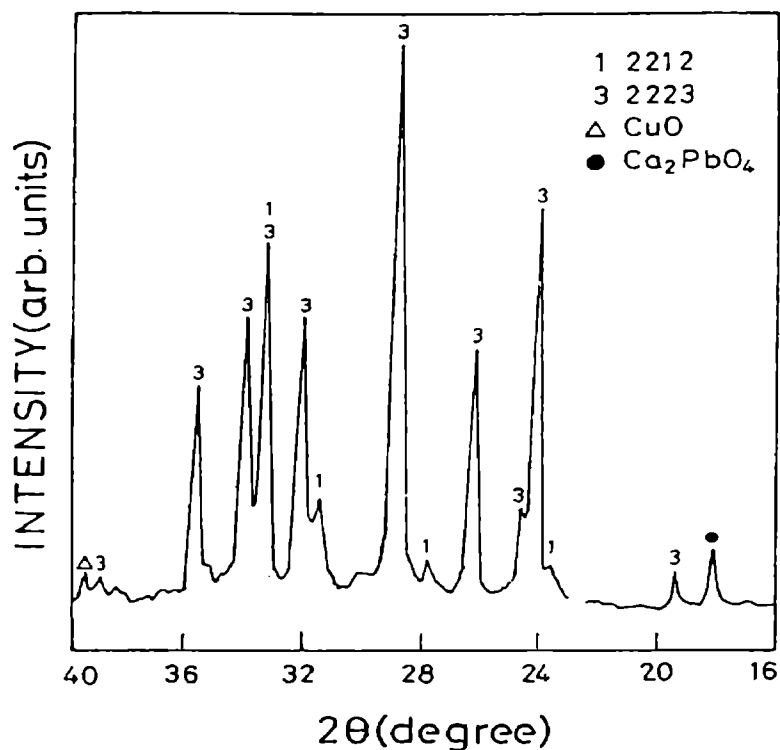


Fig. 5.2 A typical XRD pattern of the samples at the final stage of heat treatment

high T_c phase with very little quantities of secondary phases after 180 h of heat treatment.

Table 5.1 shows the variation of core density after the different stages of rolling and sintering. It can be seen that the core densities of the wires increase marginally as the groove rolling proceeds from 3 to 1 mm for all the three SPD used. Further, the flat rolling of the groove rolled wires causes a slight decrease in the core density initially. This can be understood from the fact that in groove rolling, all the sides of the wire get uniformly compressed uniformly and this can lead to a slight increase in volume of the core in the initial stages flat rolling.

Table 5.1. Core density variations during rolling and sintering (values in the parentheses are the percentage of theoretical density)

Sample	Wire stage (gcm^{-3}) (0 h)	Tape stage (gcm^{-3}) (0 h)	After 50 h sintering and rolling (g cm^{-3})	After 100 h sintering and rolling (gcm^{-3})	After 180 h sintering (gcm^{-3})
H3	4.5	4.3	4.6	4.9	5.5 (87.3%)
H2	4.6	4.4	4.7	5.2	5.6 (88.9%)
H1.3	4.7	4.5	4.9	5.4	5.6 (88.9%)
H1	4.8	4.7	5.0	5.5	5.3 (84.1%)
M3	4.3	4.1	4.5	5.0	6.0 (95.2%)
M2	4.4	4.2	4.6	5.1	6.1 (96.8%)
M1.3	4.5	4.3	4.7	5.3	6.0 (95.2%)
M1	4.6	4.5	4.9	5.3	5.8 92.06%)
L3	4.3	4.0	4.6	5.1	5.9 (93.7%)
L2	4.3	4.1	4.7	5.0	6.1 (96.8%)
L1.3	4.4	4.2	4.8	5.2	6.0 (95.2%)
L1	4.5	4.3	4.9	5.4	5.7 (90.5%)

Thereafter for each stage of rolling and sintering, the core density slightly increases and an appreciable change occurs after the final stage of heat treatment. After the final stage of sintering the core density attains values ranging from 5.2 (84% of ρ^{th}) to 6.1 g cm⁻³ (96.8% of ρ^{th}) for different samples depending on the SPD and tape width. A notable point is that all the high density (H) samples show relatively lower core density (< 90% of ρ^{th}) while the medium (M) and low density (L) samples result in high core density (up to 96.8% of ρ^{th}). At the final stage, the tape samples become very thin and the sheath thickness of the H series of samples with a higher powder fraction becomes too low to contain the core. This leads to oozing out of the transient liquid phase during the sintering process resulting in punctured tapes. The partial loss of liquid phase causes higher porosity and the poor sintered density for the H series tapes. This very well suggests that a packing density of 3.30 g cm⁻³ (powder fraction of 40 wt.%) is too high for the present tube dimensions and rolling conditions. Typical SEM image of the surface morphology of the H series samples and M series samples is shown in Fig. 5.3. On the surface of H series samples large glassy phase is visible caused by the melting and subsequent oozing of the melt from the core to the sheath. Table 5.2 gives the width of the tape samples after each stage of processing. The width increases slightly after each stage of rolling. The M series samples showed slightly lesser values of width than the corresponding H and L series samples.

Table 5.3 gives the results of the Jc measurements of the samples along with their respective core densities at the final stage. The Jc values reported here are the average values obtained for six samples of the same batch and the maximum deviation in each case is also given in

Table 5.3. In order to minimise the scattering of J_c , as generally observed in PIT tapes, utmost care was taken to keep the process parameters identical for all the samples. As a result, a fairly good reproducibility in J_c could be achieved in the present work. It is seen

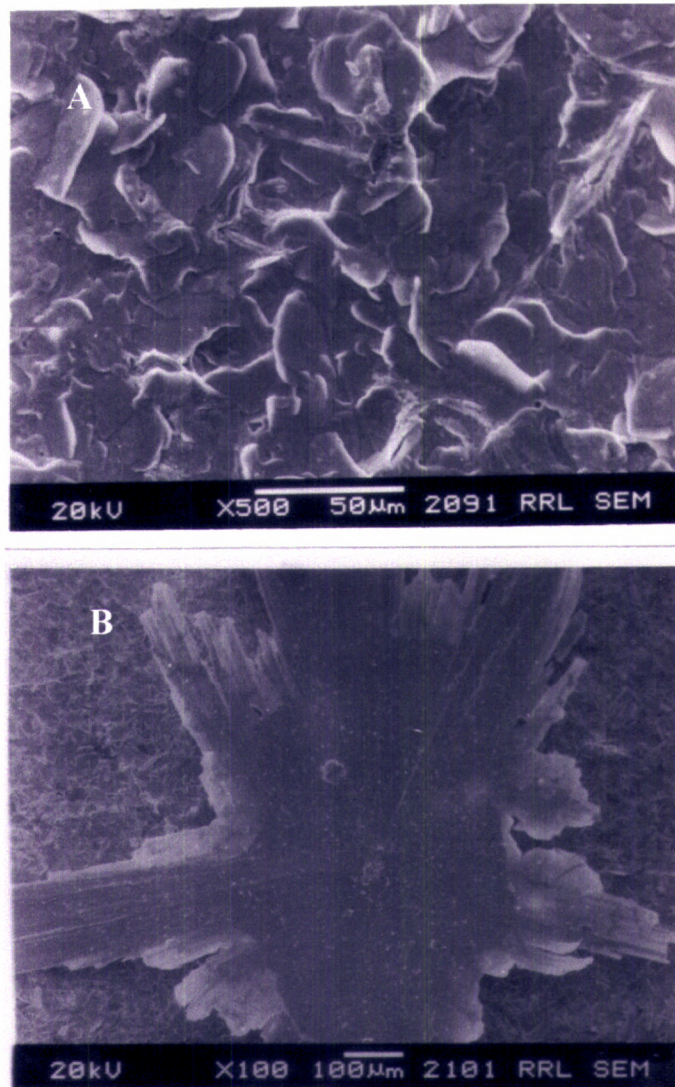


Fig. 5.3 SEM micrograph of the surface morphologies of (A) M series samples and (B) H series samples

that the J_c values show a direct dependence on their core densities. This is more clear in the cases of M and L series samples. In both these cases, tapes rolled from 1.0 mm wires, i.e., M1 and L1 show the least J_c

(8.5 and 8.1 kA cm⁻²) and core density (92.1% and 90.5% of ρ^{th}) whereas tapes rolled from 1.2, 2.0 and 3.0 mm wires show relatively higher values of J_c and core density. The best result is obtained for M2

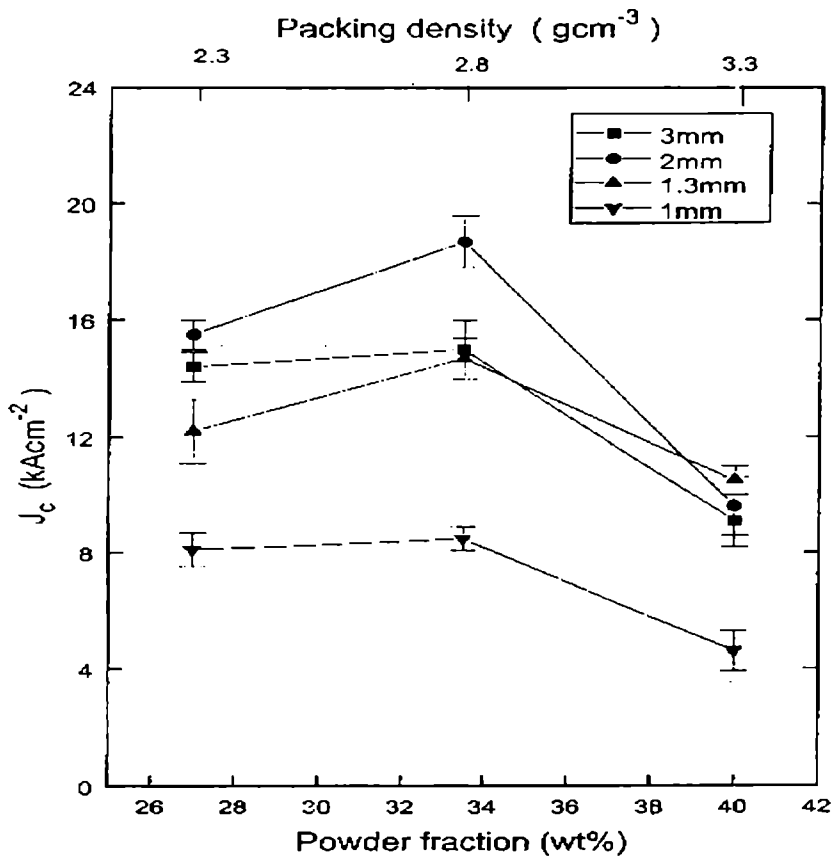
Table 5.2. Width variation at different stages of rolling

Sample	Starting wire diameter (mm)	First stage rolling (mm)	Second stage rolling (mm)	Third stage rolling (mm)
H	3.0	5.30	5.54	5.68
	2.0	3.93	4.16	4.34
	1.3	2.94	2.96	3.08
	1.0	2.12	2.22	2.30
M	3.0	5.03	5.06	5.10
	2.0	3.90	4.00	4.12
	1.3	2.70	2.80	2.94
	1.0	1.80	1.96	2.16
L	3.0	4.90	5.20	5.30
	2.0	4.00	4.10	4.20
	1.3	2.90	2.94	4.05
	1.0	1.92	2.00	2.20

samples for which the J_c and core density are 18.7 kA cm⁻² and 6.1 g cm⁻³ (96.8% ρ^{th}), respectively. The variation of J_c with respect to SPD and percentage of powder to silver fraction is shown in Fig.5.4. It is clear that tapes with SPD 3.3 g cm⁻³ for the present tube dimensions which corresponds to a powder fraction of 40% deteriorates J_c irrespective of the tape width. Similarly tapes rolled from wires less than 1.3 mm show much lesser J_c for the whole range of SPD used in this study. Best J_c values are found for samples with SPD around 2.8 gcm⁻³ corresponding to a powder fraction of 33.5 wt.%.

Table 5.3. J_c values at the final stage of heat treatment

Sample	J_c (kA/cm ²)	J_c deviation
H3	9.1	+0.9 (9.8%)
H2	9.6	+1 (10.4%)
H1.3	10.5	+0.5 (4.8%)
H1	4.6	+0.7 (15.2%)
M3	15.0	+0.8 (5.3%)
M2	18.7	+0.9 (4.8%)
M1.3	14.7	+0.7 (4.8%)
M1	8.5	+0.4 (4.7%)
L3	14.4	+2.8 (5.6%)
L2	15.5	+0.5 (3.2%)
L1.3	12.2	+1.1 (9.0%)
L1	8.1	+0.6 (7.4%)

**Fig. 5.4** Variation of J_c as function of the superconductor powder fraction (starting packing density)

The dependence of J_c on tape width for different SPD is shown in Fig.5.5. The J_c of all the samples initially increases with increase in tape width. It reaches a maximum around 4.2 mm corresponding to a wire diameter of about 2 mm for M and L series samples and decreases thereafter. The H series samples show irregular J_c variation obviously due to the different degrees of damages taken place because of insufficient sheath thickness.

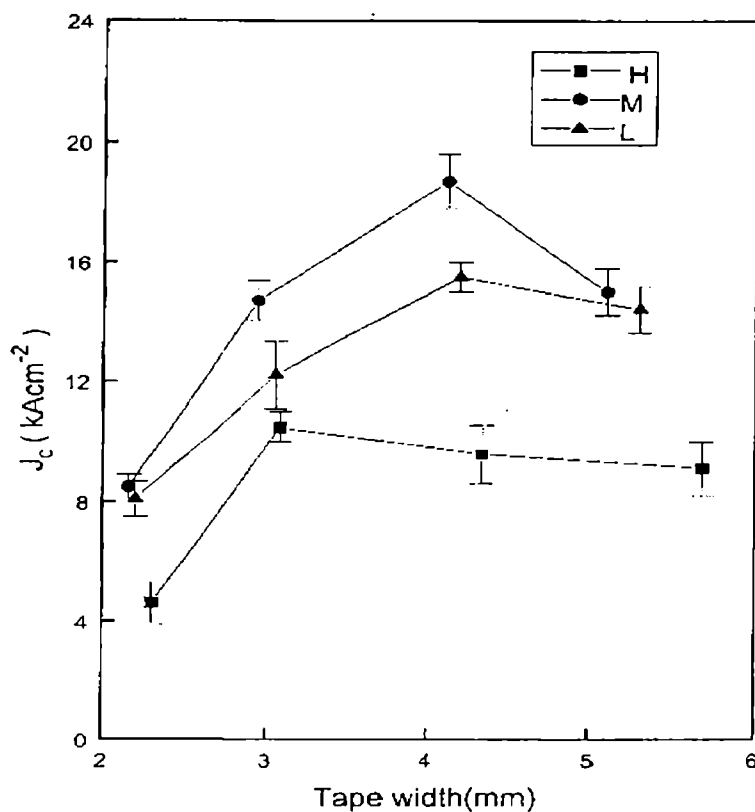


Fig. 5.5 Variation of J_c as function of the tape width(directly related to the stating wire diameter)

5.2.3. Conclusions

A systematic study on the effects of SPD and tape width on J_c in the PIT processing of (Bi,Pb)-2223/Ag tapes has been carried out. SPD

and tape width are found to be two important parameters which determine the final core density and J_c . An SPD around 2.8 g cm^{-3} for the present tube dimensions and a tape width around 4.2 mm (starting wire diameter around 2.0 mm) are found to be optimum for obtaining patch free tapes with high core density and J_c . In other words, a powder to silver fraction around 33.5 wt.% and tape width around 4.2 mm shall be optimum irrespective of the tube dimensions. Powder fractions beyond 33.5 wt.% leads to punctured tapes with poor core density and J_c .

5.3. Preparation of multifilamentary tapes: Optimization of geometrical parameters

The geometrical parameters related to the multifilamentary tape layout such as wire diameter in filling stage, number of filaments, wire diameter for tape rolling and the tape thickness are optimized and the results are presented in this section.

5.3.1. Experimental

In the previous section, it was concluded that a powder fraction of 33.5 wt.% is optimum for the preparation of monofilament tapes. In the preparation of multifilament tapes, monofilament wires of required diameter are filled in a silver tube of comparatively lesser wall thickness, groove rolled down to the required wire diameter, flat rolled and the thermomechanically processed to get the finished tapes. In order to get a smooth flow characteristics of the powder inside the sheath and to avoid the possible filament cracking that may occur during the mechanical rolling it was decided to use a lesser packing fraction

(i.e. 27.5 wt%) for the monofilament wires. Monocore wires of diameter 1.6 mm (16 Nos.), 1.1 mm (40 Nos.) and 0.75 mm (87 Nos.) were filled in Ag tubes of ID/OD – 8.5 mm/10 mm. In order to optimise the starting wire diameter, each of the above tubes were groove rolled down to three different wire diameters viz. 3 mm, 2.6 mm and 2.1 mm. The final tape thickness of individual wires were varied from 0.20 mm to 0.4 mm. Heat treatment was conducted in three stages with two intermittent rolling [50 + 50 + 100 h). The tapes were tested for the transport current at 77 K. The flow sheet for the preparation of multifilament tapes is given in Fig.5.6.

We label MFT16, MFT40 and MFT87 for the multifilamentary tapes having filament counts 16, 40 and 87 respectively.

5.3.2. Results and discussion

Figure 5.7 gives a typical optical micrograph of multifilamentary wire and tape. Fig. 5.8 gives the XRD pattern of the precursor and the tape after the final heat treatment. The precursor mainly consists of Bi-2212, the major phase, together with Ca_2PbO_4 and Bi-2201, the secondary phases. Eventhough the heat treatment was effective in converting Bi-2212 and other secondary phases of precursor into the desired Bi-2223 phase, traces of unreacted Bi-2212 is observed in the finished tape as can be seen in the XRD pattern. As the XRD is taken by exposing the etched surface of the tape, the amount of Bi-2212 left unreacted will be still high as the interior of the tape will have more unreacted material. This is because the conversion reaction of Bi-2212 and other phases into Bi-2223 is more effective in the silver ceramic interface.

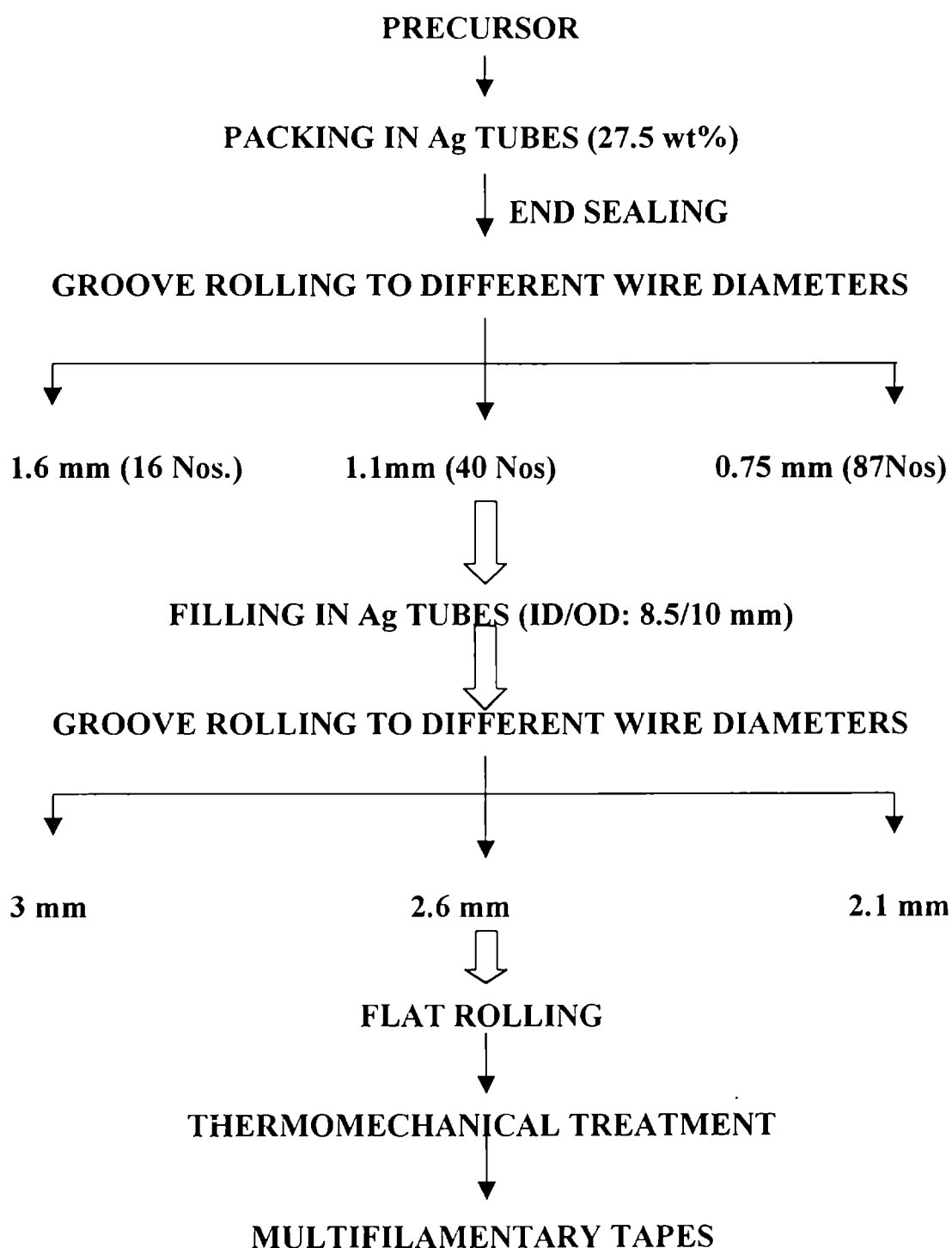


Fig. 5.6 Flow sheet for the preparation of multifilamentary tapes with different geometrical parameters

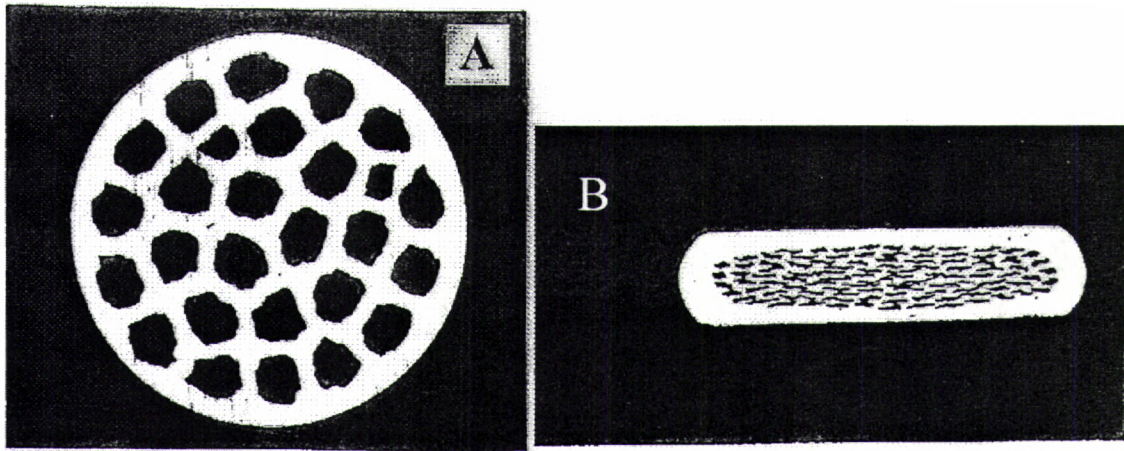


Fig. 5.7 A typical optical Micrograph of the as rolled multifilamentary wire (A) and tape (B)

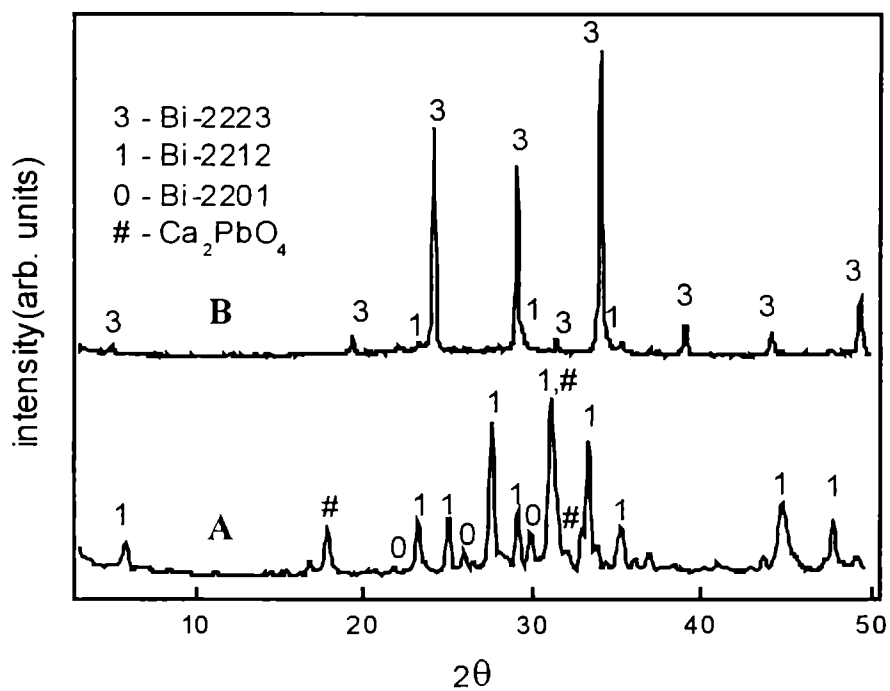


Fig. 5.8 XRD patterns of (A) precursor powder and (B) tape after the final stage heat treatment

Figures 5.9, 5.10 and 5.11 gives the variation of J_C as a function of thickness for multifilament tapes having filament counts 16, 40 and 87 respectively. For the MFT16 series samples, tapes prepared from starting wire diameter of 2.1 mm shows better J_C s for the whole range of thickness studied and the highest J_C obtained is 18.8 kA cm^{-2} for a tape

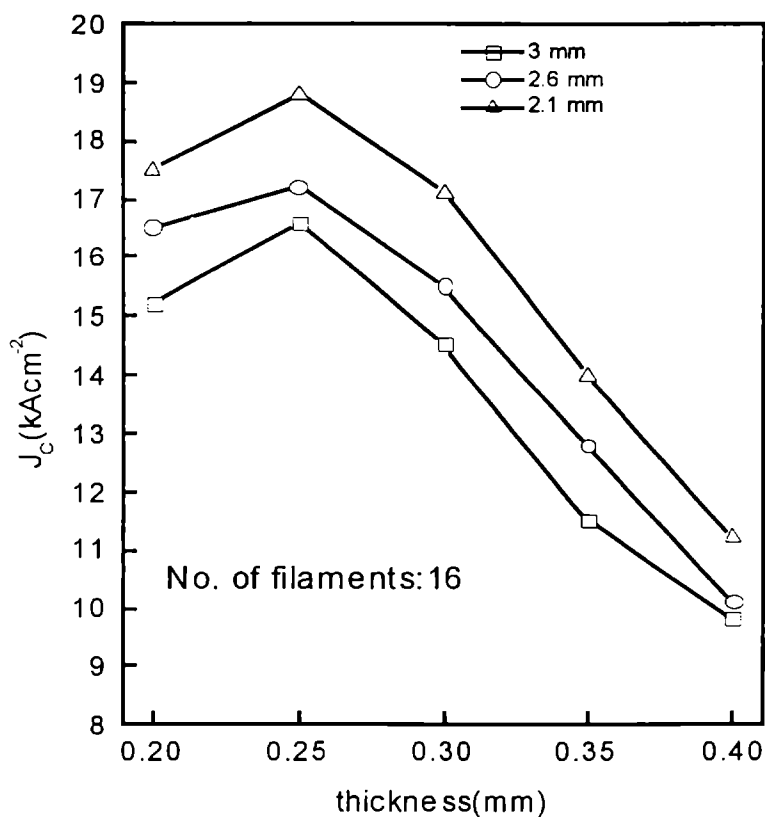


Fig. 5.9 Variation of J_C as a function of thickness for multifilamentary tapes having number of filaments 16 and with different starting wire diameters

having a thickness of 0.25 mm. For other samples also this thickness seems to be optimum and for thickness higher than this J_C s of all the samples decrease monotonically. For the MFT40 series samples tapes

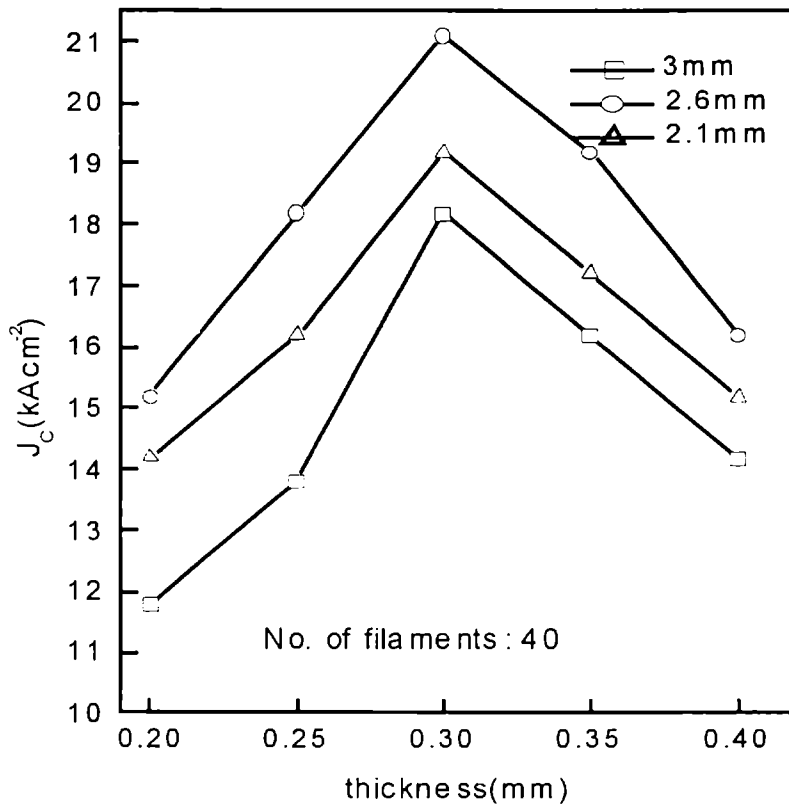


Fig. 5.10 Variation of J_C as a function of thickness for multifilamentary tapes having number of filaments 40 and with different starting wire diameters

prepared from starting wire diameter 2.6 mm show better J_C s throughout the whole range of thickness studied. In this case, a tape thickness of around 0.3 mm is found to be optimum for getting high J_C s. The highest J_C observed in this case is for a tape thickness of 0.3 mm which is 21.1 kAcm⁻². For the MFT87 series samples, the highest J_C observed is 16.8 kAcm⁻² for the tape having a thickness of 0.35 mm and starting wire

diameter 3 mm. In this case, tapes prepared from starting wire diameter 2.1 mm shows an increase of J_c with respect to the final tape thickness. For other two cases, i.e. with wire diameters 3.0 and 2.6 mm J_c

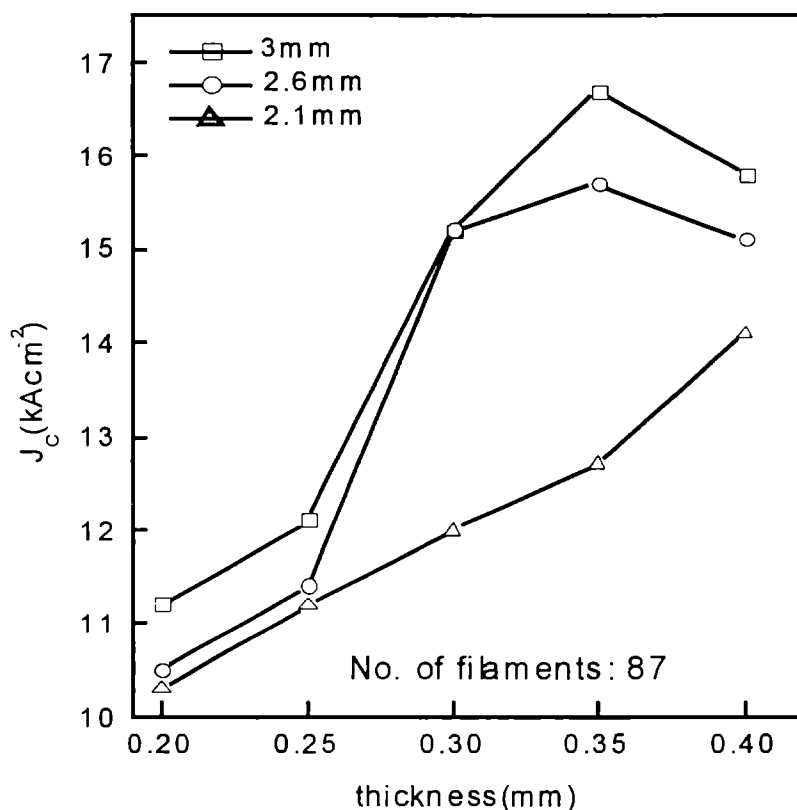


Fig. 5.11 Variation of J_c as a function of thickness for multifilamentary tapes having number of filaments 87 and with different starting wire diameters

increases from lower to higher thickness upto 0.35 mm and then decreases. Also the J_c values of all the tapes prepared from 2.1 mm wire is significantly lower compared to the other two sets.

On analysing figures 5.9 to 5.11 we can see that the final J_c values of the multifilamentary tapes do depend on the starting wire

diameter, the filament count and the final tape thickness. For a particular filament count the J_C is more dependent on the final tape thickness than the starting wire diameter. Also it is clear that as the filament count increases the optimum thickness for getting higher J_C s also increases.

For a particular value of final tape thickness in the wire-in-tube processing of (Bi,Pb)-2223/Ag multifilamentary tapes, the individual filament thickness depends on the number of filaments and starting wire diameter for flat rolling. Eventhough the thickness reduction by mechanical rolling have the advantage of improving grain alignment or texture, there is a limit value called process limit (the system limit is lower than the process limit) below which the current density of the tape will reduce due to the weak links produced by either inhomogeneity inside the filament or by the discontinuity and filament cracking. So when the filament number increases the final tape thickness also should increase for getting better J_C values as demanded by the process. This explains the observed thickness dependence of J_C with respect to the number of filaments, i.e. when the filament count increases the optimum thickness also should increase.

5.3.3. Conclusions

The dependence of the geometrical parameters of multifilamentary tape such as the number of filaments, starting wire diameter for flat rolling and the final tape thickness on the critical current density of the tapes has been understood.

It was found that the final tape thickness is a crucial parameter which has to be optimised for specific number of filaments. As the filament count in a multifilamentary tape increases the final tape

thickness also should be high for getting higher J_C values. A filament count of about 40 and a final tape thickness around 0.3 mm is optimum for preparing (Bi,Pb)-2223/Ag multifilamentary tapes.

5.4. Optimization of thermomechanical processing/heat treatment schedules of (Bi,Pb)-2223/Ag multifilamentary tapes

In the wire-in-tube process, the key to the achievement of high J_C values lies in optimizing the thermomechanical processing and heat treatment schedules. The present section describes the studies conducted to optimize the thermomechanical processing of multifilamentary tapes.

5.4.1. Experimental

Multifilamentary tapes are prepared by the wire-in-tube technique. As concluded in the previous section, the tapes prepared for the present study is the MFT40 with a starting wire diameter of 2.6mm. After an initial 30 h heat treatment and thickness reduction by mechanical rolling the tapes were divided into three batches – batch 1 (named as TP1) has gone for another 30 h heat treatment and flat rolled down to 0.3 mm; batch 2 (named as TP3) has gone for two 30h heat treatment and two rolling steps to a final tape thickness of 0.3 mm; batch 3 (named as TP4) has gone for 60 h heat treatment and flat rolled down to 0.3 mm. Now all the three batches, the samples were given a long duration heat treatment in the same furnace but for different durations; 140 h for TP1 and 110 h for TP2 and TP3; making a total of 200 h of heat treatment. XRD and SEM analysis, J_C and J_C -B measurements were done for evaluating the relative performance of the samples.

5.4.2. Results and discussion

The XRD patterns of the three batches of the samples prior to the final heat treatment is shown in Fig.5.12. The XRD of the sample after 30 h heat treatment is also given in the figure for comparison. Bi-2212 and Bi-2223 are found in varying amounts in all the samples. A quantitative estimation is made to find out the volume fraction of Bi-2223 in each sample from the X-ray peak intensities of Bi-2212 and Bi-2223. The results are shown in fig. 5.13, which is a comparative chart

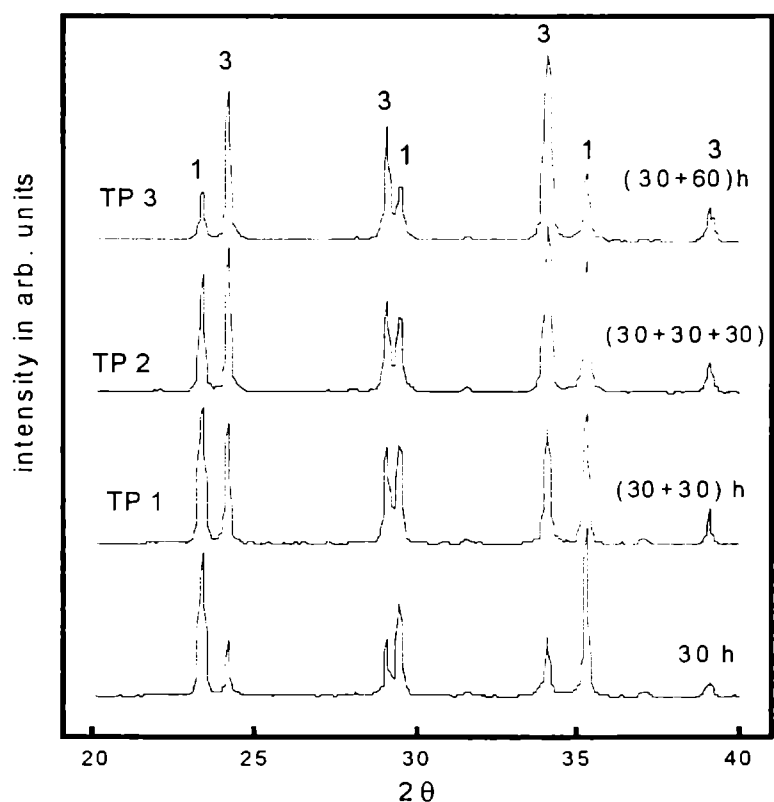


Fig. 5.12 XRD patterns of the samples prior to the last stage heat treatment: TP1 (30+30 h); TP2 (30+30+30 h); TP3 (30+60 h). XRD pattern of the tape after 30 h heat treatment is also shown in the figure.

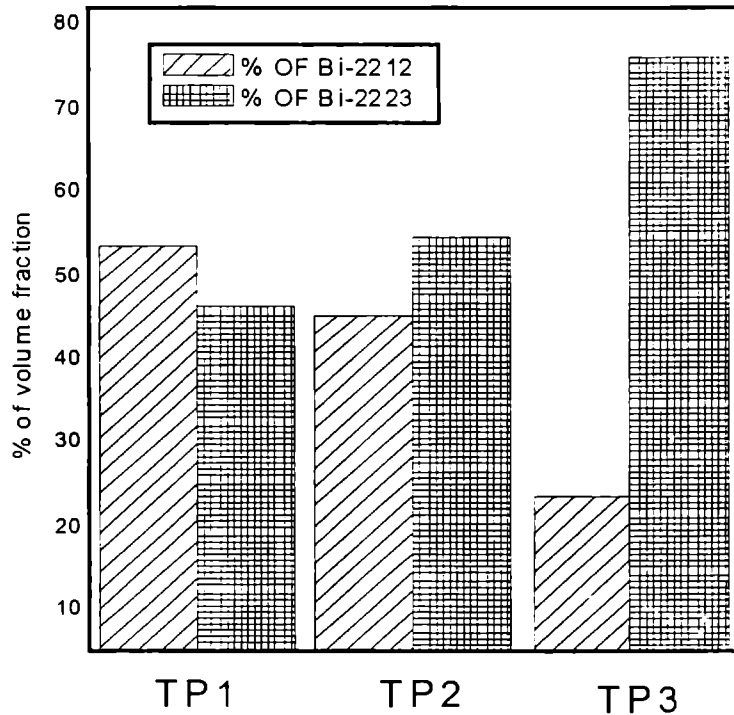


Fig. 5.13 Comparative chart showing the volume fraction of Bi-2212 and Bi-2223 prior to the last stage rolling for the different thermomechanical processing; TP1 (30+30 h), TP2 (30+30+30 h), and TP3 (30+60 h)

giving the volume fractions of Bi-2212 and Bi-2223 for each of the heat treatment schedules TP1, TP2 and TP3. The highest amount of Bi-2223 is observed for TP3 and the lowest for TP1. Eventhough both TP2 and TP3 samples had undergone a total of 90 h heat treatment, the fraction of Bi-2223 found in TP3 is about 76%, while that in TP2 is only 54%. TP1 shows a conversion of 46% of Bi-2223 after 60 h of sintering.

The lower fraction of Bi-2223 found in TP2 compared to TP3 could be understood by taking into account the incubation period required for the formation of Bi-2223. During the reaction-sintering of Bi-2223 from the precursor phases (reactants) the conversion gets initiated only after an initial gestation period. For TP2 the total 90 h heat treatment being divided into periods of 30 h each, a significant time in each period is consumed towards the gestation period required for the formation of Bi-2223, reducing the overall reaction rate.

Figure 5.14 gives the XRD patterns of the samples after the final stage of heat treatment. Eventhough the reaction-sintering is effective in converting Bi-2212 and other secondary phases into Bi-2223, Bi-2212 is found in all the samples. The results of the quantitative estimation done to determine the volume fraction of Bi-2223 and Bi-2212 are given in Fig.5.15. Bi-2212 is lowest in TP3 and highest in TP1. About 95% of Bi-2223 is formed for TP3, about 90% for TP2 and 87% for TP1. Most of the XRD peaks are originated from $00l$ reflections suggesting the texture development during the thermomechanical treatment.

Figure 5.16 shows the SEM picture of the surface morphologies of the samples after the final stage of heat treatment taken in the back scattered mode. The surface morphology of the samples differ considerably depending on the processing conditions. The striking feature is that the sample TP1 is highly porous and contains relatively smaller grains compared to that of TP2 and TP3. Large single crystalline like grains with highly dense structure are seen in TP3 which is an indication of the better processing condition. Thus as we go from sample TP1 to TP3 the density monotonically increases. This can be understood

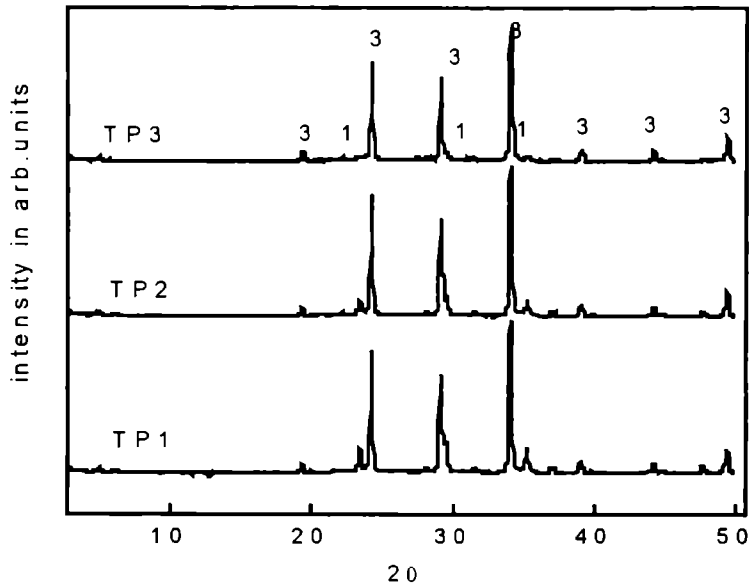


Fig. 5.14 XRD patterns of the samples after the final stage heat treatment

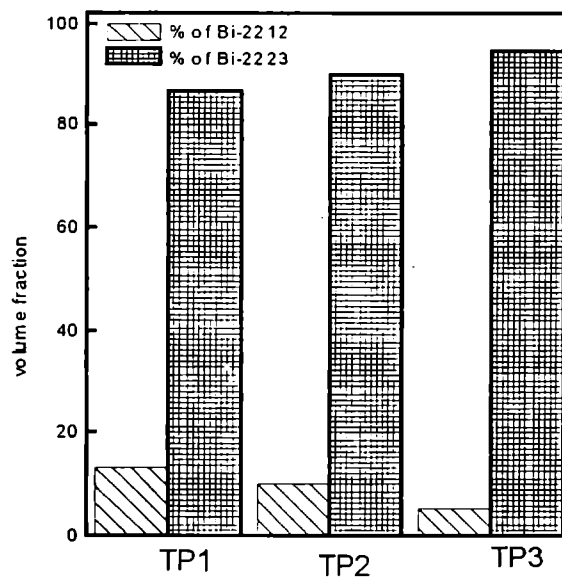


Fig. 5.15 Comparative chart showing the volume fractions of Bi-2212 and Bi-2223 after the last stage heat treatment for the different thermo mechanical processing; TP1(30+30+140 h), TP2(30+30+30+110 h), and TP3(30+60+110 h)



Fig. 5.16 SEM Micrograph of the surface morphologies of (a) TP1, (b) TP2 and (c) TP3 samples after the final stage heat treatment.

in the light of dedensification of BPSCOO during the reaction-sintering and can be correlated with the fraction of Bi-2223 present in the samples prior to the final heat treatment (TP1-46%, TP2-54% and TP3 – 76%). The results show the importance of obtaining a greater Bi-2223 conversion in the tape prior to the final heat treatment for achieving a dense microstructure.

Fig.5.17 gives the J_c variation of samples after the final stage heat treatment. The J_c values observed for the samples are in agreement with the XRD and SEM results. TP3 shows the highest J_c value and TP1 shows the lowest J_c value.

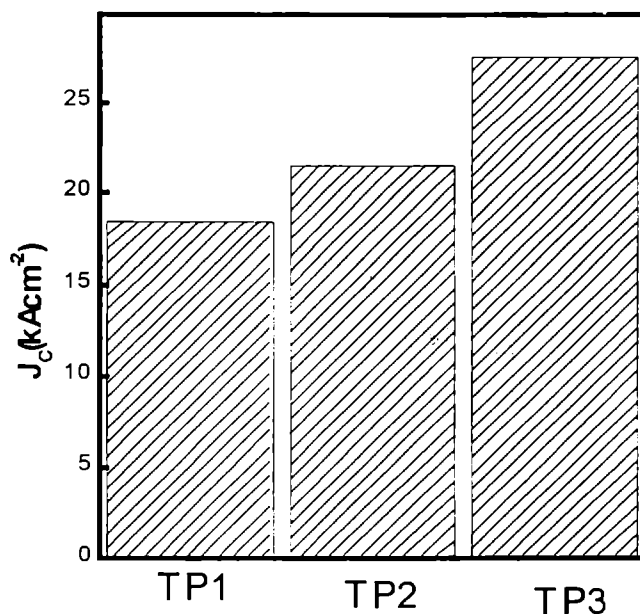


Fig. 5.17 Bar graph showing the J_c variation for the three samples viz. TP1, TP2 and TP3 after the final stage of heat treatment

Fig. 5.18 shows the J_c -B characteristics of the samples. Magnetic field is varied from 0 to 3500 G and is applied parallel to the c-axis of

the tape. It is obvious that TP3 shows a better J_c - B characteristics, i.e. less reduction of J_c in applied magnetic fields. The J_c -B characteristics of TP2 is close to that of TP3 and TP1 shows a poor behaviour on applied field. The observed difference in the J_c -B characteristics can be understood when we analyse the J_c values, XRD, and SEM results of the samples. Better J_c - B characteristics of TP3 when compared to TP2 and TP3, is obviously due to the J_c enhancement by better phase purity, and microstructure of the sample.

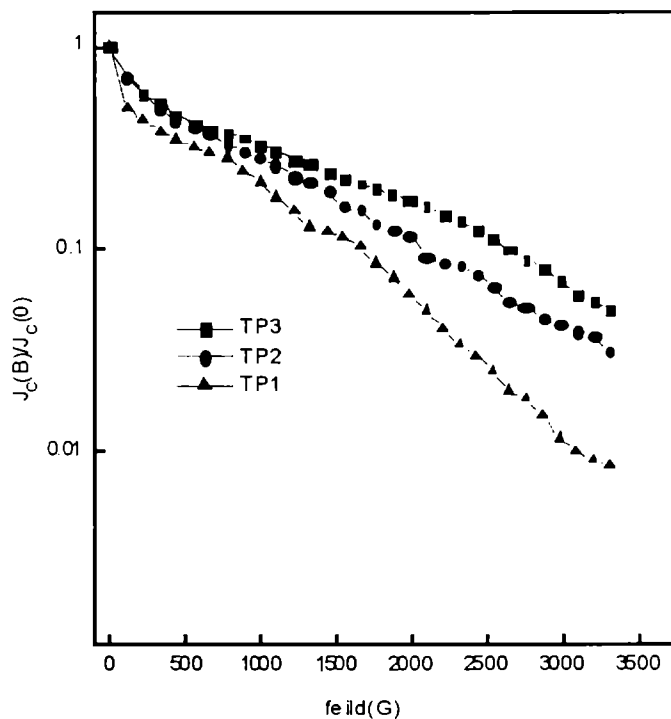


Fig. 5.18 J_c -B characteristics of multifilamentary tapes prepared by the different thermomechanical processes: TP1, TP2, and TP3. Y-axis is normalised with respect to the zero field J_c of individual samples.

It is generally observed that retrograde densification occurs during the formation of Bi-2223 phase [18-20]. That is, during the

formation or heat treatment stage Bi-2223 gets dedensified and the intermediate deformation/rolling redensifies the grains. Therefore prior to the last stage heat treatment, phase assemblage of the tape should be critically adjusted so that there is enough room for the reaction sintering to be effective and improve the density of the final product. Another problem to tackle with is that during the mechanical deformation grains get fragmented and these must be effectively healed during the final sintering stage. In the case of TP3 after 90 h of heat treatment (prior to the last stage rolling) more than 75% of the grains are of Bi-2223 and are getting realigned and densified during the final stage deformation, so that the final density and texture are improved. But for TP2 and TP1 the amount of aligned and densified Bi-2223 grains prior to the last stage sintering is comparatively lesser, and that the amount of Bi-2212 is comparatively high, resulting in a lower current density and a poor $J_C - B$ characteristics.

5.4.3. Conclusions

The phase assemblage of the tape prior to the last stage deformation and heat treatment is a crucial parameter affecting the J_C , $J_C - B$ and microstructure of the finished tapes. A fraction of more than 75% for Bi-2223 prior to the last stage rolling and a final sintering duration of >100 h seem to be optimum for the preparation of multifilamentary tapes. Moreover the heat treatment schedules must be so adjusted that after every heat treatment stage significant amount of conversion must take place.

References

- [1] N.N. Merchant, J.S. Luo, A.K. Fischer, V.A. Maroni, E.R. Podtburg, W.L. Carter, Q. Li, A. Otto, M.W. Rupich and G.N. Riley Jr., *Supercond. Sci. Technol.* 12 (1999) 327.
- [2] H. Eckelmann, M. Daumling, M. Quilitz and W. Goldacker, *Physica C*, 295 (1998) 198.
- [3] C.H. Kato, H.Y. Tang, Y.S. Hhine, S.R. Sheen, M.K. Wu, C.C. Tsuel, C.C. Chi and D.T. Shaw, *Supercond. Sci. Technol.* 7 (1994) 470.
- [4] J.T. Dawley, S.E. Dorris, E.P. Kvam and R.B. Poeppel, *Supercond. Sci. Technol.* 7 (1994) 587.
- [5] K. Matzuzaki, K. Shimizu, A. Inone and Masumoto, *Jpn. J. Appl. Phys.* 33 (1994) L308.
- [6] L. Martin, J. Bechtold, M. Mazaros, V. Ottoboni, U. J-C. Uallier and Zanella, *S. Supercond. Sci. Technol.* 7 (1994) 24.
- [7] V.E. Sytniko, V.A. Mitrokhin, P.I. Dolgosheev, M.V. Polyakova, I.P. Radchenko, G.G. Svavlov and G. Ziemek, *Supercond. Sci. Technol.* 7 (1994) 115.
- [8] K. Endo, H. Yamasaki, S. Misawa, S. Yohida and K. Kajimura, *nature*, 355 (1992) 324.
- [9] Y. Hakuraku and Z. Mori, *J. Appl. Phys.* 73 (1993) 309.
- [10] H. yamasaki, K. Endo, S. Kosaka, M. Umeda, S. Yoshida and K. Kajimura, *Phys. Rev. Lett.* 80 (1994) 3331.
- [11] P. Wasner, U. Frey, F. Hillmer and H. Adisian, *Phys. Rev. B.* 51 (1993) 1206.
- [12] L. Martin, *Supercond. Sci. Technol.* 11 (1998) 231.

- [13] M.W. Rupich et al. 1998. Proc. (1998) ISTECS-MRS Workshop on superconductivity (Okinawa, Japan) Tokyo: ISTECS) p147.
- [14] M.S. Sarma, U.Syamaprasad, P.S. Murkherjee, P.Guruswamy, K.G.K. Warriar and A.D. Damodaran. Supercond. Science and Technology (UK) 10, 337-341 (1997).
- [15] J. Jiang, X.Y. Cai, A.A. Polyanski, L.A. Schwartzkopf, D.C. Larbalestier, R.D. Parella, Q. Li, M.W. Rupich and G.N. Riley Jr., Supercond. Sci. Technol. 14 (2001) 548.
- [16] Larbaleslier, D.C. et. Al. Advances in Superconductivity XI, 1999 (Tokyo: Springer) p805.
- [17] J.A. Parrell, A.A. Polyanski, A.E. Pashitski and D.C. Larbaleslier, Supercond. Sci. Technol. 9 (1996) 393.
- [18] X.Y. Cai, A. Polyanski, Q. Li, G.N. Riley Jr. and D.C. Larbaleslier, Nature, 392 (1998) 906.
- [19] Y. Yamada, M. Satou, S. Murase, T. Kitamura and Y. Kamisada, Advances in Superconductivity X (Tokyo: Springer) (1998) 909.
- [20] Y. Yamada, M. Satou, T. Masegi, S. Nomura, T. Koizumi and Y. Kamisada, Advances in Superconductivity VI (Tokyo: Springer) (1998) 609.
- [21] B. Wolf, P. Paufler, M. Schuber, C. Rodig and K. Fisher, Supercond. Sci. Technol. 9 (1996) 589.

CHAPTER 6

PREPARATION AND CHARACTERIZATION OF HTS CURRENT LEADS USING MULTIFILAMENTARY (Bi,Pb)- 2223/Ag AND Ag-ALLOY SHEATHED TAPES

6.1. Introduction

Based on the results of the previous studies, it is possible to prepare multifilamentary tapes of reasonable current density and with other necessary properties needed for the current leads. But one of the important factors to be considered when going to the application prototypes is the homogeneity of J_c along the length of the tape and its consistency. Recent magneto optical imaging (MOI) studies [1-4] conducted on filaments extracted from good quality tapes led to the conclusion that the actual supercurrent carrying area of BPPSCO tape is very much lower than the total area of superconductor core. The main reason suggested was the poor connectivity between the grains due to the presence of a large number of incipient cracks which remain unhealed even after the final stage of heat treatment. The cracks were originated due to filament fragmentation during rolling process. Moreover rolling produces transverse cracks which are more severe as the current percolation between the grains is considered compared to the cracks produced by uniaxial pressing, applied perpendicular to the tapes surface, which are longitudinal and doesn't severely affect the current percolation path [2]. To minimize the cracks and to enhance the density and texture of the finished tapes researchers are exploring the possibility

of over pressure processing in BSCCO tapes at the sintering temperature [5]. In the present case as an effort to maximize the current density as well as the J_c homogeneity along the length of the tape a detailed investigation has been carried out to study the effect of uniaxial pressing applied prior to the last stage heat treatment of the multifilamentary tapes and the results are discussed in the first part of this chapter.

The second part of this chapter describes the preparation and characterization of prototype current leads using the multifilamentary tapes processed in the optimized conditions. Development of large current capacity current leads with minimized heat leak using Bi-2223 tapes in different configurations is being actively pursued by various research groups around the world [6-15] for high current magnets such as LHC, ITER etc. The current lead described here is a general purpose type that can be operated in the conduction cooled mode.

6.2. Optimization of Uniaxial pressure for the preparation of multifilamentary tapes

The effect of uniaxial pressing applied prior to the last stage sintering on the superconducting properties of the multifilamentary tapes will be discussed in this section.

6.2.1. Experimental

Multifilamentary tapes were prepared by the wire-in-tube technique. Based on the results of the previous experiments, the filament count was taken as 40 and the starting wire diameter for flat rolling was 2.6 mm. After a two step heat treatment and an intermediate rolling (30+60 h) the multifilamentary tapes of thickness 330 μm were

given uniaxial pressure from 25 to 100 Mpa. Then all the samples were heat treated for another 110 h making the process schedule identical to the conditions for TP3 described in the previous chapter. The samples were labelled as MFT25, MFT50, etc for the samples pressed with the pressure 25 Mpa, 50 Mpa etc. The tapes were characterized by J_c (0 T, 77 K) and J_c -B measurements and SEM analysis to evaluate the relative performance of the samples.

After the optimization of pressure, multifilamentary tapes of length > 15 cm were prepared by both pressing and rolling prior to the last stage sintering. In order to press the samples having length > 15 cm a rectangular die has been fabricated in die steel with the dimensions suited for pressing the tapes. The final tape thickness of both samples was $300 \mu\text{m}$. The tapes were tested for J_c (0 T, 77 K), J_c - homogeneity along the length of the tape and the J_c -B behaviour. The homogeneity tests were conducted by taking voltage terminals at an interval of 1 cm along the length of the tape and measuring the I_c between two consecutive terminals using the criterion $1 \mu\text{v cm}^{-1}$. The tapes were coated with a thin layer of GE varnish before immersing in liquid nitrogen to avoid the possible blistering caused by evaporation of trapped liquid nitrogen.

6.2.2. Results and discussion

Fig.6.1 shows the variation of J_c with applied pressure for the multifilamentary tapes after the final stage heat treatment. It is evident from the figure that a pressure of 50 MPa is optimum as the J_c of MFT 50 is 35.2 kAcm^{-2} , the highest compared to all other samples. Beyond

this pressure, J_c decreases sharply and reaches 13.2 kAcm^{-2} for MFT 100. The J_c of MFT 25 is 30.5 kAcm^{-2} .

Fig. 6.2 gives the variation of normalised J_c ($J_c(B)/J_c(0)$) as a function of the applied field which is parallel to the c-axis of the tape. It is noteworthy that the J_c -B behaviour of MFT 25 and MFT 50 are almost same and are superior to compared to the behaviour of MFT75 and MFT100. The remenant J_c s at a field of 0.375 T is 4.5% of the zero

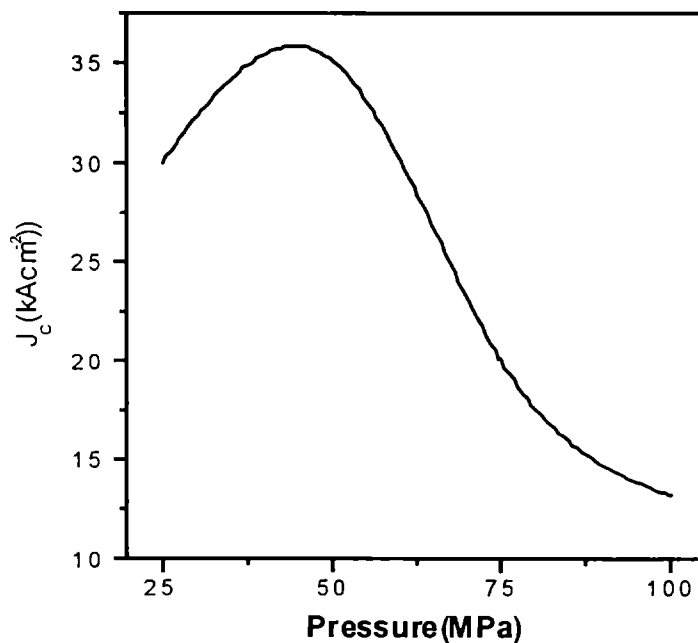


Fig. 6.1 Variation of J_c as function of uniaxial pressure applied to the multifilamentary tapes prior to the last sintering

field value for both MFT 25 and MFT 50, but that of MFT 75 is only 0.6% and for MFT 100 is below the detectable limits used in the present study.

In fig. 6.3(a) to (d) shows the SEM picture of the cross sectional views of the samples after the final stage of heat treatment. The sectional morphology of both MFT25 and MFT50 seems to be the same. But the grains are more densely packed and level of orientation is also better for MFT50 compared to MFT25. Moreover for both the samples the grain structure seems to be continuous with lesser number of grain boundaries. On going to figure 6.3(c) which is the structure of MFT75, it can be noted that the grains are still densely packed but the grain size is smaller and the continuity in terms of the length of a single grain is

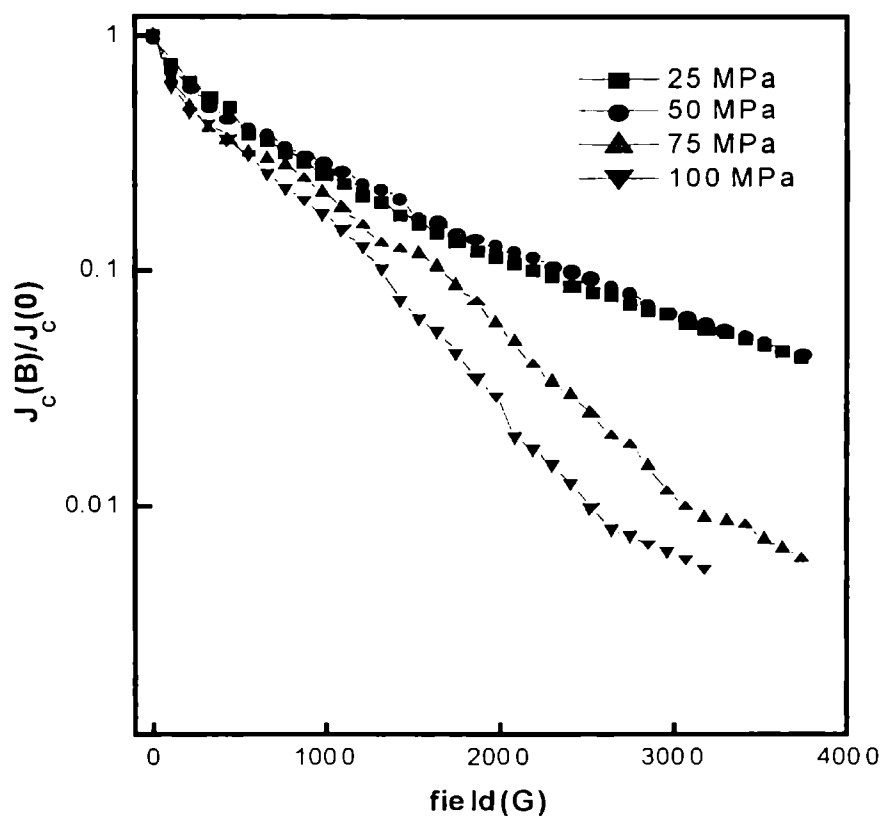


Fig. 6.2 Variation of J_c as a function of applied field for the tapes prepared with different pressures

also lesser making more number of grain boundaries. In the case of Fig. 6.3 (d) the continuity of the grains is further reduced and the grain boundaries are discontinuous making the intergrain connectivity very poor. Also it can be noted that there is no substantial improvement in the density or texture of MFT 100 compared to that of MFT 75.

The observed difference in J_C as well as the J_C -B behaviour of the samples can be explained by taking into account of the different structural morphologies seen in the samples. On increasing the pressure beyond 50 MPa the grain structure is distorted and more weak links are

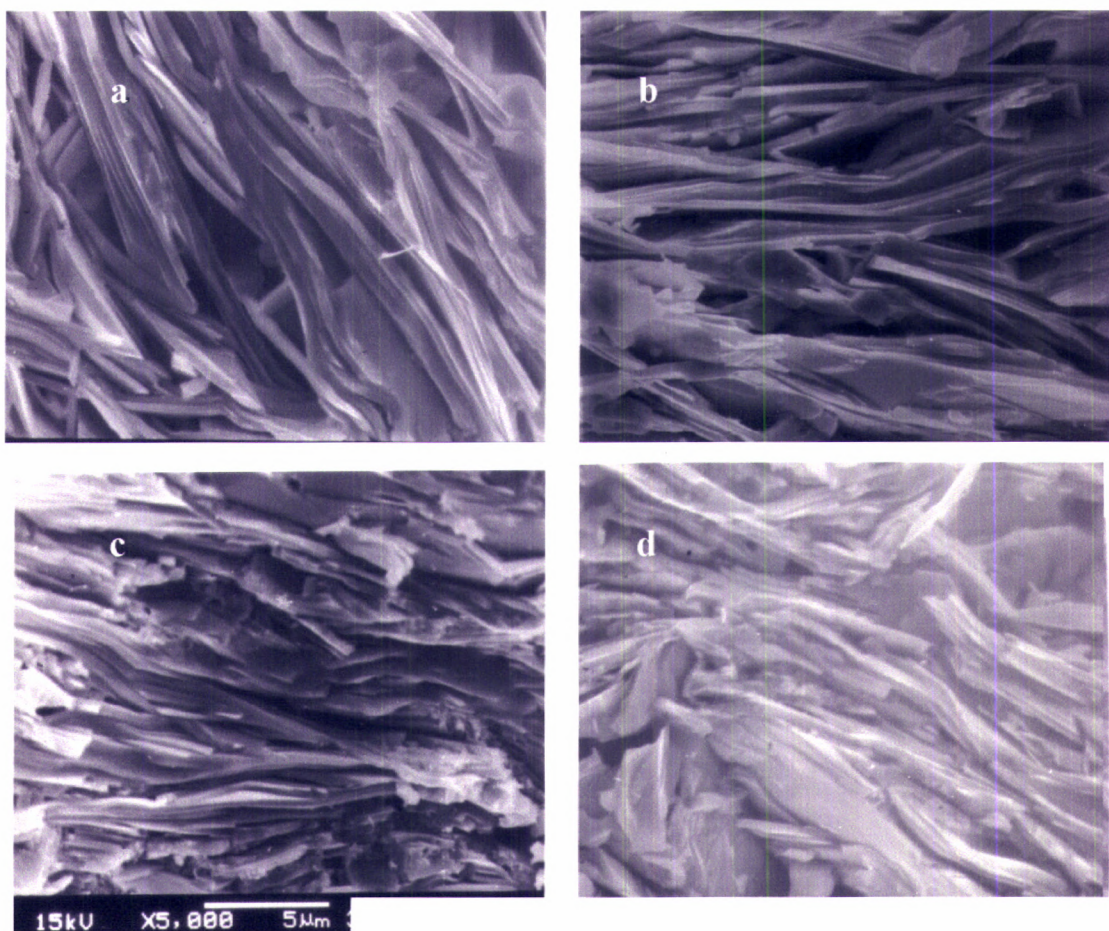


Fig. 6.3 SEM micrograph of the transverse section of samples pressed with (a) 25MPa, (b) 50 MPa, (c) 75 MPa and (d) 100 MPa

produced, yielding a lower J_C and a poor J_C -B behaviour for the MFT 75 and MFT 100 samples. For MFT 100 even the grain boundaries are discontinuous and that is why the very poor J_C and J_C -B behaviour.

Fig. 6.4 shows the variation of J_C along the length of the multifilamentary tape prepared by pressing and rolling applied prior to the last stage heat treatment. Both the J_C as well as J_C homogeneity of the pressed tapes are better compared to the rolled one. While there is

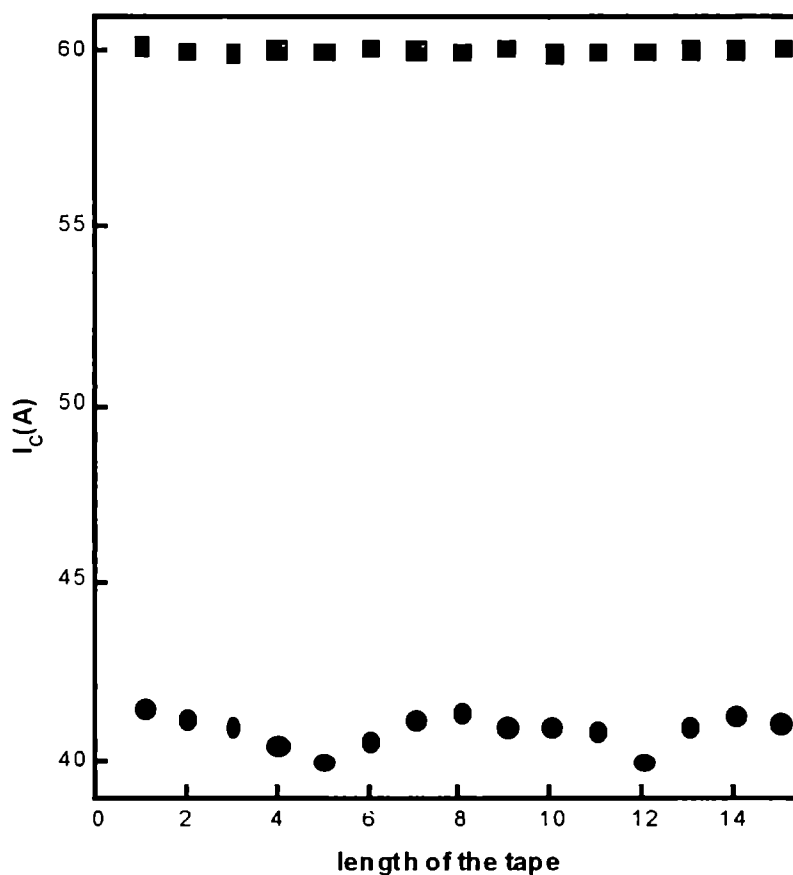


Fig. 6.4 Variation of J_C as function of the length of the tape

only a variation of 0.3% in J_C in the pressed tapes, the rolled tape has an inhomogeneity of $J_C \sim 4\%$ along the length of the tape.

Fig. 6.5 gives the J_C -B characteristics of pressed and rolled tapes. It is obvious that the macroscopic connectivity of pressed tapes is better and the weak links are reduced compared to the rolled one, smoothening the current percolation between the grains.

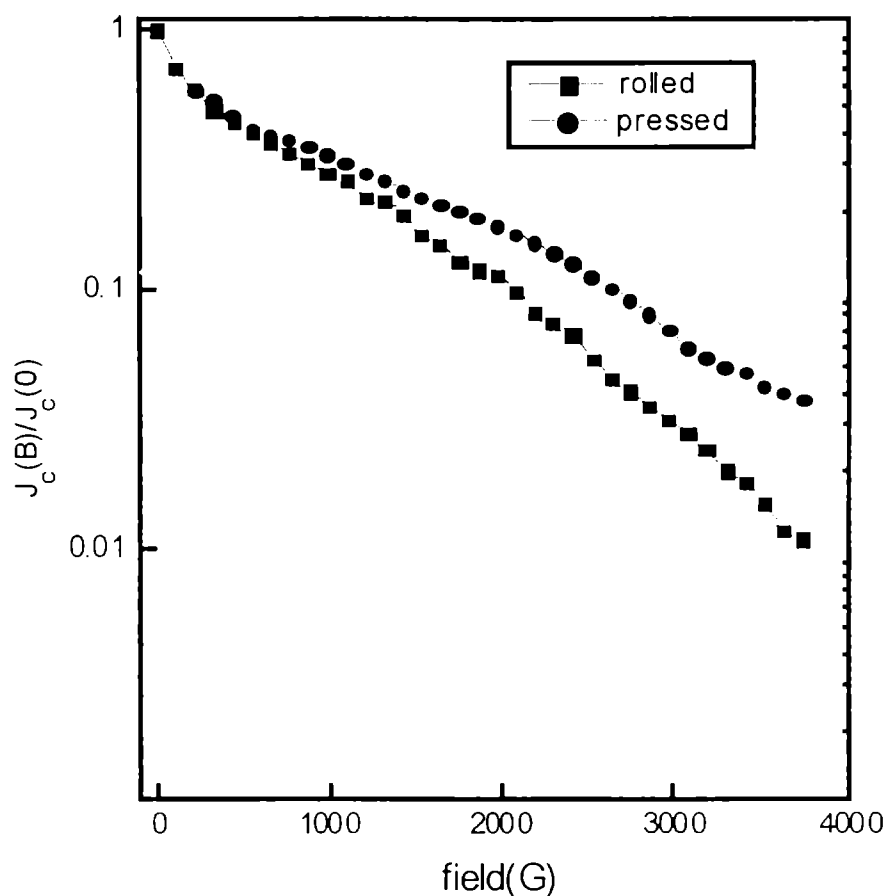


Fig. 6.5 Variation of normalised J_C as a function of applied field for the rolled and pressed samples

6.2.3. Conclusions

The following points can be concluded from the present investigation.

- (i) Compared to the deformation by mechanical rolling uniaxial pressing has greater advantages such as improving the core density, texture and connectivity of the grains.
- (ii) The level of J_C and its homogeneity along the length of the tape as well as J_C -B characteristics of the pressed tapes are much superior compared to the rolled tape.
- (iii) The observed scattering in J_c along the length of the pressed tape is only 0.3% of the maximum measured, while that of a rolled tape is ~4% of the maximum.

Eventhough uniaxial pressing is not suitable for the preparation of long length tapes, laboratory scale samples of length ~20 can be successfully prepared by uniaxial pressing applied prior to the last stage sintering.

6.3. Preparation and Characterization of Prototype HTS Current Leads

Having been optimized the material properties and processing conditions of the multifilamentary tape so as to suit for the preparation of current leads, it is necessary to identify the design criteria for the current leads. The main design requirements are the current rating and the operational environment viz. temperature and field. The preparation

and characterization of a pair of general purpose current lead with a rating of > 100 A at 77 K, 0 T for operation in conduction cooled mode will be described in the following section.

6.3.1. Experimental

The flow sheet for the preparation of HTS current lead is given in Fig. 6.6. As concluded from the previous studies, 0.3 wt.% nanosize MgO particles were added to the precursor powder to enhance the $J_C - B$ characteristics of the final tape. The precursor is filled in an AgAu6 (Au – 6 at.%) tube of ID/OD : 8/10 mm and groove rolled down to 1.1 mm. 40 Numbers of such wires were filled in an AgCu6 (Cu – 6 at.%) tube of ID/OD 8.5/10 mm and groove rolled down to 2.6 mm. Then the composite wire is flat rolled to 400 μ m. Initial two stages of heat treatment (30 + 60 h) was done with one intermediate rolling to 330 μ m. Heat treatment was done at 831°C in air in a large volume muffle furnace with temperature stability and accuracy better than $\pm 1^\circ\text{C}$. The tapes were then pressed uniaxially at a pressure of 50 MPa and again heat treated for another 110 h at 831°C. The final tape thickness being 0.3 mm. The multifilamentary tapes were then tested for $V - I$ and $J_C - B$ characteristics. Two such tapes of I_C 60 A at 77 K, 0T were packed in a cryostable glass fibre reinforced epoxy (GFRE) tube with compatible thermal expansion coefficient with the alloy used. Ni coated Cu end terminals were soldered to the HTS element as end connectors for the use of integration with the superconducting system. The prototype leads were tested for the current rating, thermal recycling tolerance and quench stability. Heat leak of the lead pair is estimated assuming a warm end temperature of 77 K and the cold end temperature of 4.2 K.

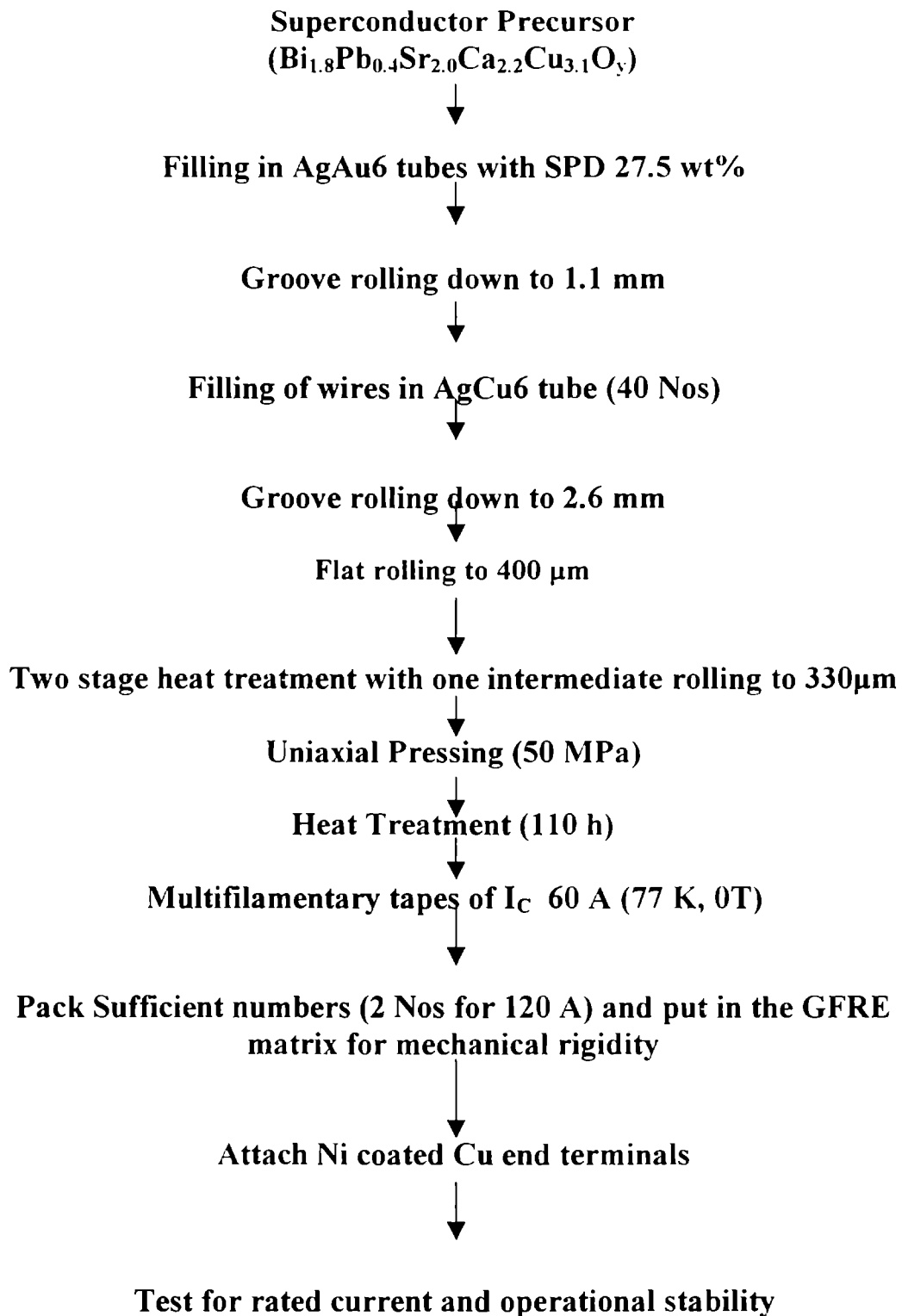


Fig. 6.6 Flowsheet for the preparation of current leads.

6.3.2. Results and discussion

Fig. 6.7 gives the $V - I$ characteristics of the multifilamentary tapes. The distance between voltage terminals was 10 cm. In the inset of the figure, $R-T$ plot of the same is given. Fig. 6.8 gives the J_c-B characteristics of the multifilamentary tapes with the applied field both parallel and perpendicular to the tape's surface. One should take care when anchoring the leads into superconducting systems so that any magnetic field present should be parallel to the tape's surface as the reduction of J_c in this direction is minimum. Three types of GFRE were tested for its thermal compatibility with the alloy matrix of HTS used. The types of GFRE tested were

- (i) GFRE I –Glass Cloth Reinforced Epoxy tube
- (ii) GFRE II –Glass Fibre (woven rovings) reinforced Epoxy tube
- (iii) GFRE III –Glass Fibre (chopped strand) reinforced Epoxy tube

and some of the important physical properties of these GFRE's are given in Table 6.1.

Table 6.1 Some of the important physical properties the three different GFREs tested for its suitability as housing matrix for current leads.

Property	Unit	GFRE I	GFRE II	GFRE III
Specific gravity	g/cc	1.85+0.05	1.80+0.03	1.70+0.05
Tensile strength	N/mm ²	300	280	240
Shear strength	N/mm ²	140	120	100
Insulation resistance	M ohm	50000	20000	10000

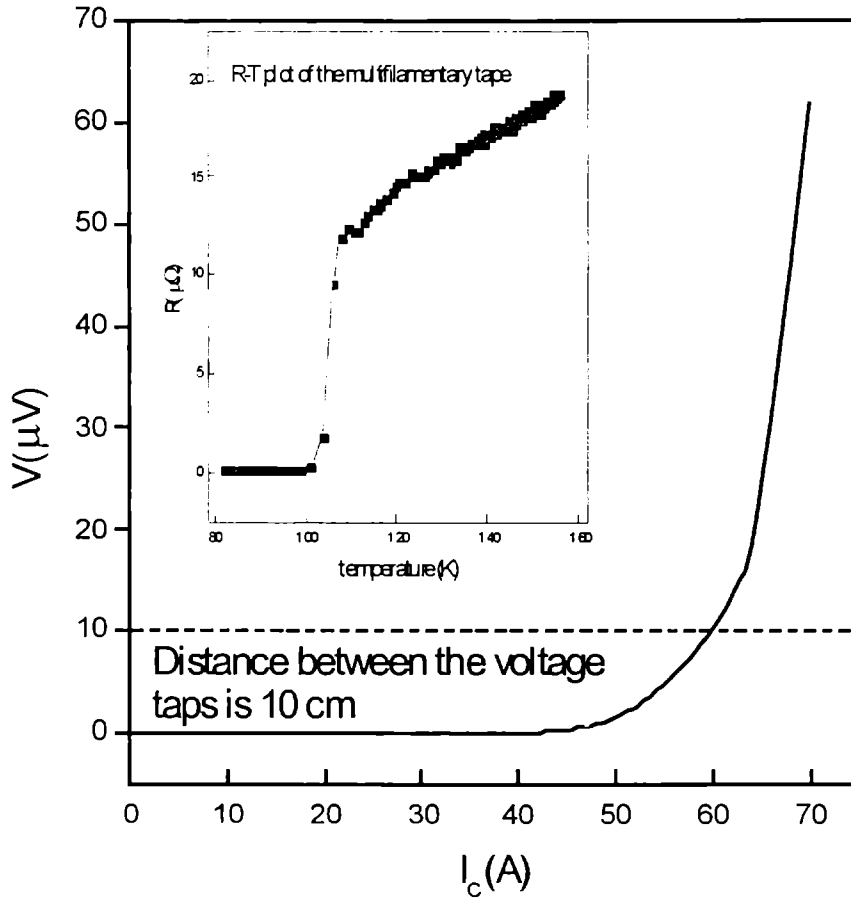


Fig. 6.7 V-I characteristics of the multifilamentary tape of length >10 cm used for the preparation of current leads

Fig. 6.9 gives the percentage of linear thermal expansion of three GFREs between RT and 77 K. For comparison, the thermal expansion coefficient of the alloy is also presented in the figure. Based on this result the GFRE II: Glass Fibre (woven rovings) reinforced epoxy tube is selected for the housing of current leads.

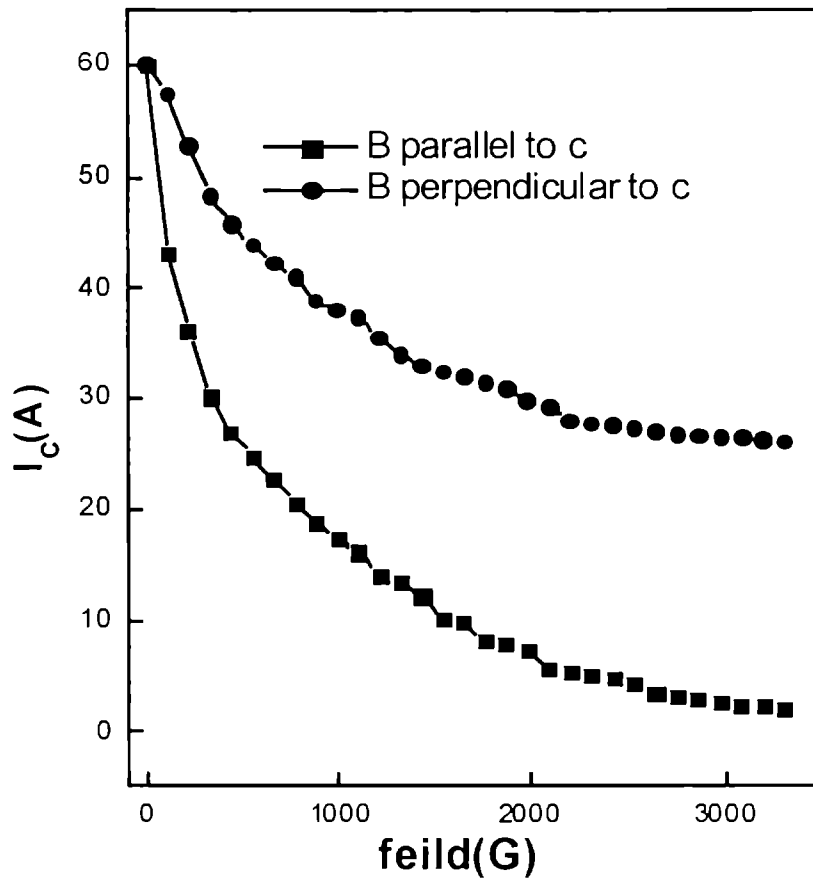


Fig 6.8 Variation of I_c as a function of the applied field, B, both parallel and perpendicular to the c-axis of the tape.

6.3.3. Testing of the current leads

(i) Thermal recycling tolerance

The thermal recycling tolerance has been tested by about 100 temperature excursions from RT to 77 K and back and measuring the critical current after each temperature excursions. No degradation of the properties was observed even after 100 recycling.

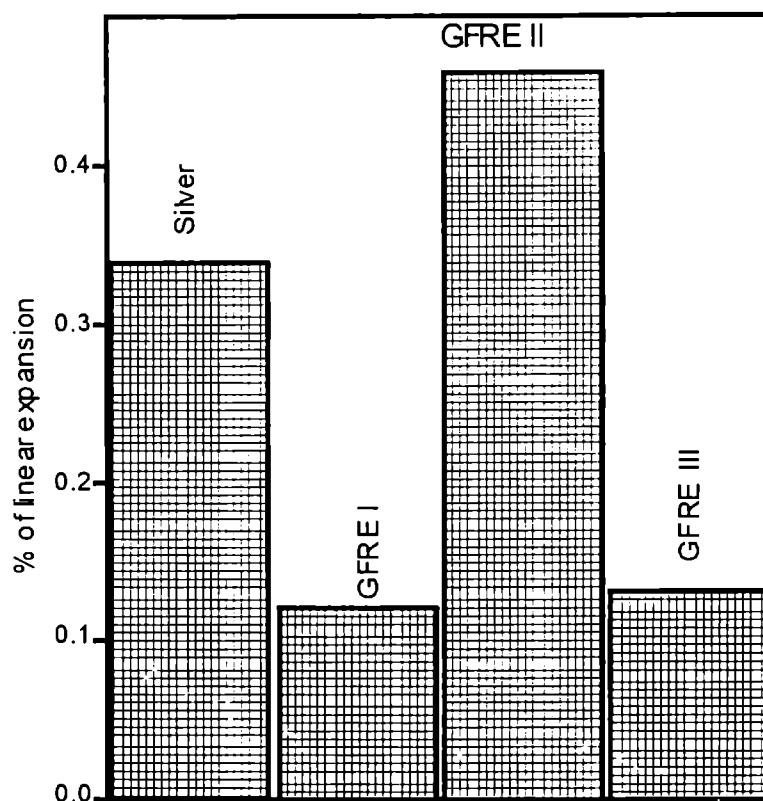


Fig 6.9 Comparative chart showing the variation of the percentage of linear expansion of silver and different types of GFREs

(ii) Transient Quench stability

Quench stability has to be tested by keeping the cold end of the lead at a constant temperature and slowly rising the hot end temperature near to the T_C of the material and passing the rated current, observing the heat dissipation and temperature profile along the length of the lead. If the lead is not protected for quench stability, a burn out will occur and the lead will be destroyed. In the present case, as we are unable to go to temperatures below 77 K, the quench stability of the prototype lead has

been tested for half of the rated current by keeping the hot end temperature at 100 K and cold end at 77 K. Neither any burn out nor any degradation of I_C was observed after ten such tests.

(iii) Heat leak estimation

Heat leak Q (W) through the superconducting tapes depends on the thermal conductivity 'K' (W/K cm) and the cross section $f \times S$ (cm^2) of the alloy sheath of the current lead, where f is the cross section ratio of the sheath to the total area S . The heat leakage Q of the current lead when anchored between 77 K (hot end) and 4.2 K (cold end) is given by

$$Q = (f \times S \div L) \int_{4.2}^{77} KdT \quad (1)$$

where L (cm) is the length of the current lead and T (K) is the temperature. Defining overall J_C (J_E) by the critical current density divided by the cross section of the tape, S is written as

$$S = I/J_E \quad (2)$$

From equations (1) and (2), it is understood that the rated current I and the heat leakage Q of the current lead depend on the thermal conductivity K of the alloy sheath, the sheath ratio, f and the J_E of the tape. On the basis of equations (1) and (2), the heat leak of the pair of prototype current lead for the rated current is 72 mW. In comparison, the heat leak produced by a current lead made of pure Ag as the sheath material under the same conditions is 14 W.

Fig. 6.10 shows the photograph of a pair of current leads of rating >100 A at 77 K.

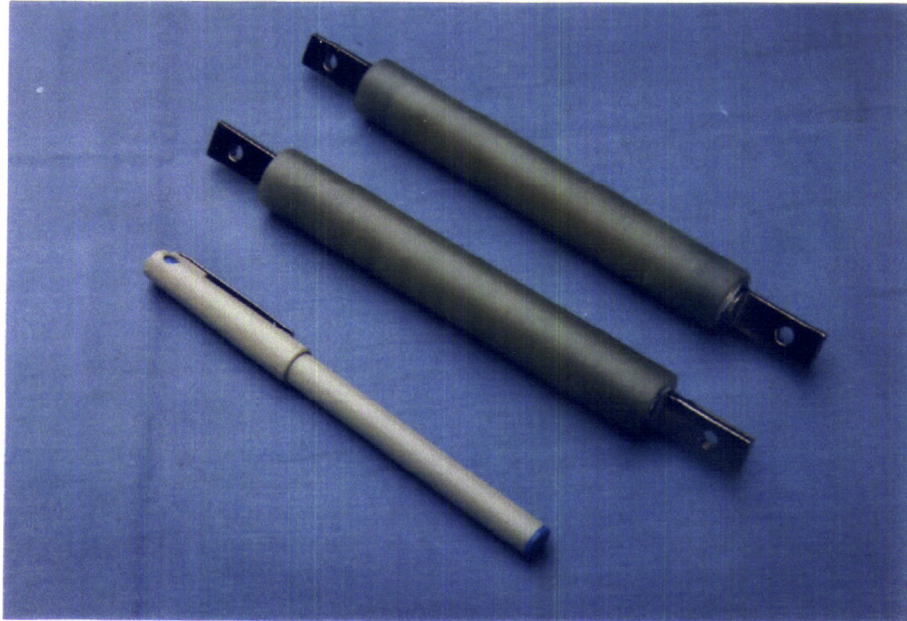


Fig. 6.10 Photograph of the prototype current leads

6.4. Conclusions

HTS prototype current leads of 10 cm length having a rating > 100 A at 77 K is prepared using multifilamentary (Bi,Pb)-2223 tapes comprising of inner AgAu (Au – 6 at.%) as sheath and outer AgCu (Cu = 6 at.%). This combination is helpful in reducing the thermal conductivity of the sheath and improving the mechanical stability of the tape. The estimated heat leak for the pair of current lead is 72 mW. In comparison, the heat leak of a pair of current leads of identical dimension prepared from pure Ag as sheath is 14 W.

References

- [1] A. Polyanski, D.M. Feldmann, S. Patnaik, J. Jiang, X. Lai, D. Larbalestier, K. DeMoranville, D. Yu, R. Parrella, *IEEE Trans. Appl. Supercond.* **11** (2001) 3269.
- [2] H.K. Liu, A. Polyanski, W.M. Chen, Y.G. Guo, S.X. Don, M. Apperley, *Presented at the Applied Superconductivity Conference*, Sept. 2000, Virginia.
- [3] D.C. Larbalestier, J.W.A. Anderson, S.E. Babcock, X.Y. Cai, S.E. Dowis, M. Feldmann, J.Jiang, Q. Li, J.A. Rarrell, R. Parrella, M. Polak, A. Polyanski, G.N. Riley Jr., M. Rupich and Y. Wu, *11th International Symposium on Superconductivity* Fukuoka, Japan, Nov. 1998.
- [4] X.Y. Cai, A. Polyanski, Q. Li, G.N. Riley Jr., D.c. Larbalestier, *Nature*, **392** (1998) 906.
- [5] M. O. Rikel, R.K. Williams, X.Y. Cai, A. A. Polyanskii, J.Jiang, D. Wesolowski, E.E. Helstrom, D.C. Larbalestier, K. DeMoranvillae, and G.N. Riley, Jr., *IEEE. Trans. on. Appl. Supercond.* **11(2)** (2001) 3026.
- [6] Y.Aoki, T.Koizumi, N.Ohtani, T.Hasegawa, L.Motowidlo, R.S.Sokolowski, R.M.Scanlan, S.Nagaya, *Physica C* **335(1-5)** (2001) 1
- [7] R.Heller, G.Friesinger, A.M.Fuchs, T.Mito, S.Satoh, K.Takahata, M.Tasca, M.Vogel, *Cryogenics* **41** (2001) 539
- [8] Darren M Spiller, C Beduz, M.K. Al-Mosawi, C.M.Friend, P.Thacker, A.Ballarino, *Supercond.Sci.Technol.* **14** (2001) 168

- [9] M.Putti, M.R.Cimberle, C.Ferdeghini, G.Grasso, A.Manaca, W.Goldacker, *IEEE Trans.App.Supercond.* **11(1)**, (2001) 3285
- [10] J. Le Bras, T. Dechambre, P. Regnier, K. Gagnant, *IEEE Trans.App.Supercond.* **9 (2)** (1999) 503

- [11] L. Martini, F.Barberis, R. Berti, G. Volpini, L. Bigoni, F. Curcio, *Physica C* **341-348** (2000) 2513
- [12] S. Odaka, S. B. Kim, A. Ishiyama, Y. Sato, S. Honjo, Y. Iwata, S. Shingo *IEEE Trans.App.Supercond.* **9** (1999) 491
- [13] L.Martini, F.Barberis, R.Berti, L.Bigoni, F.Curcio, G.Volpini, *IEEE Trans.App.Supercond.* **9** (1999) 420
- [14] R.Heller, G. Friesinger, W. Goldacker, M. Quilitz, M. Tasca, A. M. Fuchs, W. Pfister, M. Vogel, *IEEE Trans.App.Supercond.* **9** (1999) 507
- [15] L.Tkachenko, I.Bogdanov, A.Harchenko, S.Kozub, K.Myznikov, A.Olyunin, V.Sytnik, V.Zubko, I.Akimov, D.Gusakov, D.Rakov, A.Shikov, Bochvar, Proceedings of EPAC (2002), Paris

CHAPTER 7

SUMMARY AND CONCLUSIONS

Over the widespread application areas of HTS, current leads are of the first generation type, which is used to connect a superconducting system with a room temperature power service. There are two types of current leads viz. conduction cooled (cooling is provided by the conduction from the low temperature system) and vapour cooled (cooling is provided by the cold He vapours externally supplied or generated by boil off from the system itself). Conduction cooled current leads are implemented in superconducting systems operating with the help of closed cycle cryocoolers/refrigerators, enhancing its efficiency. Vapour cooled current leads are used mostly in LTS systems and reduce the boil off of liquid He. While vapour cooled current leads are efficient in terms of its low heat leak, conduction cooled current leads are of more general type, easy to fabricate and find application in medium and relatively high field superconducting magnets such as MRI/NMR etc. Compared to the bulk form of current leads prepared from YBCO, Bi-2222 or Bi-2223 either in the form of a ceramic tube or rod, the metal ceramic composite form prepared from (Bi,Pb)-2223 tapes have many advantages in terms of its electrical, thermal and mechanical properties. The work presented in this thesis is a systematic investigation carried out to optimize the superconducting, mechanical and thermal properties of (Bi,Pb)-2223 tapes in the multifilamentary configuration to use it as the raw material for HTS current leads. Also it is the aim of the present investigation to prepare prototype current leads using the optimized

(Bi,Pb)-2223/Ag alloy sheathed tapes and to test it for the operational stability.

The thesis presents a brief review on the properties and processing aspects of HTS superconductors in general and BPSCCO system in particular. The distinguishing characteristics of Cu-O superconductors compared to other types conducting ceramic oxides are discussed along with the theoretical developments in the field of HTS. The type II nature and low irreversibility field of HTS is also mentioned. Along with the application environments of HTS, the wire requirement in terms of ampere meter of HTS conductor for certain high current applications are mentioned. The structural features and the problems specific to powder-in-tube processing of Bi-2223 tapes such as formation and stability of Bi-2223 phase, critical current density, importance of flux pinning, weak links and other possible current limiting mechanisms are also mentioned. The importance of multifilamentary geometry for application developments is highlighted. Also the achievements and the state-of-the-art developments for Bi-2223 tapes both on the international and national scenario are mentioned. The salient features of HTS current leads and the material choices for it taking into account of operational stability requirements are mentioned together with the state-of-the-art developments in this field.

Against this background, the scope of the work includes investigations on to the optimization of superconducting, mechanical and thermal properties of (Bi,Pb)-2223/Ag multifilamentary tapes. Investigations were focused on (i) finding suitable alloy sheath to replace pure Ag having reduced thermal conductivity and better

mechanical properties, (ii) enhancing the field tolerance or the $J_c - B$ characteristics of the tapes, (iii) optimization of geometrical and the processing parameters of the multifilamentary tapes so as to increase the final J_c as well as J_c homogeneity along the length of the tape and finally (iv) preparation prototype current leads of rating > 100 A (0T, 77 K) and characterize it.

In the present study, the main analytical methods used are phase analysis using XRD, microstructural examination using optical microscopes and SEM, mechanical properties using tensile testing machine, thermal analysis like DTA etc. Characterization of the superconductors have been done at 77 K, for obtaining critical current I_c , its field dependence ($J_c - B$), its dependence on stress ($J_c - \sigma$) and strain ($J_c - \epsilon$). Also the preparation technique for the multifilamentary wire-in-tube tapes are discussed.

The studies on alternate alloy systems included Ag-Cu and Ag-Au with varying Cu and Au content in the sheath. Results showed that on alloying with Cu both the phase formation and the ultimate phase fraction of Bi-2223 is significantly affected by Cu percentage in the sheath. Moreover the optimum Cu percentage in the sheath is dependent on the Cu stoichiometry in the system and a Cu deficient precursor is favoured for making Bi-2223 tapes with Ag-Cu as alloy sheath. A Cu doping percentage of 6 at% in the sheath for a precursor with Cu stoichiometry of 3.0 is found to yield better phase formation and J_c after the final stage heat treatment.

Superconductivity measurements, XRD results and microstructural examinations of the Au doped samples showed no

significant change compared to the pure Ag sheathed tape. However the $J_c - B$ characteristics showed a slight enhancement with respect to Au doping on the sheath.

Coming to the mechanical behaviour of the composite tapes, strength of the sheath is found to be the critical factor enhancing the mechanical strength of the tape. While the UTS of Ag-Cu alloys are considerably enhanced, that of Ag-Au alloys are comparable to that of pure Ag. It was found that both the bend strain tolerance ($I_c - \epsilon$) and the stress tolerance ($I_c - \sigma$) of Ag-Cu alloy sheathed tapes improve remarkably as the level of Cu doping in the sheath increases. Also the multifilamentary tapes were found to withstand higher mechanical strains and stresses due to their fine filamentary structure and comparatively lower superconductor fill factor.

Both the electrical and thermal conductivity of Ag-Au alloys are considerably lower than that of Ag-Cu alloys and both in turn are very much lower than that of pure Ag. At 77 K thermal conductivity of AgAu₆ is 128 W/cmK while that of AgCu₆ is 376 W/cmK. At the same condition, K of pure Ag is 671 W/cmK.

After a critical analysis of the superconducting, mechanical and thermal properties of both Ag-Cu and Ag-Au alloys, it was decided to use AgAu (Au – 6 at.%) sheath for the inner filaments and AgCu (Cu -6 at.%) as the outer sheath for the preparation of multifilamentary tapes for HTS current leads.

As required by any application of Bi-2223 tapes, the flux pinning strength should be enhanced either by processing adjustment or by

adding extra impurity phases on to the system acting as flux pinners. After a thorough literature survey, it was decided to use nanosize (~30 nm) MgO particles into the system as flux pinners. Investigations such as XRD analysis, SEM observations and superconductivity measurements showed that 0.3 wt.% MgO is the optimum for enhancing the flux pinning strength and the self field J_C of the tapes. The essential pinning mechanism is the 'δI' pinning, where the pinning force for the fluxons is provided by the normal particles of size of the order of coherence length (ξ).

One of the objectives of the thesis was the optimization of geometrical and thermomechanical processing parameters of the multifilamentary tapes. As the preparation of multifilamentary tapes essentially involves the filling of monocoil wires of optimized diameter and number, a detailed investigation has been carried out to optimize the starting packing density (SPD) and the wire diameter prior to flat rolling stage of monolayer tapes. The results of core density measurements and J_C after the final stage heat treatment showed that a powder fraction of 33.5 wt.% is the optimum for obtaining defect free tapes with higher sintered density and J_C . Higher powder fractions yielded punctured tapes, caused by oozing out of the liquid phase during the sintering process due to insufficient sheath thickness, with poor J_C and lower sintered density. But for the preparation of multifilament tapes a powder fraction of 27.5 wt.% was used as a precautionary measure to avoid the possible filament cracking and discontinuity that may happen during the mechanical deformation steps.

The geometrical parameters selected for the optimization study were the filament number, wire diameter prior to tape rolling stage and the final tape thickness. The filament count was varied from 10 to 100 and the final tape thickness from 0.2 to 0.4 mm. J_C results after the final stage heat treatment showed that the final tape thickness had a controlling factor and it should be optimized with respect to the filament count used. A filament count of ~40 and a final tape thickness of 0.3 mm prepared from a starting wire diameter of 2.6 mm showed the highest J_C among all the samples and these optimum parameters were used for the subsequent studies conducted.

Thermomechanical processing schedule has a vital importance in the processing of multifilamentary tapes as the process essentially involves repeated thermomechanical cycles. Studies conducted to optimize the thermomechanical processing schedules showed that the phase assemblage of the tape prior to the last stage deformation plays a significant role in governing the final J_C , J_C -B and microstructure of the tapes. Out of the three different schedules the one with maximum Bi-2223 content prior to the last stage rolling showed highest J_C and better microstructure.

In order to enhance J_C as well as the J_C homogeneity along the length of the tape studies were conducted to optimize the uniaxial pressure applied prior to the last stage heat treatment. A pressure of 50 MPa was found to optimum with respect to the final superconducting properties, J_C homogeneity along the length of the tape as well as microstructure. Based on the studies conducted to optimize the process and geometrical parameters in the wire-in-tube processing of

multifilamentary tapes an I_c of 60 A (77 K, 0T) has been achieved in tapes of length > 15 cm.

For the preparation of HTS current leads of length > 10 cm multifilamentary tapes with inner AgAu (6 at. % Au) and outer AgCu (6 at.% Cu) were prepared under the optimized conditions. A suitable glass-fibre reinforced epoxy with compatible thermal expansion coefficient with the sheath alloy was selected as the housing matrix for mechanical rigidity. Ni coated copper end caps were used as the interconnectors. The estimated heat leak of the prepared current lead for a hot end temperature of 77 K and cold end temperature of 4.2 K was found to be two orders of magnitude lower than that prepared using pure Ag sheath.

